NASA Contractor Report 185297

Oscillating-Flow Loss Test Results in Rectangular Heat Exchanger Passages

J. Gary Wood, Consultant
Albany, Ohio
for
Sunpower Inc.
Athens, Ohio

September 1991

Prepared for
Lewis Research Center
Under Contract NAS3-23885

Date for general release September 1993

National Aeronautics and
Space Administration

[redacted]

ABSTRACT

Presented in this report are test results of oscillating-flow losses in rectangular heat exchanger passages of various aspect ratios. This work was performed in support of the design of a free-piston Stirling engine (FPSE) for a dynamic space power conversion system. The FPSE design was done by Sunpower Inc. under contract to NASA-Lewis Research Center as part of the SP-100 program. Oscillating-flow loss testing was performed using an oscillating-flow loss rig which is based on a variable stroke and variable frequency linear drive motor. Tests were run over a range of oscillating-flow parameters (Re_{max}, Re_{ω}, and Ar) encompassing the flow regimes of the proposed engine design. Test results are presented in both tabular and graphical form and are compared against analytical predictions.

INTRODUCTION

The work described in this report was performed in support of a free-piston Stirling Space Engine (SSE) design performed by Sunpower Inc. for NASA-Lewis Research Center. Details of this conceptual design were presented by Penswick (1).

The flow losses through the heat exchangers of a free-piston Stirling engine influence the dynamics of the reciprocating displacer and piston and, therefore, have a magnified effect on engine performance. The SSE design incorporated rectangular gas flow passages in the heater and cooler and operated at relatively high reciprocating frequencies. Understanding oscillating-flow losses through these types of passages at the design operating conditions was a primary goal of this study.

An oscillating-flow pressure drop test rig and a steady-flow rig were previously designed and fabricated by Sunpower Inc. for NASA-Lewis and used to generate test information for regenerators and round heat exchanger passages. These test rigs have been described by Wood (2) and test results for this testing were reported by Koester et al (3).

In support of the SSE design, various aspect ratio, rectangular flow passage test samples were fabricated and tested on both the oscillating- and steady-flow test rigs. This report presents and discusses the results and findings which resulted from this work.

Further, this report is intended to supplement the earlier report on regenerators and round flow passages. General descriptions of the test rigs are given in a following section, but for detailed descriptions of the data acquisition system and the data reduction techniques,the reader is referred to reference 3.

AUTHOR'S NOTE

The testing on which this report is based was conducted by an engineer who left Sunpower before writing the final report. This report is a reconstruction of the notes, graphs and materials studied after the conclusion of the program work.

Although the author of this final report was not responsible for this testing, he had designed the original test rig and was familiar with earlier test programs conducted with this rig. He made a conscientious effort to assemble the test results and reach meaningful conclusions based on the available test data.

DESCRIPTION OF THE TEST RIGS

Detailed descriptions of both test rigs are given in reference 2. The following contains a brief description.

Steady Unidirectional Flow Rig

A schematic of this rig is shown in Figure 1. Gas flow is provided by an oilless piston-type compressor. The flow rate of gas is set by adjusting the speed of the compressor which is accomplished by varying the voltage supplied to a DC drive motor.

Downstream of the compressor is an accumulator. Gas exits this accumulator through a high density filter. The main purpose of this filter is to act as a flow restriction, so the accumulator and filter act together to suppress pressure pulsations which would otherwise be caused by the compressor.

Gas then proceeds to the section where the mass flow rate is measured by a Teledyne-Hastings mass flowmeter. This flowmeter determines flow rate by measuring the temperature difference upstream and downstream of a heated section of tubing. Actually, a laminar flow element is placed in the flow path, which causes only a portion of the flow to pass through the flowmeter.

The element labeled small pressure vessel is located next in the flow path. This element allows access for changing the sample and turns the flow direction of the gas back toward the main pressure vessel of the rig.

Gas then passes through the test sample and back to the main pressure vessel. A differential pressure transducer measures the pressure drop of the gas passing through the test sample.

Oscillating-Flow Rig

A schematic of the oscillating-flow rig is shown in Figure 2, while an assembly drawing is shown in Figure 3. This rig is based on a 2 kW linear drive motor. A variable voltage and variable frequency electronic driver provides the electrical excitation which powers this motor.

The drive motor is directly connected to a gas displacement section consisting of a close-fitting piston in a cylinder. The piston diameter is 19.05 mm (0.750 in.). The gas seal of the displacement section is accomplished by the relatively long clearance seal.

To reduce the driving force required of the motor, the mass of the reciprocating parts is resonated by mechanical springs. These springs are selected so the reciprocating components of the rig are in mechanical resonance close to the desired frequency for testing. Frequency variations around the mechanical resonance point are accomplished with the electronic driver (approximately ±5 hertz).

The entire linear drive motor, displacement section, and test section are enclosed within a pressure vessel to allow testing at elevated mean gas pressures. Dynamic instrumentation for the rig consists primarily of a linear displacement transducer which measures piston position and a close-coupled pressure transducer in the displacement section.

The end of the test sample away from the displacement section is open to the large internal volume of the pressure enclosure. Because of the large volume of the pressure vessel, the pressure here remains essentially constant during gas cycling through the test sample. This allows for the measurement of pressure drop across the sample by means of the close-coupled pressure transducer. The back side of the sensing element (diaphragm) of this transducer is ported to the internal volume of the pressure vessel. Thus, dynamic pressure drop is measured without the use of sensing lines which commonly can cause measurement errors.

The range of operating parameters of the test rig are:

Stroke (mm)	0 to 30*
Frequency (Hz)	0 to 120*
Mean Pressure (MPa)	0 to 15
Working Gas	He, N_2, Ar, etc.

*Because of the use of Teflon-based bearing surfaces which have a peak velocity limitation of 5.66 m/s, maximum values of stroke and frequency are not allowed simultaneously. For example, at maximum frequency, stroke is limited to 15 mm.

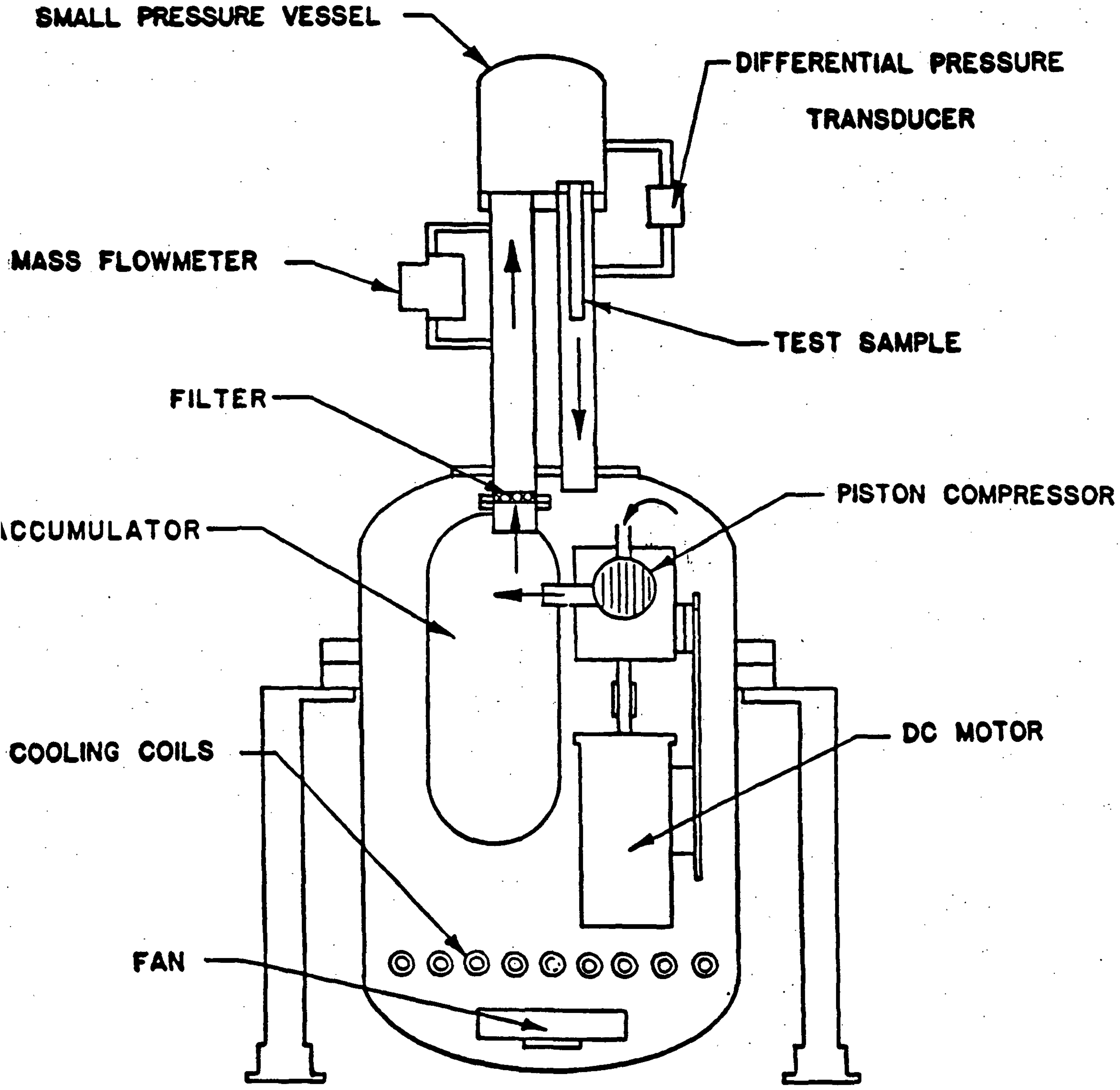

Figure 1 Steady-Flow Test Rig

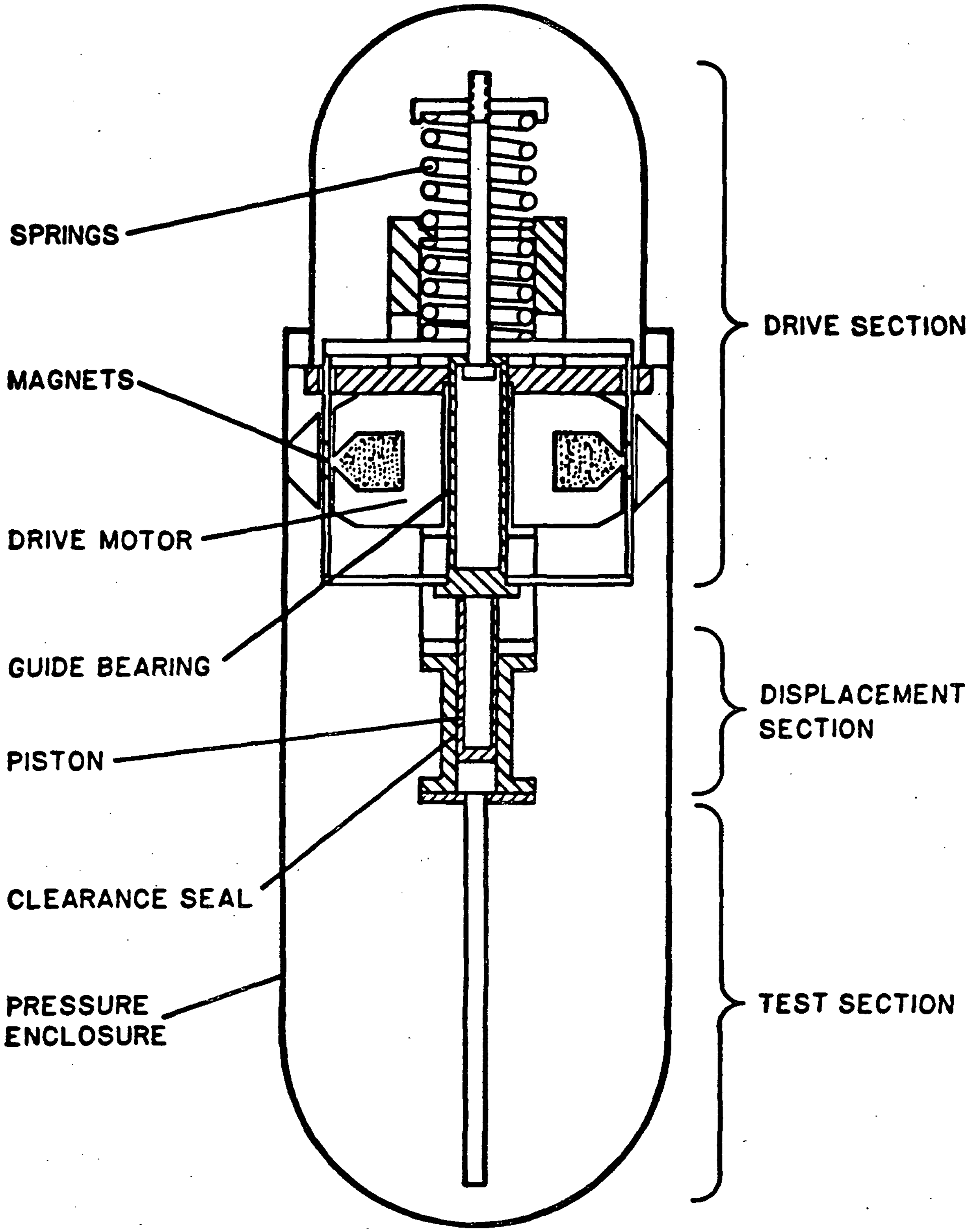

Figure 2 Oscillating-Flow Test Rig

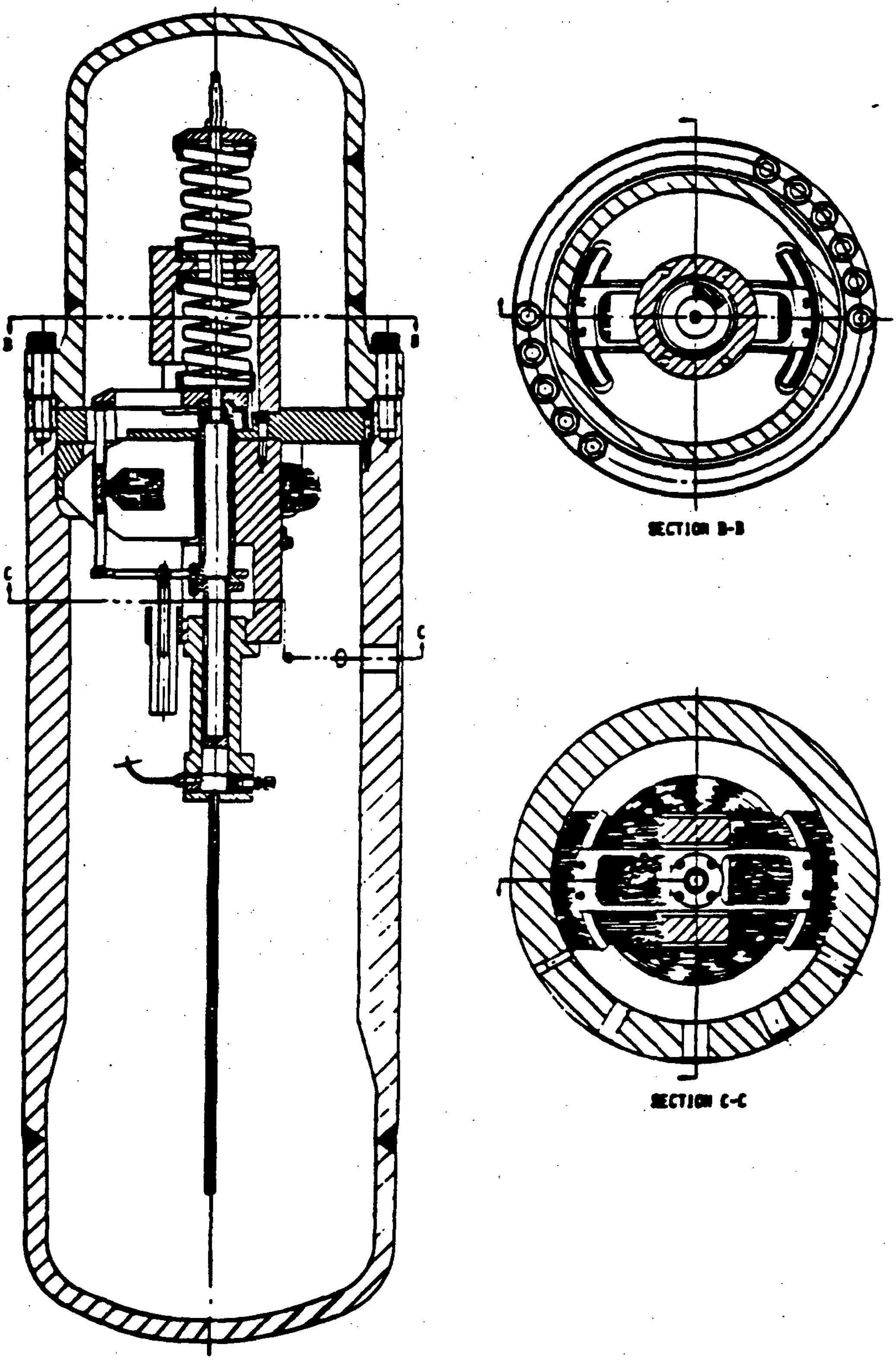

Figure 3 Oscillating-Flow Test Rig

DESCRIPTION OF THE TEST SAMPLES

The test samples were comprised of rectangular cross-section flow passages with various aspect ratios. Geometrical parameters of these samples are given in Table 1. As is shown in this table, aspect ratios ranged from 0.127 to 0.805. Most samples were 120 mm long (the length of the heat exchanger modules of the SSE design) and were designed to have square entrance/exit edges. Three 10 mm long samples were also fabricated: two with square entrance and exit edges (aspect ratios of 0.127 and 0.442) and one with rounded edges (aspect ratio of 0.442).

Pictures of these samples are shown in Figure 4. Figures 5 and 6 present typical detailed drawings of the two component parts which were pressed together to form a single test sample. Both of the component parts were fabricated from aluminum. Note that channel dimensions given in the table are presented in the order of the slot width by slot depth machined in the inner aluminum part.

The reader will notice that the table indicates two flow passages for all samples, while Figure 4 shows that most samples appear to have 12 flow passages. Although many of the samples were originally fabricated with 12 slots, 10 of these were blocked with epoxy prior to testing.

It was originally intended that 12 flow passages would be used; however, early testing on the oscillating-flow rig with the 12 flow passages resulted in significant Helmholtz-type acoustic oscillations of gas through the test sample.

Basically, acoustic oscillations would occur whenever the rig frequency was an odd order subharmonic of the Helmholtz frequency of the combined displacement section and test sample system. The higher the number of passages, the higher is the Helmholtz frequency of the system. This placed the odd order subharmonics very close to one another and made it impossible to avoid these during testing. By reducing the number of passages and, thus, the Helmholtz frequency, it was possible to essentially eliminate the problem.

The samples with 12 passages, shown in the picture, were fabricated before this acoustic problem was realized and understood. Ten of the passages were, therefore, blocked off with epoxy for testing. However, for two of the samples (aspect ratios of 0.147 and 0.805), some partial epoxy blockage was later found in the open passages. This is described later in this section where the results of inspection of the samples are given.

Table 1
Geometric Parameters of Rectangular Channel Test Sections

Aspect [1] Ratio	No. of [2] Channels	Channel [3] Dimensions (mm)	Flow Area (m^2)	Hydraulic Diameter (m)	Length (m)	L/D	Entrance Configuration
0.805	2	2.36 x 1.90	8.97E-6	2.11E-3	0.12	57.0	Square Edge
0.667	2	1.64 x 2.46	8.07E-6	1.97E-3	0.12	61.0	Square Edge
0.456	2	1.46 x 3.20	9.34E-6	2.00E-3	0.12	59.8	Square Edge
0.444	2	1.40 x 3.17	8.88E-6	1.94E-3	0.01	5.15	Square Edge
0.444	2	1.40 x 3.17	8.88E-6	1.94E-3	0.01	5.15	Round Edge
0.352	2	1.35 x 3.84	1.04E-5	2.00E-3	0.12	60.1	Square Edge
0.220	2	1.00 x 4.55	9.10E-6	1.64E-3	0.12	73.2	Square Edge
0.147	2	0.84 x 5.71	9.59E-6	1.46E-3	0.12	81.9	Square Edge
0.127	2	1.00 x 7.90	1.58E-5	1.78E-3	0.12	67.6	Square Edge
0.127	2	1.00 x 7.90	1.58E-5	1.78E-3	0.01	5.63	Square Edge

1. Smaller dimension divided by larger dimension
2. No. of channels in the test sample
3. Channel width x channel height

ORIGINAL PAGE
BLACK AND WHITE PHOTOGRAPH

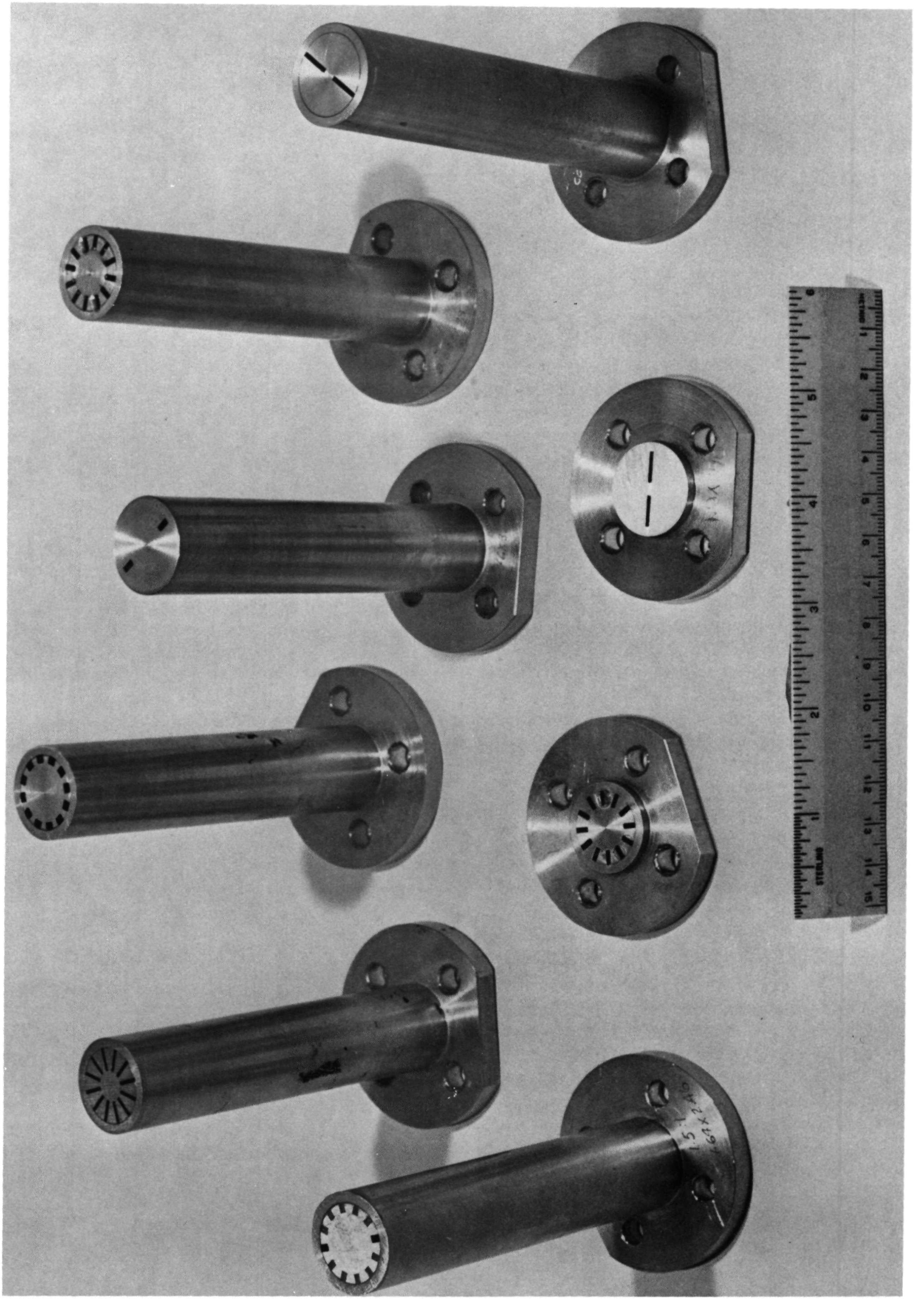

Figure 4 Test Samples

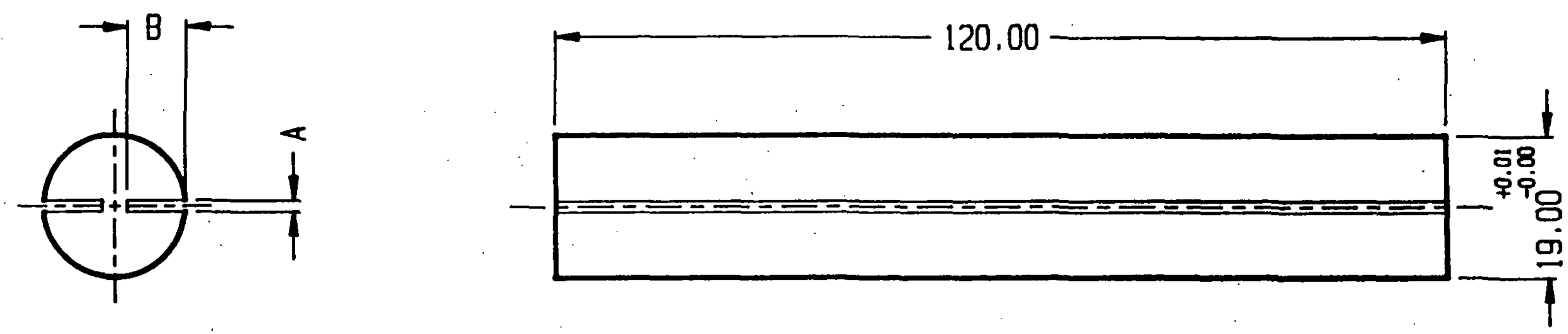

ALL DIMENSIONS IN MILLIMETERS. UNLESS OTHERWISE SPECIFIED: TOOL RADIUS = 0.4 or 0.8 SURFACE FINISH = 1.5µm (RMS) OR BETTER DEBURR ALL EDGES	ANGLES: ± 1.0° X. ±1.0 X.X ±0.25 X.XX ±0.10	CHECKED BY:	DATE:	SUNPOWER, INC. Athens, Ohio
		DRAWN BY: TC	DATE: 3/87	
FILE NAME: TESTSECT	PROJ. NO. 6050	DESIGN BY: GK	QTY/UNIT 1	
MATERIAL: 6061-T6 AL		SIZE: A	SCALE: FULL	TITLE SSE HEATER TEST SECTION
TREATMENT: N/A		DRAWING NO.		

Figure 5 Test Sample Inner Slug

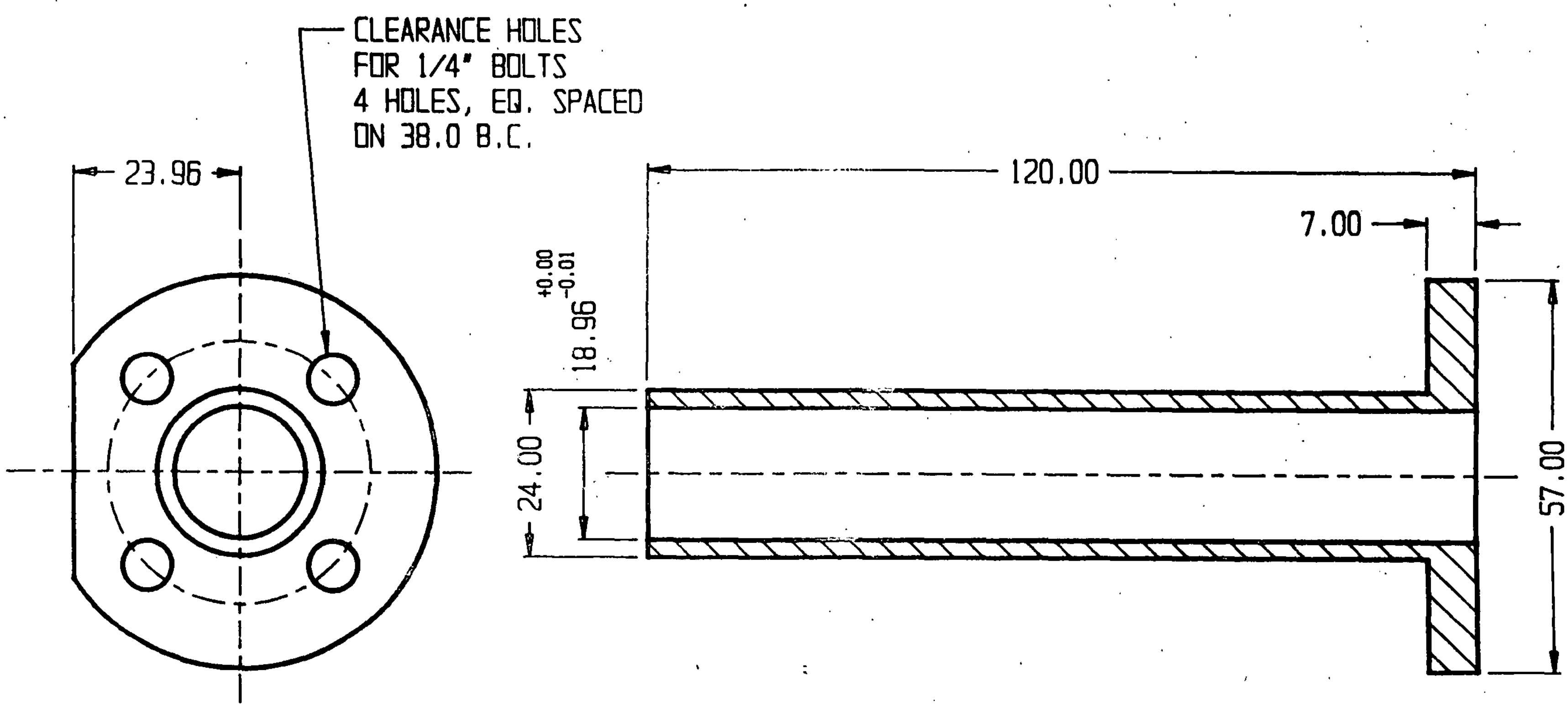

ALL DIMENSIONS IN MILLIMETERS. UNLESS OTHERWISE SPECIFIED: TOOL RADIUS = 0.4 or 0.8; SURFACE FINISH = 1.5μm (RMS) OR BETTER; DEBURR ALL EDGES. ANGLES: ±1.0°; X. ±1.0; X.X ±0.25; X.XX ±0.10	CHECKED BY:	DATE:	SUNPOWER, INC. Athens, Ohio
	DRAWN BY: TC	DATE: 3/87	
FILE NAME: CYLINDER / PROJ. NO. 6050	DESIGN BY: GK	QTY/UNIT 1	
MATERIAL: 6061-T6 AL	SIZE: A	SCALE: FULL	TITLE: CYLINDER SHEATH
TREATMENT: N/A	DRAWING NO.		

As discussed later in the section Preliminary Comments on the Test Results, both the steady- and oscillating-flow results are sensitive to the exact geometry of the test samples, both to the passage flow area and the shape of the entrance/exit corner edges. The test samples were fabricated on a horizontal milling machine using a slitting saw. The alignment of the part being fabricated and the cutting saw in such a machining operation is critical toward the resulting slot width. The greater the misalignment, the wider the resulting passageway.

Apparently the test samples were not examined in detail prior to testing. Only during the writing of this report, while trying to better understand the test results, were the full length samples inspected and the findings recorded. These samples were examined with an optical comparator having graduations of 0.001 in., as well as with a 30 power microscope and an 8 power magnifying glass. The total scale length of the optical comparator was 0.100 in., which did not allow measurement, by this means, of the depth of cut of the deeper slots.

The dimensions obtained from this examination were in general agreement with the values given in Table 1. The conditions of the entrance/exit edges, however, often varied significantly from an ideal square edge. Ends of some passages were found to have significant machining burrs, while some edges had small chamfers, apparently the result of a deburring operation. The following gives details of the major findings of this examination of the 120 mm long samples.

0.127 Aspect Ratio (1.00 x 7.90 mm)
The width of the sample passages were fairly accurate, measuring between 0.99 mm and 1.02 mm (0.039 in. to 0.040 in.). Three of the four ends had a 50 μm to 75 μm (0.002 in. to 0.003 in.) chamfer on the edges, while the fourth end had what appeared to be a significant zone of machining burrs which restricted passage width to 0.94 mm (0.037 in.).

0.147 Aspect Ratio (0.84 x 5.71 mm)
This sample originally was fabricated with 12 slots, 10 of which were then blocked with epoxy. However, examination showed that some small amounts of glue had gotten into the open passages and would be expected to slightly restrict the gas flow at one end of the sample. Some small burrs also existed, but generally the edges were quite square.

0.220 Aspect Ratio (1.00 x 4.55 mm)
The edges of this sample were found to be quite good. On one end, the two passages were both uniform and very close to 1.02 mm (0.040 in.) wide. The other end showed some taper in the cross-section of both passages; here, toward the center of the sample, the passages were 1.02 mm (0.040 in.) wide but, at the outer edge, one tapered to 1.07 mm

(0.042 in.) and the other to 1.12 mm (0.044 in.). A large dent (probably the result of the sample having been dropped at some point) existed on the non-tapered end of one passage which restricted passage width to 0.89 mm (0.035 in.). It is not known if this dent had occurred before or after the sample was tested.

0.352 Aspect Ratio (1.35 x 3.84 mm)
This was the best looking sample, having quite square edges, few burrs, and a uniform width of between 1.35 mm and 1.37 mm (0.053 in. to 0.054 in.).

0.456 Aspect Ratio (1.46 x 3.20 mm)
This sample measured somewhat oversize at about 1.52 mm (0.060 in.); edge chamfers varied from 50 μm to 100 μm (0.002 in. to 0.004 in.).

0.667 Aspect Ratio (1.64 x 2.46 mm)
Reasonably square corners were found, except one end had a large burr. Width was generally uniform at 1.63 mm (0.064 in.), except one end of one of the passages was closer to 1.65 mm (0.065 in.) wide. The depth, however, varied from 2.44 mm (0.096 in.) on one end of the sample to 2.36 mm (0.093 in.) on the other end for one passage; the other passage depth varied from 2.46 mm (0.097 in.) to 2.39 mm (0.094 in.) from end to end.

0.805 Aspect Ratio (2.36 x 1.90 mm)
This sample had the poorest accuracy and end conditions of all the samples. On one end, width was uniform at 2.34 mm (0.092 in.); on the other end, one passage was 2.29 mm (0.090 in.) wide and the other 2.31 mm (0.091 in.). One passage was 1.96 mm (0.077 in.) deep on the one end, but the other end apparently was offset in machining causing the depth to vary from one side of the slot to the other from 1.83 mm to 1.93 mm (0.072 in. to 0.076 in.) The other slot started with a depth variation of 1.78 mm to 1.90 mm (0.070 in. to 0.075 in.) across the width. The other end was 1.90 mm (0.075 in.) deep on both sides but had a large machining burr over most of the width that restricted depth to 1.78 mm (0.070 in.); this end also had two areas where epoxy was seen in the passage.

PRELIMINARY COMMENTS ON TEST RESULTS

Many of the results presented and discussed later make use of comparisons to steady-flow correlations. In the case of steady-flow testing, a term Pratio is calculated which is the ratio of measured pressure drop to that predicted by common steady-flow correlations. For the oscillating-flow results, a Total Dissipation Factor (TDF) is given which is the ratio of measured pumping power to that obtained by integrating over the cycle using the instantaneous flow rate applied to steady-flow correlations.

The steady-flow correlation used in these calculations is:

$$\Delta P = (fL/D+K)\rho u^2/2$$

where:

- ΔP = pressure drop
- L = Flow passage length
- D = Hydraulic diameter (4 x Area / Perimeter)
- K = 1.5 (combined entrance and exit loss coefficient, for square-edged sample)
- ρ = gas density
- u = gas velocity

and:

Case: Re>4000 $\quad f = 0.316\ Re^{-0.25}$

Case: Re<2000 $\quad f = 64\ b\ Re^{-1}$

where:

- $b = 1.47-1.48\ a+0.92\ a^2$
- a = aspect ratio of passage (smaller dimension divided by larger dimension)

Case 2000<Re<4000 uses a linear interpolation between f@2000 and f@4000:

$$f = (Re/2000-1)(f@4000-f@2000)+f@2000$$

Note that the above makes use of the Blasius correlation for the turbulent friction factor. This correlation is not recommended above Reynolds numbers of 10^5. However, only under steady-flow testing was this limit exceeded, and even here not by an amount that would have given significantly different results.

Also, due to the short L/D of the test samples, the entrance and exit loss coefficient is a significant contributor to overall pressure drop. This further reduces the difference that would have been obtained from the use of a different friction factor correlation. Benedict (4) in his Table 6.1, presents a good comparison of alternate correlations which are considered applicable to Reynolds numbers above 10^5.

The influence of the passage aspect ratio on the turbulent friction factor is neglected in the equations above. Idelchik (5) in his diagram 2.6, indicates that the turbulent flow friction factor of rectangular passages exceeds that of a round tube by an enhancement that falls linearly from 10 to 0 percent as aspect ratio increases from 0 to 1. Again, including this effect would have resulted in small changes to either the Pratio or TDF values.

It is important to emphasize that the test results presented here are sensitive to both the flow area of the passageways and the squareness of the entrance/exit edges. Turbulent flow pressure drop is approximately inversely proportional to the square of the area of the passage. In narrow passages, such as those in many of the samples tested, minor machining errors can have significant influences on overall pressure drop. For example, a rather small error of 25 μm in the width of a 1.00 mm slot will change the pressure drop by 5 percent. This 25 μm variation in width is fairly representative of the samples examined.

As an example of the effect of the form of the entrance and exit corners, consider the roughly 75 μm deburring break which existed on several of the test samples. Using representative values for the test samples of 2.0 mm for hydraulic diameter, an L/D of 70, an assumed break angle of 45 degrees, and a Reynolds number of 5×10^4, the fL/D term is calculated as 1.48 . Using diagram 3.7 of Idelchik (5) gives a total entrance and exit loss coefficient of approximately 1.38 instead of 1.50 for a square edge. The total pressure drop is then calculated as about 96 percent of that with a sharp corner.

For comparison, the enhancement on turbulent flow friction factor (for rectangular passages compared to circular) given by Idelchik (5) would be expected to result in a Pratio variance between the extremes of sample aspect ratios on the order of 3 percent. Thus, the problems of geometrical accuracy of both the passage cross-section and the entrance/exit edges can be expected to shadow any discernible aspect ratio effect in the test results.

STEADY-FLOW TEST RESULTS

Steady unidirectional flow testing was performed only on four samples. The samples tested were all full length with aspect ratios of 0.127, 0.220, 0.352, and 0.805.

From the test results, a parameter termed Pratio was calculated. Pratio is defined as the ratio of the measured pressure drop to that predicted, using commonly accepted equations. (See the earlier section titled: Preliminary Comments on the Test Results.)

Steady unidirectional flow test results are presented graphically in Figures 7 through 11. Figures 7 through 10 give results for each of the samples tested. Figure 11 shows the results presented together with an expanded scale for the ordinate. Tabular test results are given in Appendix A-1.

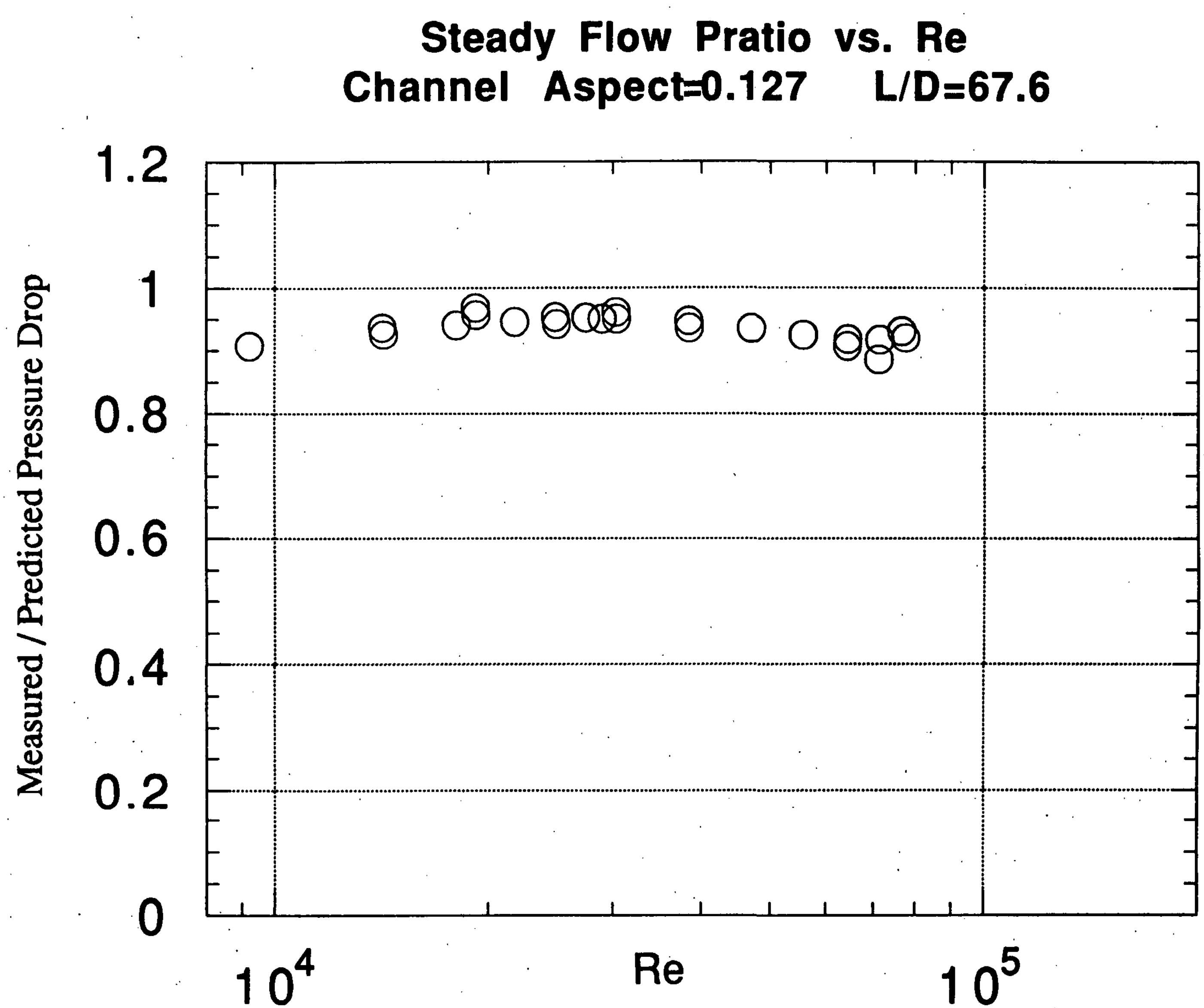
Steady Flow Pratio vs. Re
Channel Aspect=0.127 L/D=67.6
1.2
1
0.8
0.6
0.4
0.2
0
Measured / Predicted Pressure Drop
10^4
Re
10^5

Figure 7

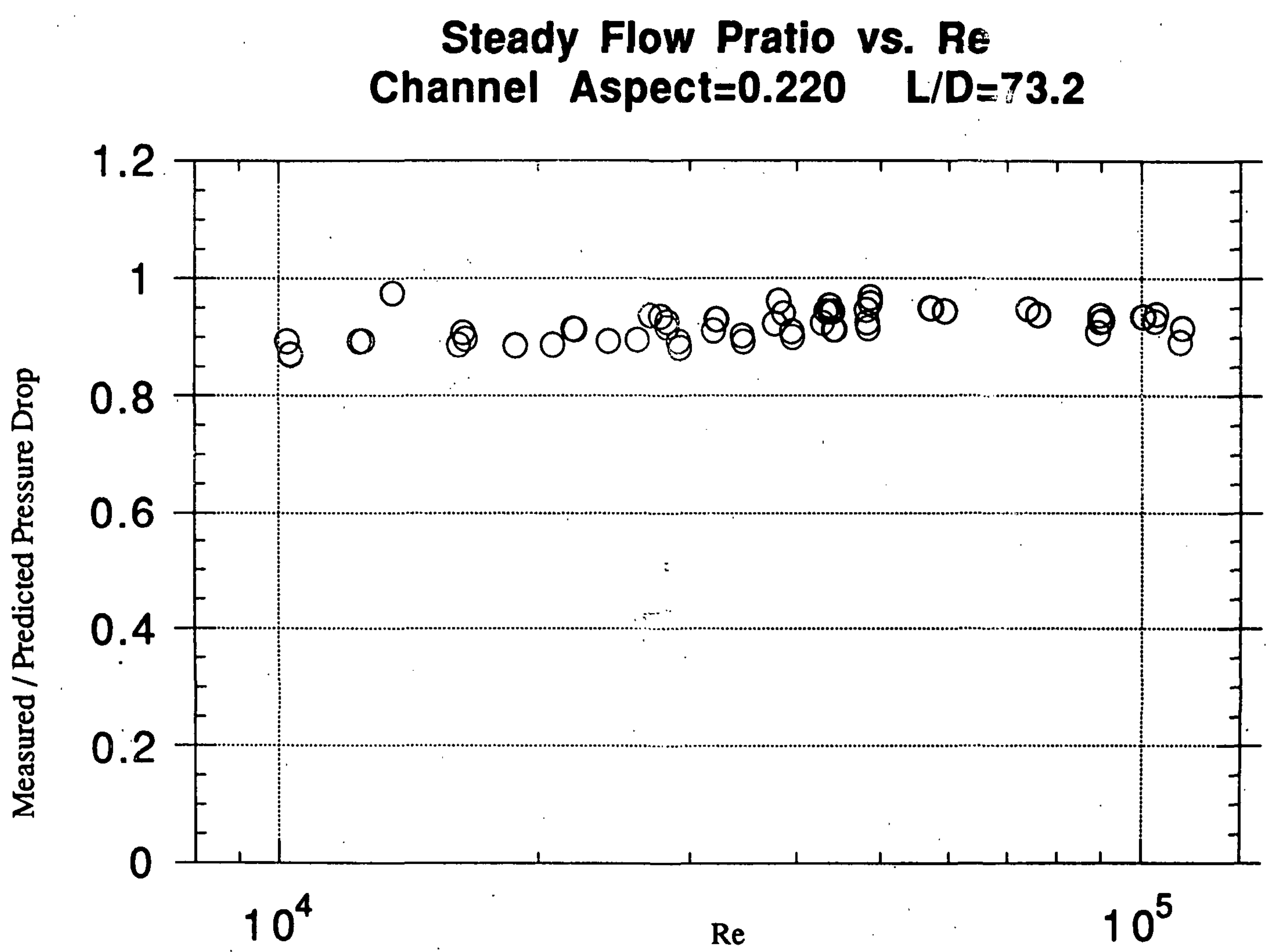
Steady Flow Pratio vs. Re
Channel Aspect=0.220 L/D=73.2
Measured / Predicted Pressure Drop
1.2
1
0.8
0.6
0.4
0.2
0
10^4
Re
10^5

Figure 8

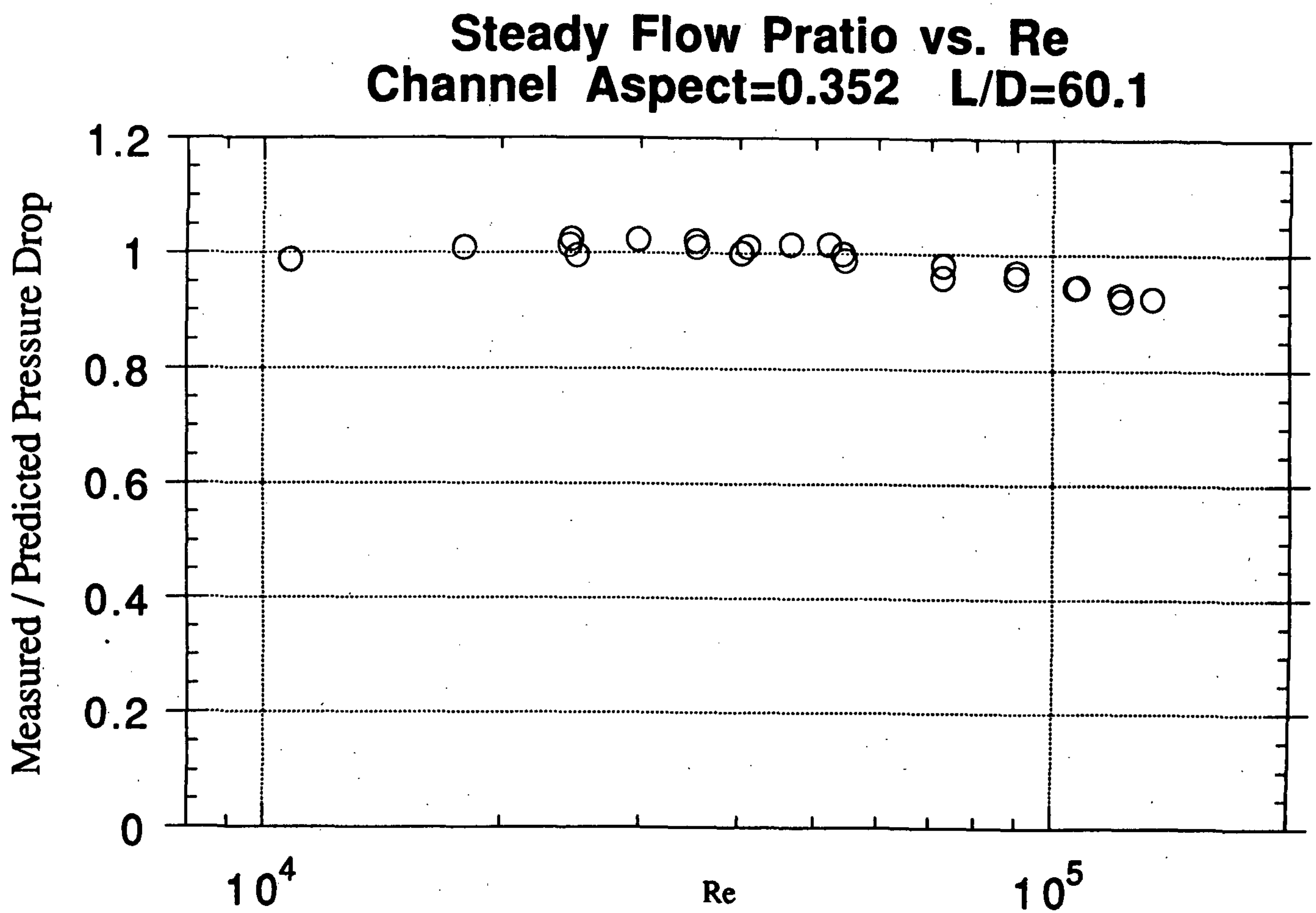
Steady Flow Pratio vs. Re
Channel Aspect=0.352 L/D=60.1
1.2
1
0.8
0.6
0.4
0.2
0
Measured / Predicted Pressure Drop
10^4
Re
10^5

Figure 9

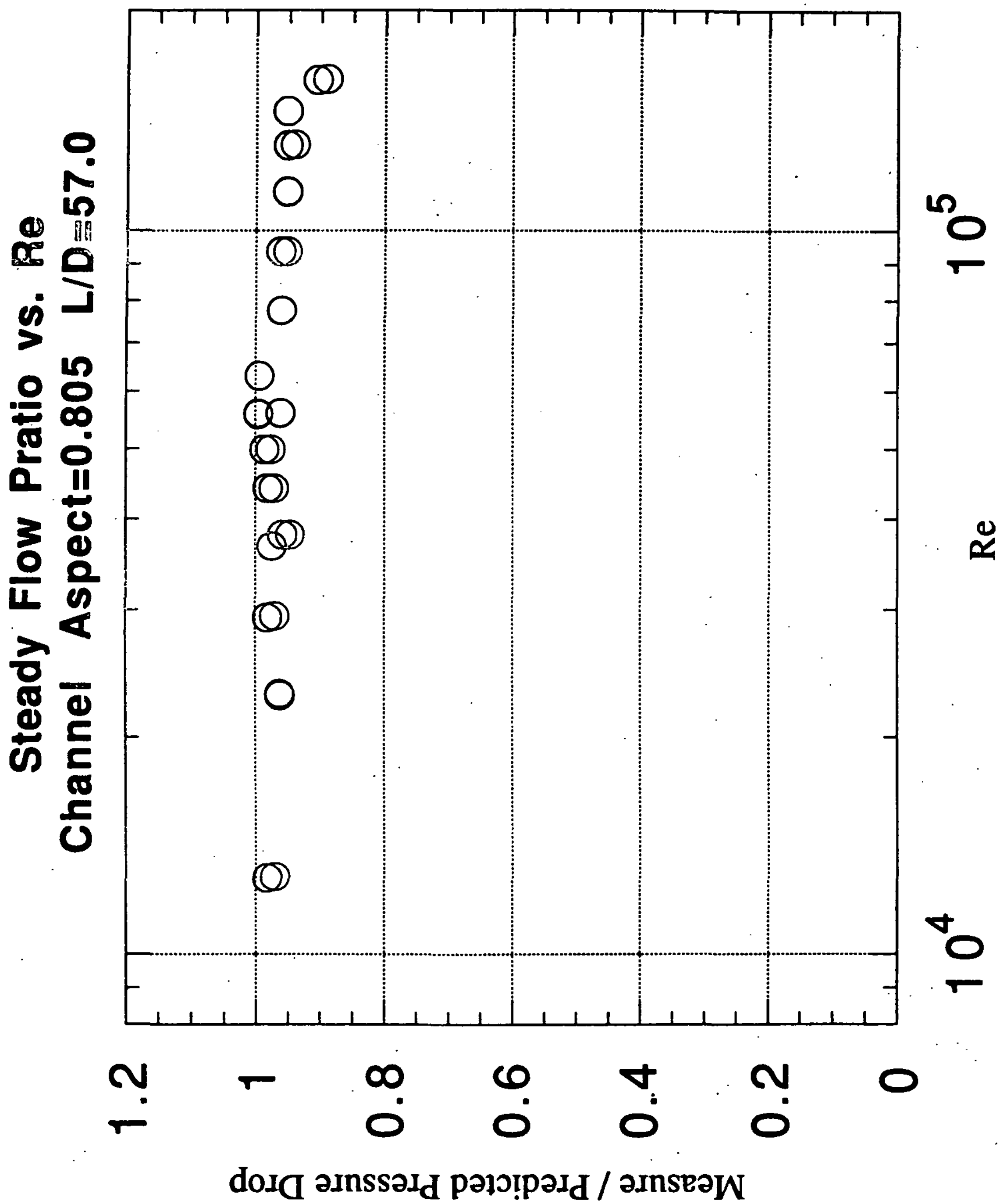
Steady Flow Pratio vs. Re
Channel Aspect=0.805 L/D=57.0
1.2
1
0.8
0.6
0.4
0.2
0
10^4
10^5
Re
Measure / Predicted Pressure Drop

Figure 10

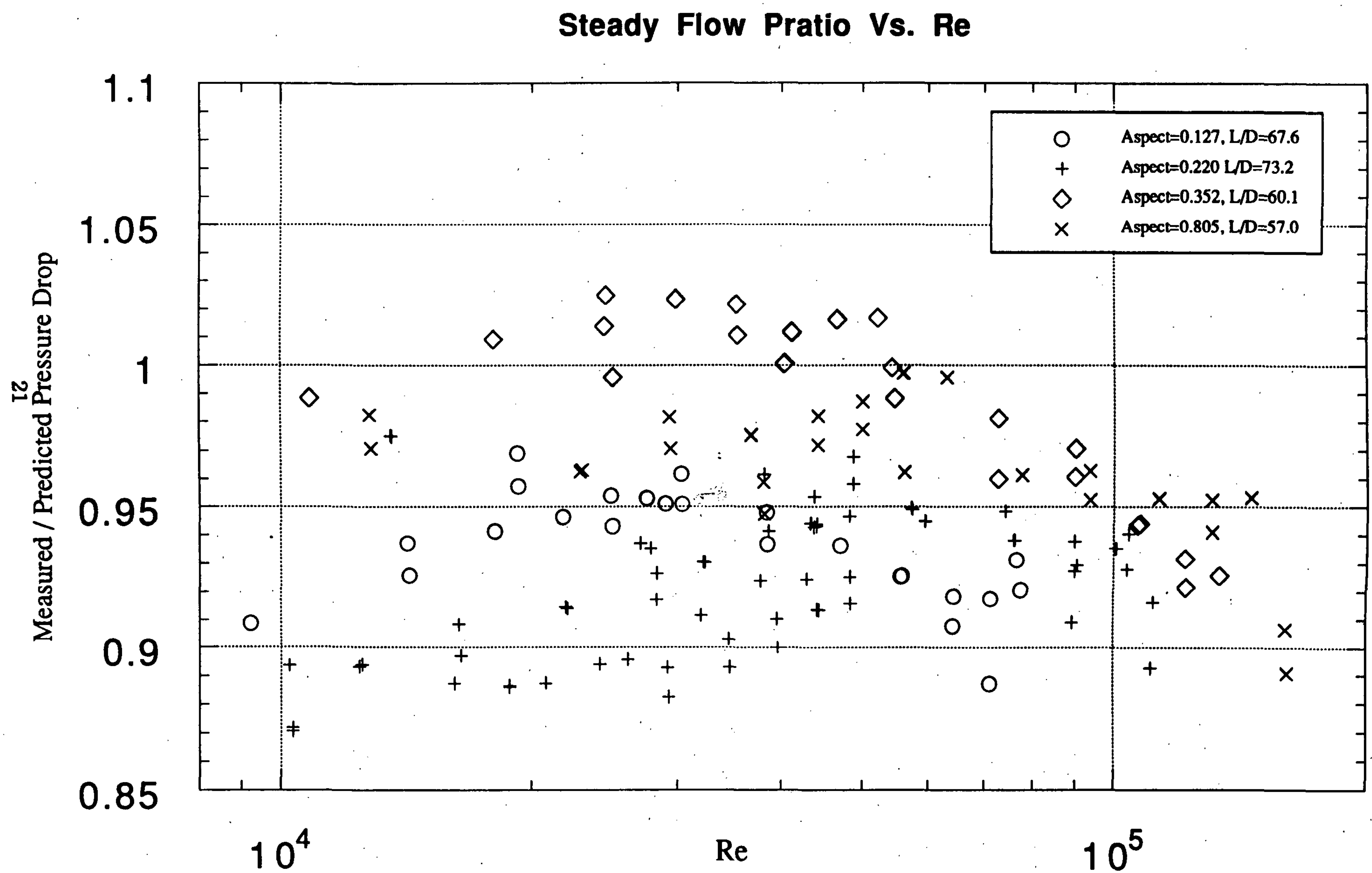
Steady Flow Pratio Vs. Re
1.1
1.05
1
0.95
0.9
0.85
Measured / Predicted Pressure Drop
10^4
Re
10^5
Aspect=0.127, L/D=67.6
Aspect=0.220 L/D=73.2
Aspect=0.352, L/D=60.1
Aspect=0.805, L/D=57.0

Figure 11

DISCUSSION OF STEADY-FLOW TEST RESULTS

Pratio for all the tested samples is close to a value of 1. Considering the samples tested as a group, as in Figure 11, Pratio has an average value of approximately 0.95 and all results fall within ±8 percentage points of this value.

Values for experimental errors in Pratio are given with the tabular data of Appendix A-1. As is shown in this appendix, experimental errors on Pratio increase at the lower Reynolds numbers. At Reynolds numbers above 10^5, the error band on Pratio is always less than ±3 percent, but this error increases with decreasing Re to ±7 to 10 percent near a Reynolds number of 4×10^4.

In studying these results, it was noticed that the Pratio for all samples was falling off at higher Reynolds numbers where the accuracy of the results was supposedly the best. It was concluded that this was an indication of a leak which would allow more gas to bypass the test sample as the pressure drop increased.

In pursuit of this possibility, the steady-flow test rig was examined in the area where the test sample is mounted. Indeed, it was found that the possibility of a leak in this area was very likely. This was the combination of several things all of which led toward an increased probability of a leak.

First, a weld in an adjacent area had been located closer to a seal surface than had been intended. This had melted away some material on the face against which the O ring seal of the sample holder mates. Secondly, the clearance holes for the bolts which mount the sample holder in the rig were considerably oversize, due either to a design or a fabrication error. These oversize clearance holes allowed considerable lateral play in the positioning of the holder and made it likely that the seal holder could not consistently be mounted to ensure a good seal.

In light of the considerations discussed above and the previous discussions on the passage geometry effects, the test results appear fairly good. The steady-flow testing was neither intended nor used to obtain pressure-drop correlations. The purpose of this testing was to provide a comparison of measured pressure drop to that predicted by accepted correlations. These accepted correlations were then used to calculate the Total Dissipation Factor for the oscillating-flow test results.

OSCILLATING-FLOW TEST RESULTS

Oscillating-flow tests were performed on seven full length (120 mm) samples. Aspect ratios for these full length samples were 0.127, 0.147, 0.220, 0.352, 0.456, 0.667 and 0.805. Three short (10 mm long) samples were tested: two square-edged entrance and exit samples of aspect ratios 0.127 and 0.442, and a round-edged entrance and exit sample of aspect ratio 0.442 . Tabular results for this oscillating-flow testing are contained in Appendix A-2.

Figures 12 through 32 present test results for the full length samples as follows:

Figures 12 through 18—TDF vs Ar and Re_ω
Figures 19 through 25—TDF vs Re_{max} and Re_ω
Figures 26 through 32—Eu vs Ar and Re_ω

Figures 33 through 35 present the short sample test results as follows:

Figure 33—Eu vs Re_{max} and Re_ω for Aspect Ratio = 0.127, square edged (L/D=5.63)
Figure 34—Eu vs Re_{max} and Re_ω for Aspect Ratio = 0.442, square edged (L/D=5.15)
Figure 35—Eu vs Re_{max} and Re_ω for Aspect Ratio = 0.442, round edged (L/D=5.15)

Where:

TDF = Total Dissipation Factor = $$\frac{2\int \Delta P u}{\int\left(\left(f\frac{L}{D}+K\right)g\,|u|\right)u}$$

The ratio of measured dissipated power to that calculated using steady-flow correlations applied to the instantaneous mass flow rate and integrating over the cycle

Ar = Amplitude Ratio, The ratio of the distance a theoretical gas particle sweeps divided by the tube length = 2 x flow distance amplitude/L

Re_ω = Kinetic Reynolds (or Valensi) Number = $\omega D^2 \rho / (4\mu)$

Re_{max} = Maximum Instantaneous Reynolds Number

Eu = Euler Number = $2\,\Delta P max / \rho\, u_{max}^2$

g = ρu = Mass flow rate per unit area

u = Velocity

ω = Circular Frequency

Note that Re_ω, Re_{max} and Ar are not all independent for a sample of fixed length.

$Re_\omega = \omega D^2 \rho / (4\mu)$

$Re_{max} = u_{max} D \rho / \mu$

$Ar = 2 X_{max} / L = D\, Re_{max} / (2 L\, Re_\omega)$

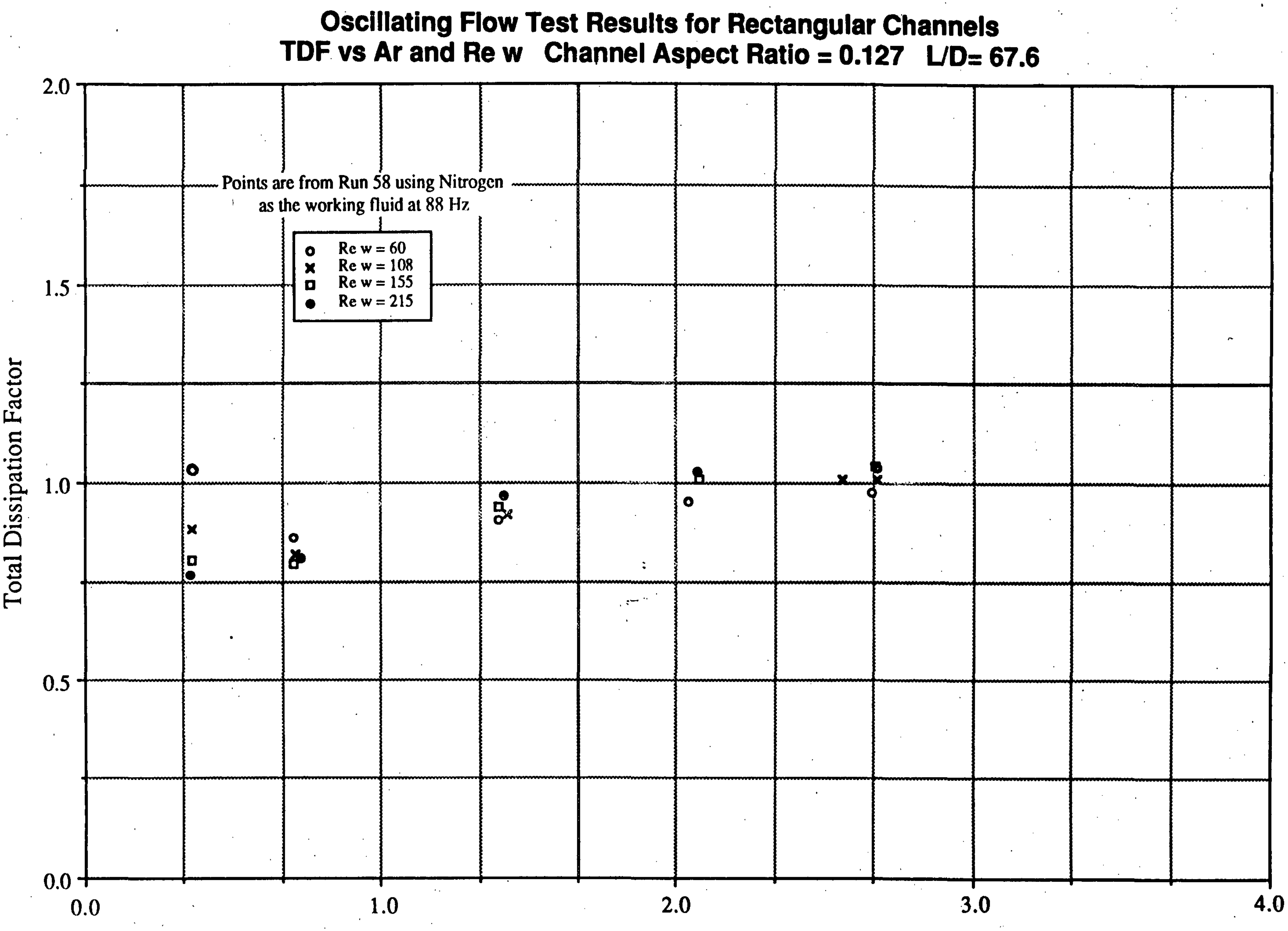
Oscillating Flow Test Results for Rectangular Channels
TDF vs Ar and Re w   Channel Aspect Ratio = 0.127   L/D= 67.6
Points are from Run 58 using Nitrogen
as the working fluid at 88 Hz
Re w = 60
Re w = 108
Re w = 155
Re w = 215
Total Dissipation Factor
2.0
1.5
1.0
0.5
0.0
0.0
1.0
2.0
3.0
4.0
Ar
Figure 12

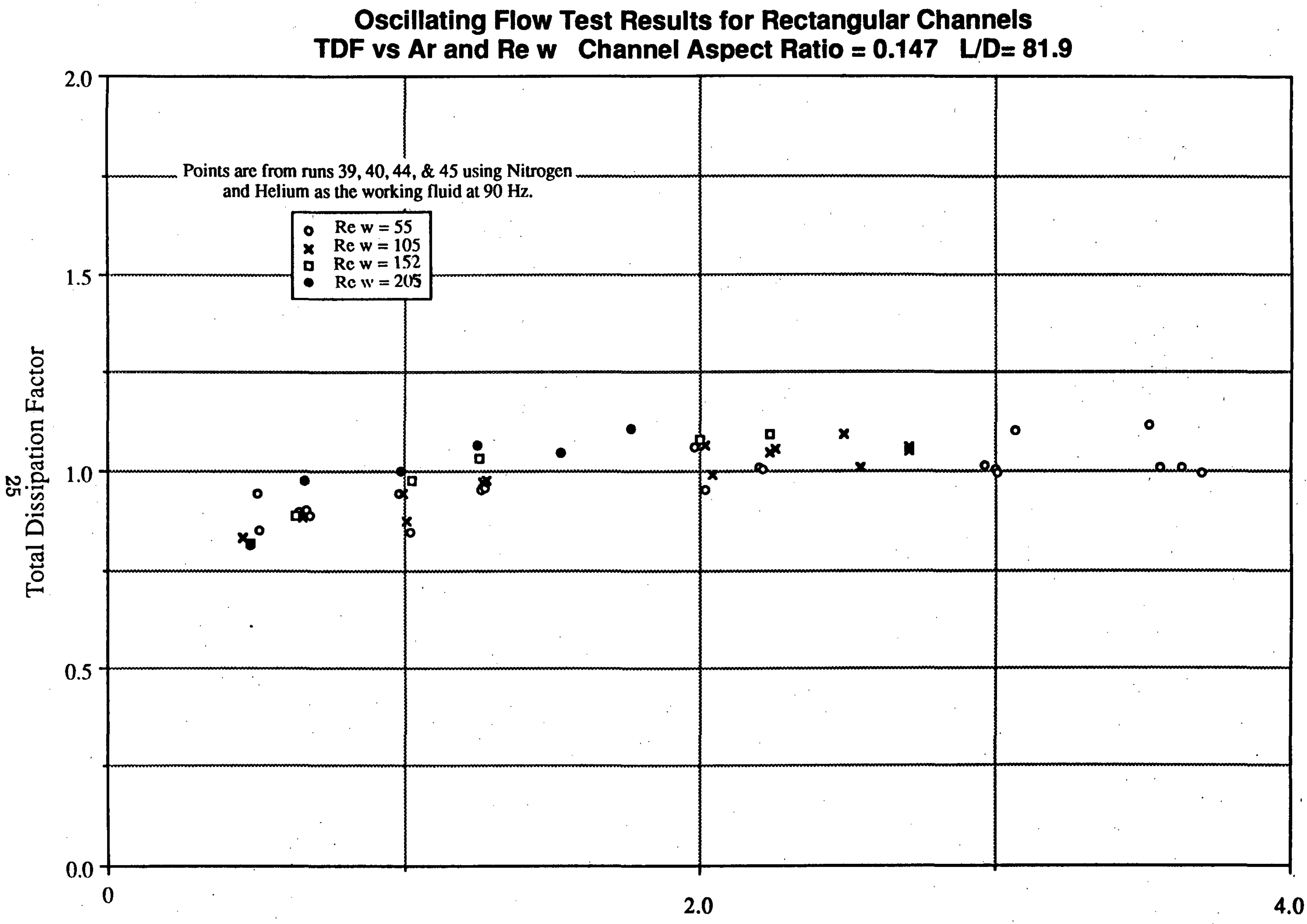
Oscillating Flow Test Results for Rectangular Channels
TDF vs Ar and Re w Channel Aspect Ratio = 0.147 L/D= 81.9
Points are from runs 39, 40, 44, & 45 using Nitrogen and Helium as the working fluid at 90 Hz.
Re w = 55
Re w = 105
Re w = 152
Re w = 205
Total Dissipation Factor
2.0
1.5
1.0
0.5
0.0
0
2.0
4.0
Ar

Figure 13

Oscillating Flow Test Results for Rectangular Channels
TDF vs Ar and Re w   Channel Aspect Ratio = 0.220   L/D= 73.2

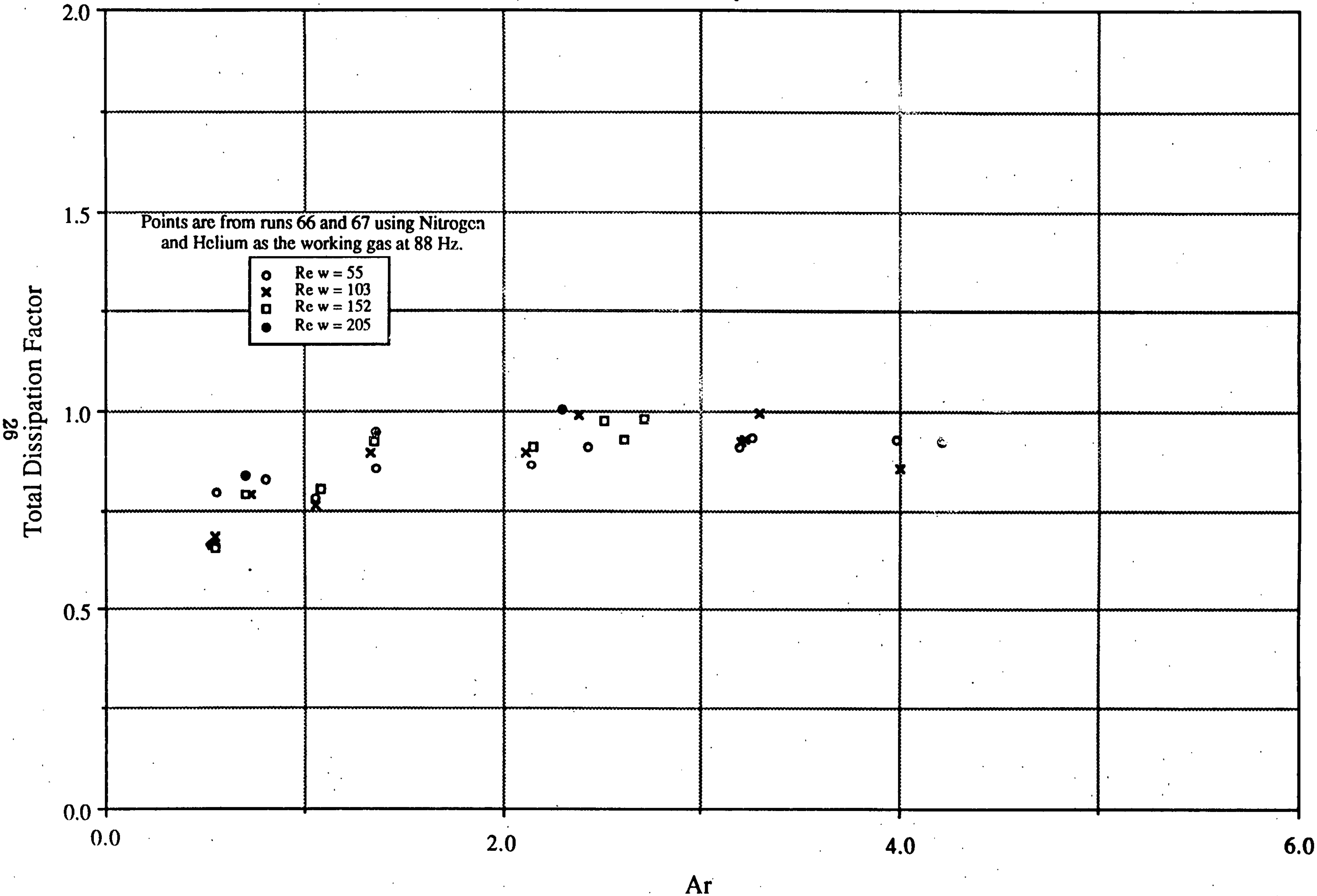

Figure 14

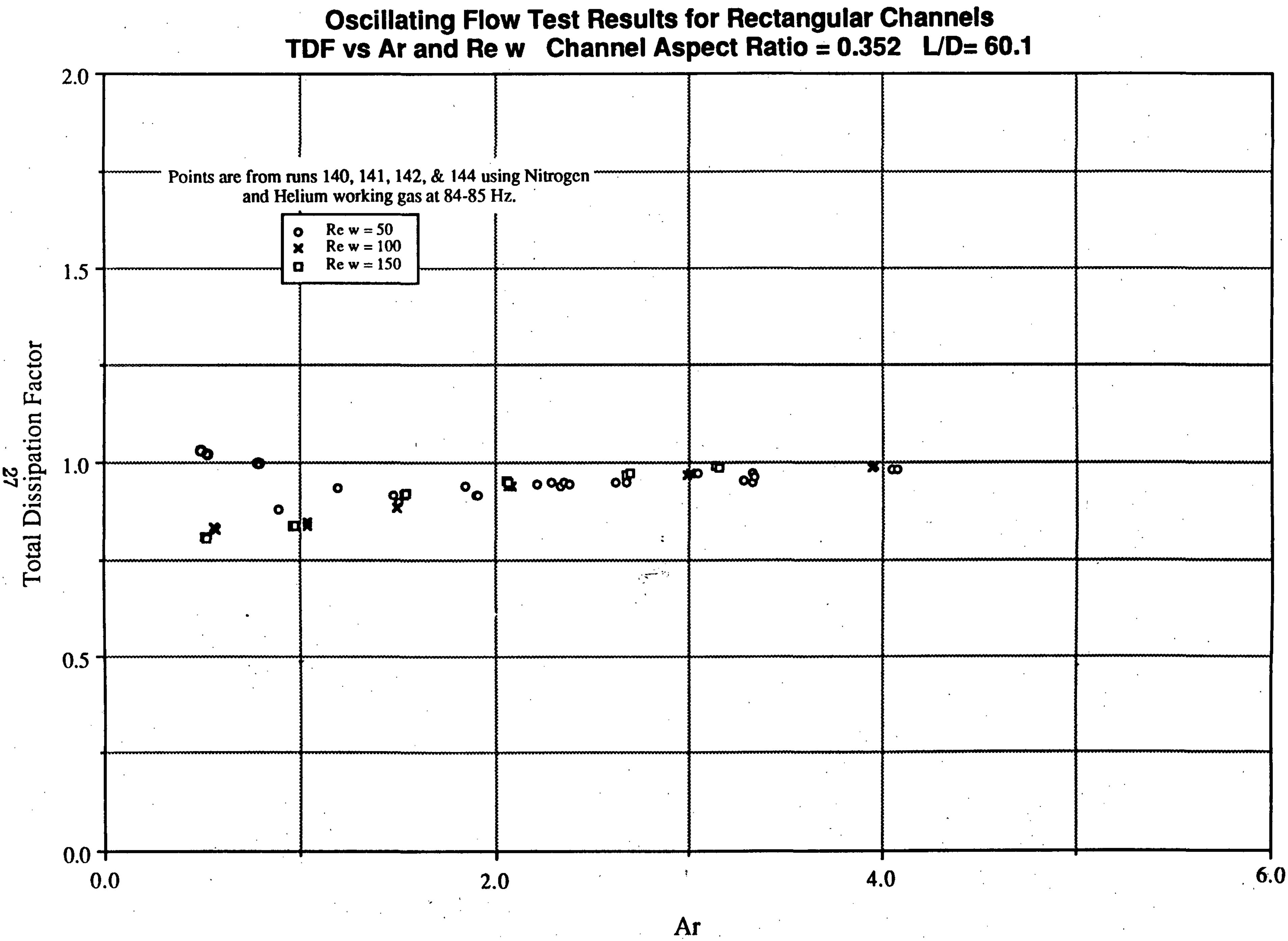

Oscillating Flow Test Results for Rectangular Channels
TDF vs Ar and Re w   Channel Aspect Ratio = 0.352   L/D= 60.1
Points are from runs 140, 141, 142, & 144 using Nitrogen and Helium working gas at 84-85 Hz.
Re w = 50
Re w = 100
Re w = 150
2.0
1.5
1.0
0.5
0.0
Total Dissipation Factor
0.0
2.0
4.0
6.0
Ar

Figure 15

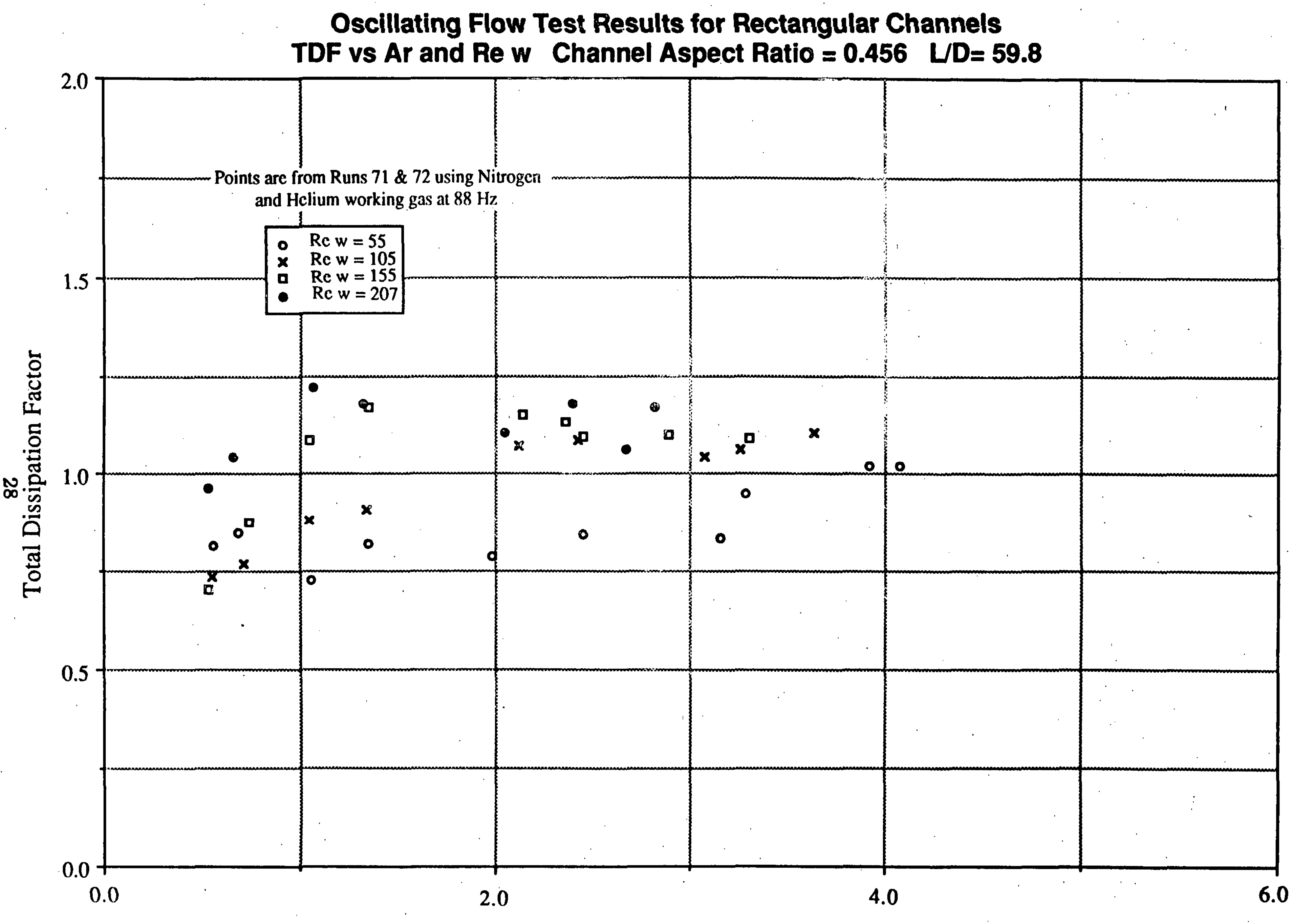
Oscillating Flow Test Results for Rectangular Channels
TDF vs Ar and Re w Channel Aspect Ratio = 0.456 L/D= 59.8
Points are from Runs 71 & 72 using Nitrogen
and Helium working gas at 88 Hz
Re w = 55
Re w = 105
Re w = 155
Re w = 207
2.0
1.5
1.0
0.5
0.0
0.0
2.0
4.0
6.0
Total Dissipation Factor
Ar

Figure 16

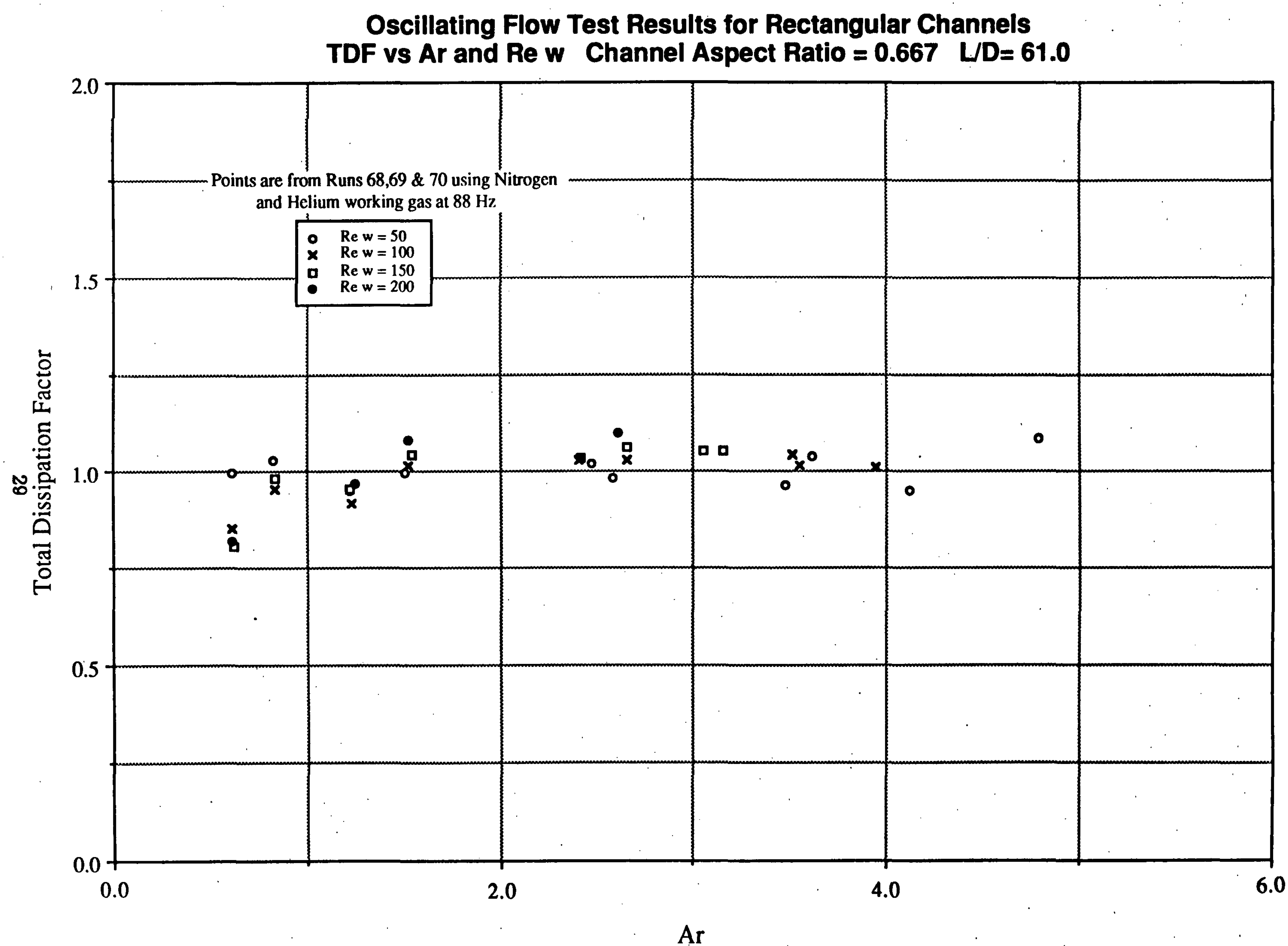
Oscillating Flow Test Results for Rectangular Channels
TDF vs Ar and Re w Channel Aspect Ratio = 0.667 L/D= 61.0
Points are from Runs 68,69 & 70 using Nitrogen and Helium working gas at 88 Hz
Re w = 50
Re w = 100
Re w = 150
Re w = 200
2.0
1.5
1.0
0.5
0.0
Total Dissipation Factor
0.0
2.0
4.0
6.0
Ar

Figure 17

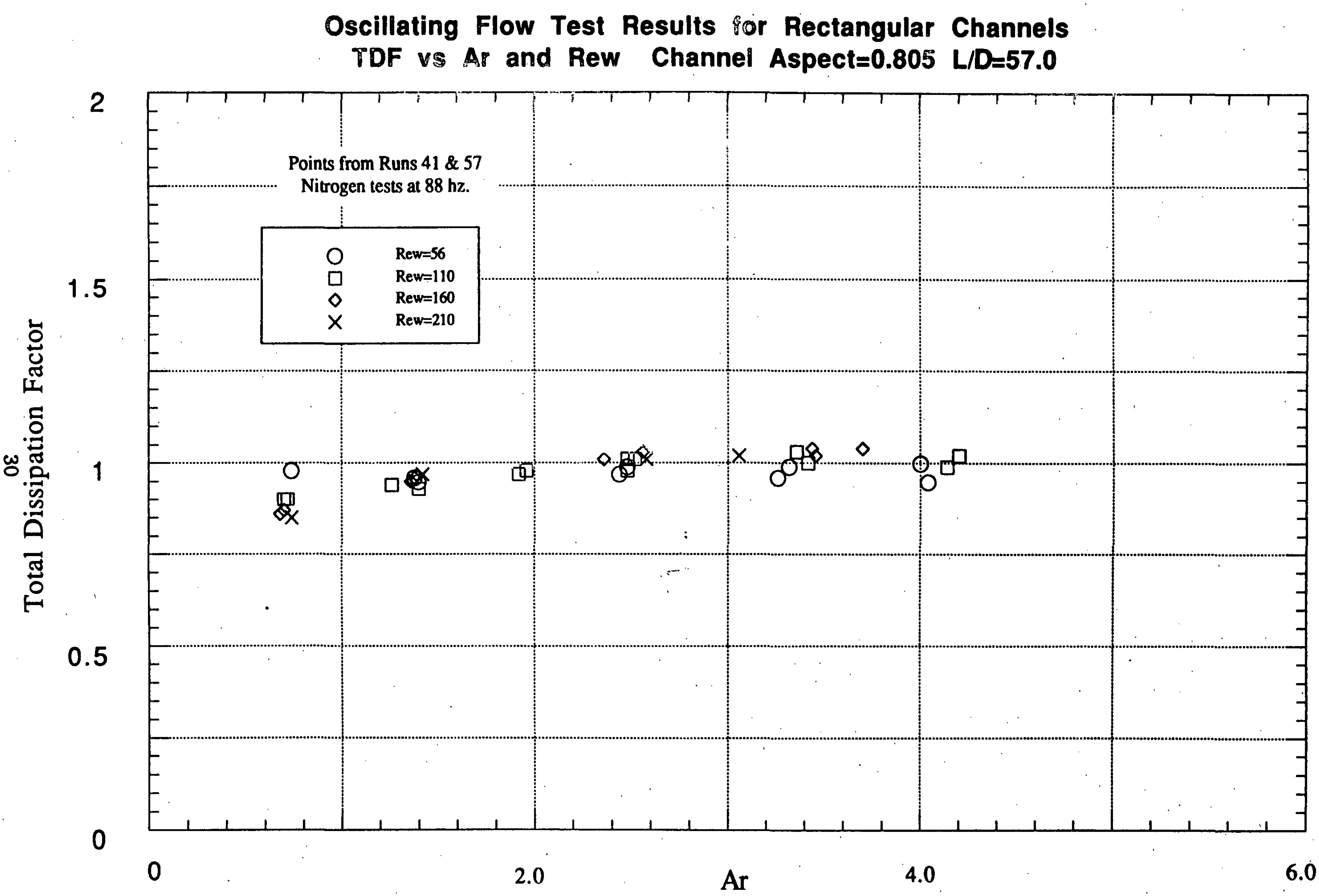
Oscillating Flow Test Results for Rectangular Channels
TDF vs Ar and Rew Channel Aspect=0.805 L/D=57.0
Points from Runs 41 & 57
Nitrogen tests at 88 hz.
Rew=56
Rew=110
Rew=160
Rew=210
2
1.5
1
0.5
0
0
2.0
4.0
6.0
Ar
Total Dissipation Factor
Figure 18

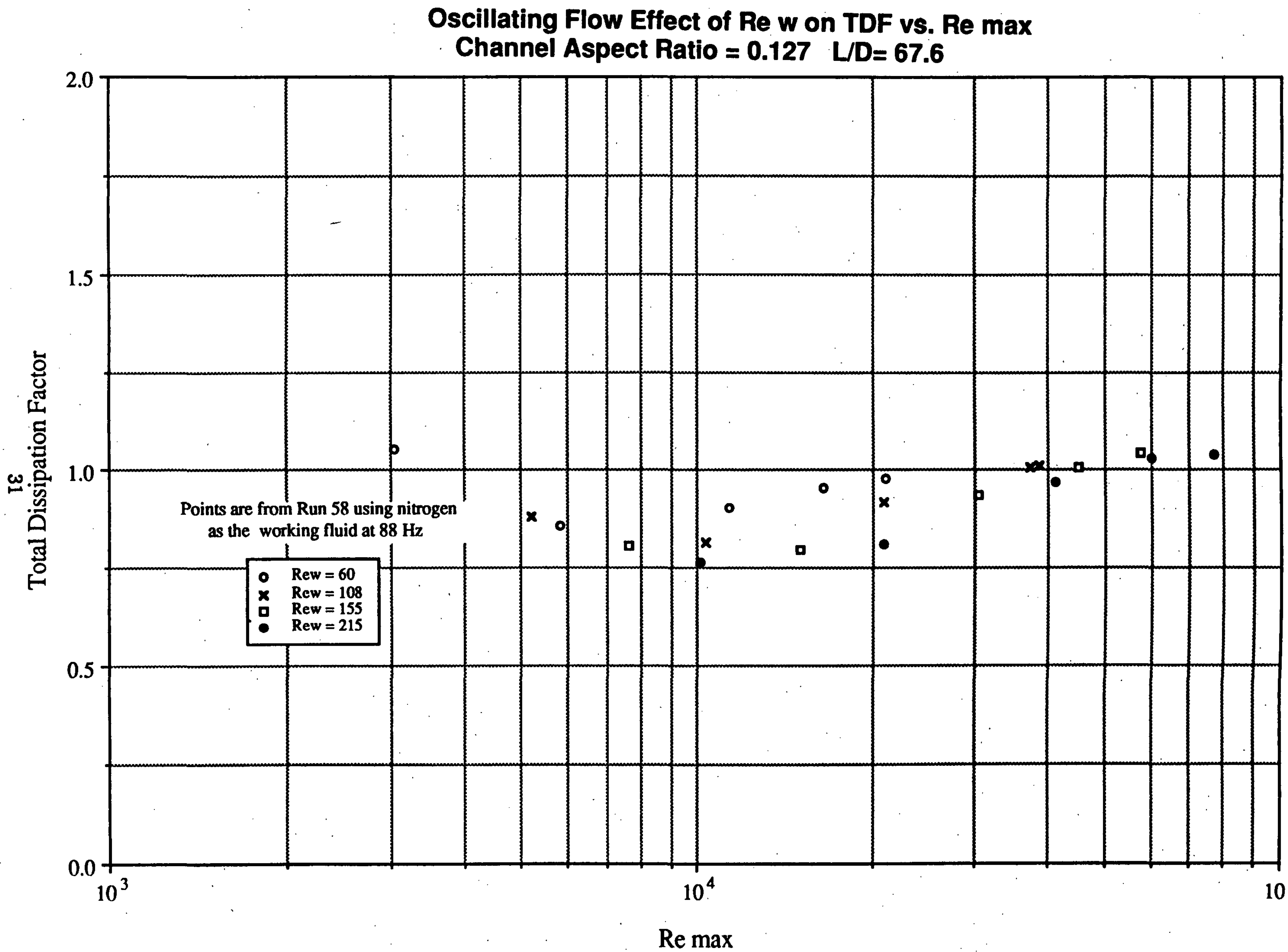

Oscillating Flow Effect of Re w on TDF vs. Re max
Channel Aspect Ratio = 0.127   L/D= 67.6
Total Dissipation Factor
2.0
1.5
1.0
0.5
0.0
Points are from Run 58 using nitrogen
as the working fluid at 88 Hz
Rew = 60
Rew = 108
Rew = 155
Rew = 215
10^3
10^4
10^5
Re max

Figure 19

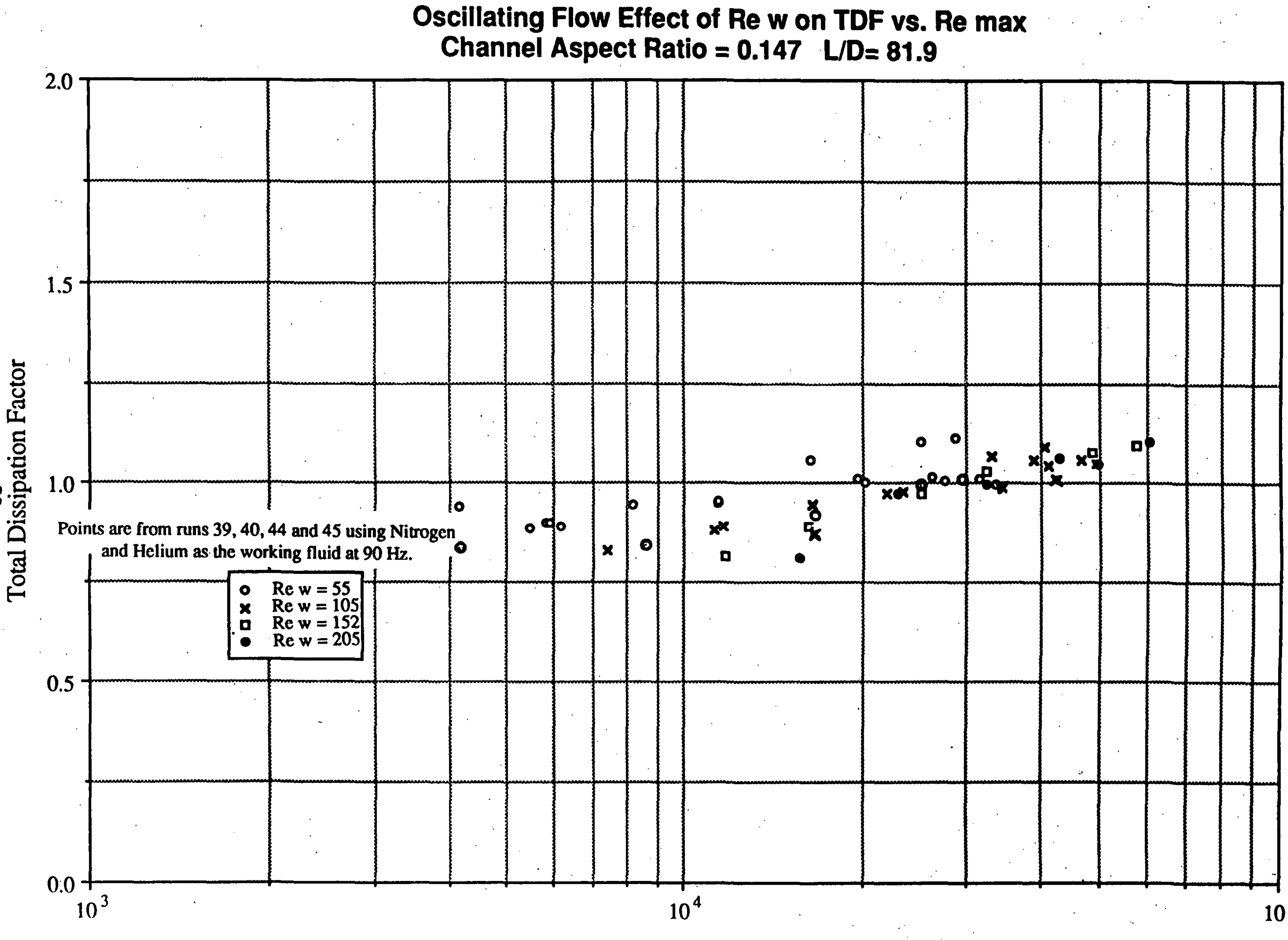

Oscillating Flow Effect of Re w on TDF vs. Re max
Channel Aspect Ratio = 0.147 L/D= 81.9
Total Dissipation Factor
2.0
1.5
1.0
0.5
0.0
Points are from runs 39, 40, 44 and 45 using Nitrogen and Helium as the working fluid at 90 Hz.
Re w = 55
Re w = 105
Re w = 152
Re w = 205
10^3
10^4
10^5
Re max

Figure 20

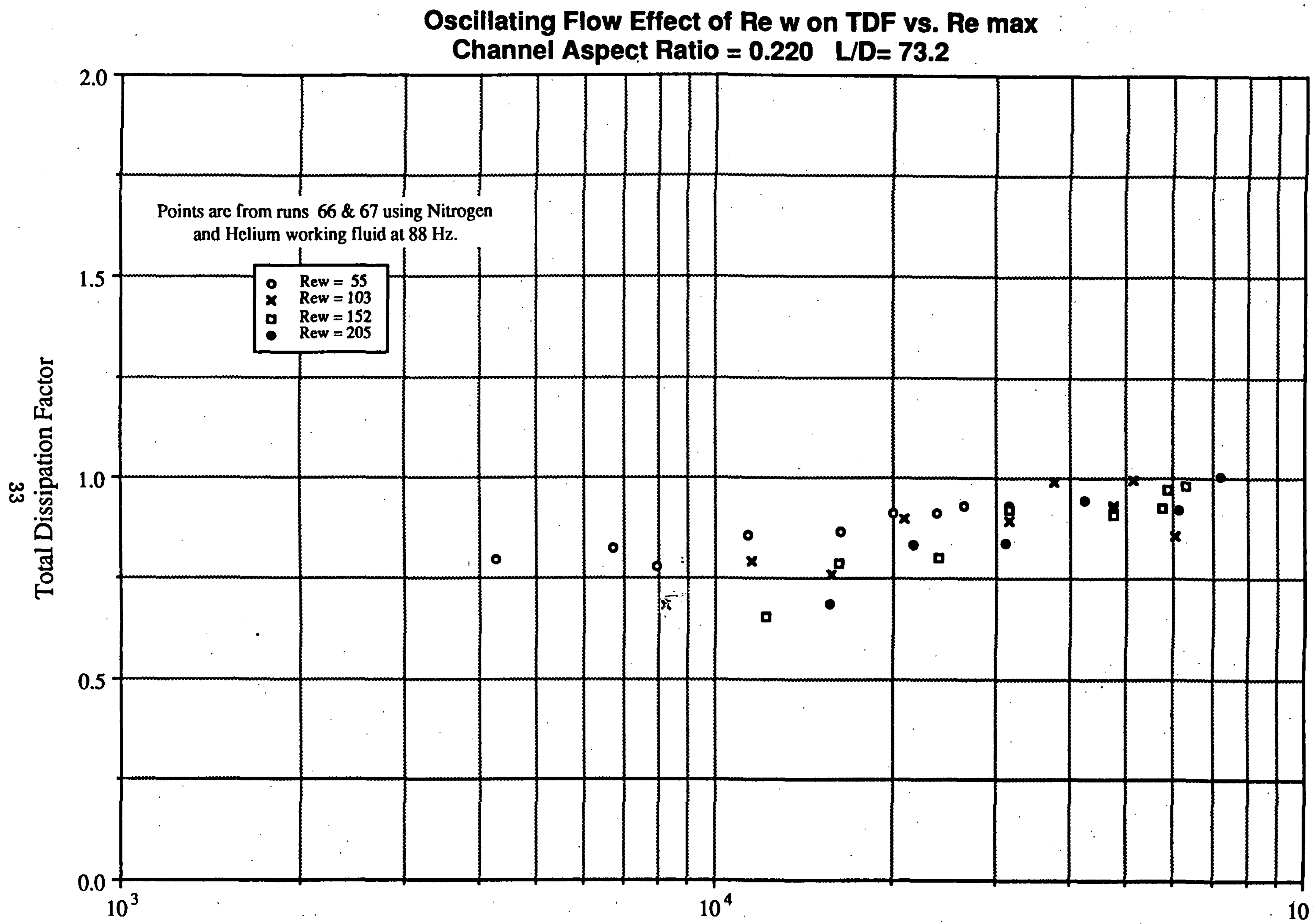

Oscillating Flow Effect of Re w on TDF vs. Re max
Channel Aspect Ratio = 0.220 L/D= 73.2
Points are from runs 66 & 67 using Nitrogen and Helium working fluid at 88 Hz.
Rew = 55
Rew = 103
Rew = 152
Rew = 205
Total Dissipation Factor
Re max
2.0
1.5
1.0
0.5
0.0
10^3
10^4
10^5

Figure 21

Oscillating Flow Effect of Re w on TDF vs. Re max
Channel Aspect Ratio = 0.352   L/D= 60.1

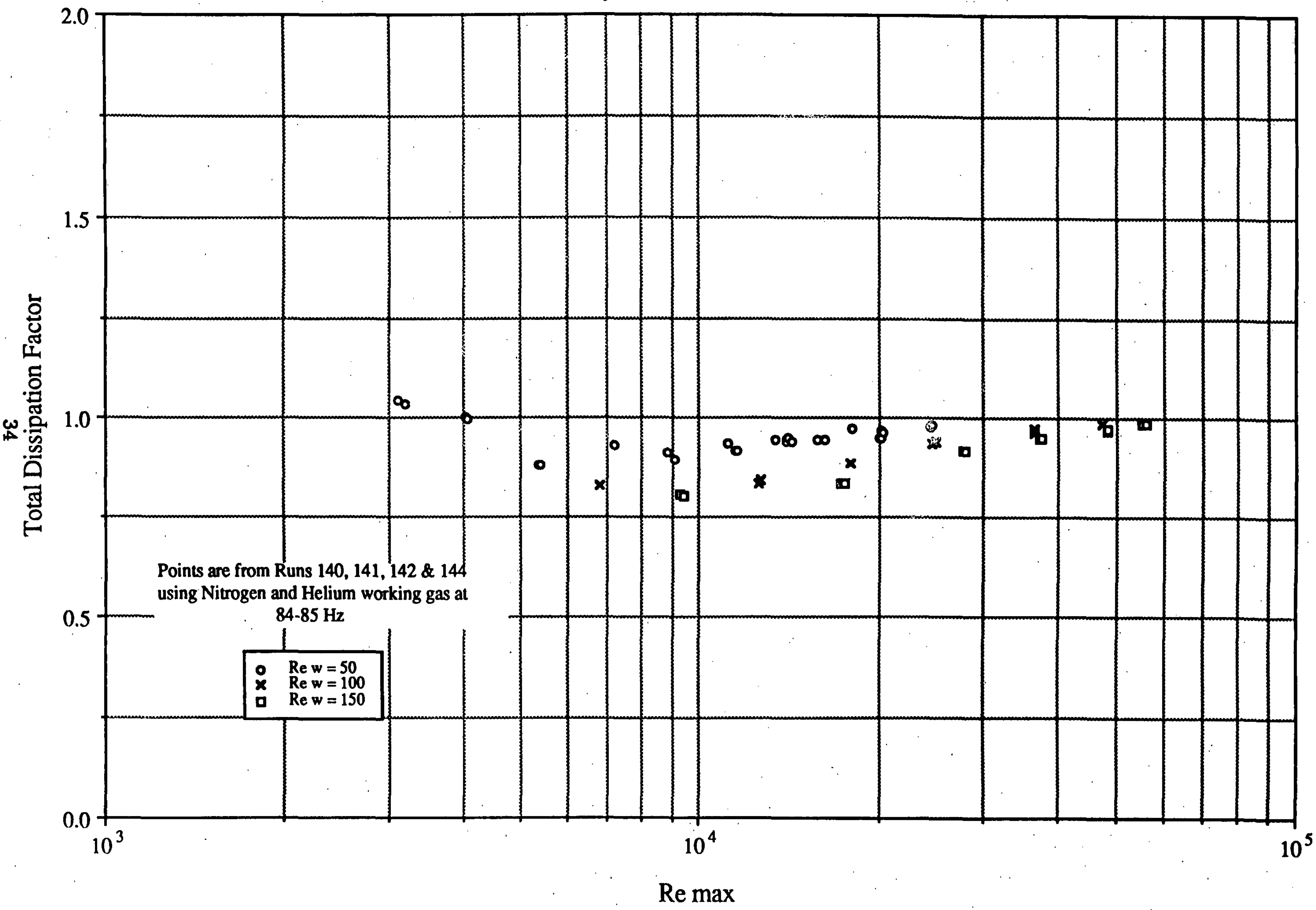

Figure 22

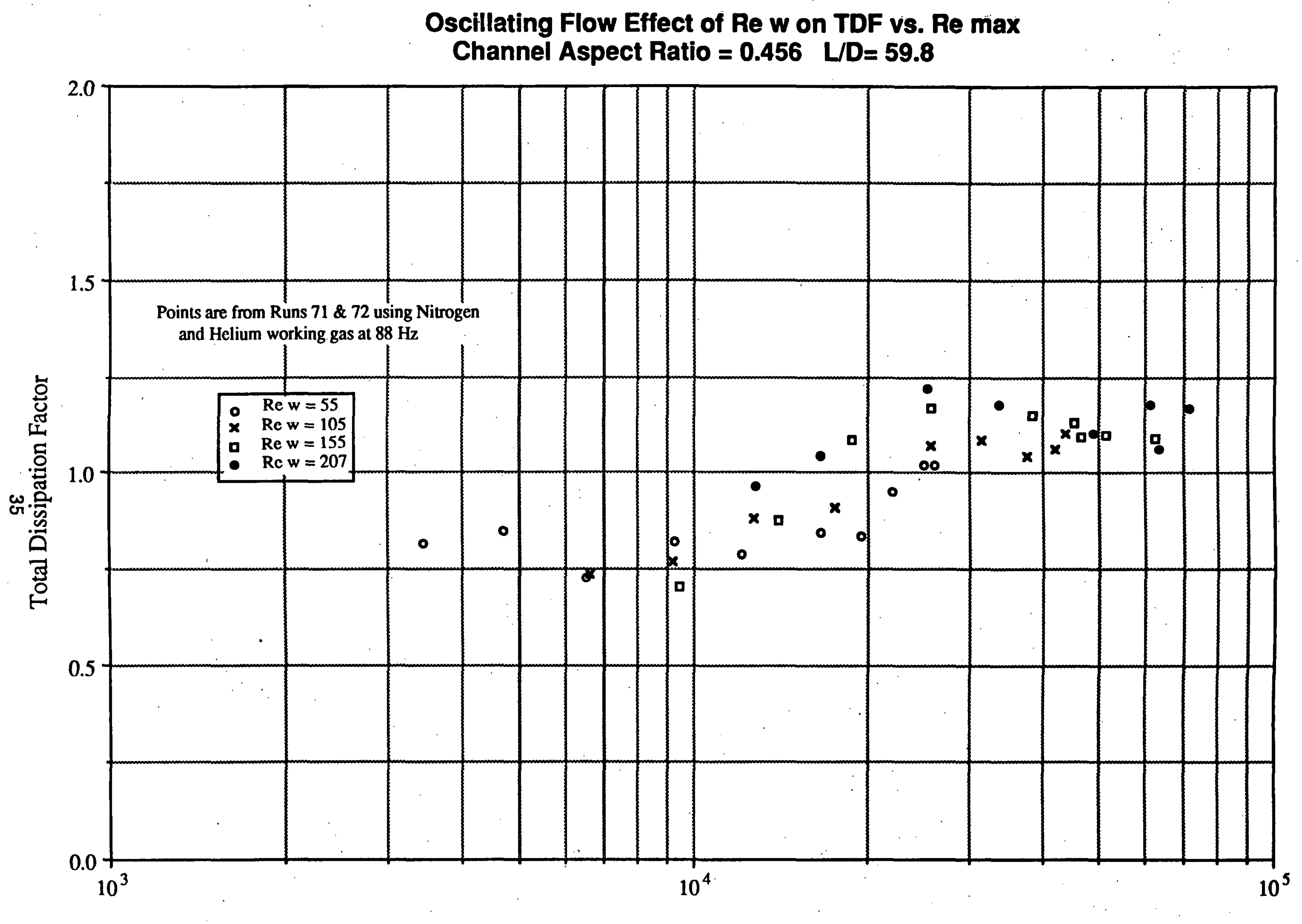

Oscillating Flow Effect of Re w on TDF vs. Re max
Channel Aspect Ratio = 0.456   L/D= 59.8
2.0
1.5
1.0
0.5
0.0
Total Dissipation Factor
Points are from Runs 71 & 72 using Nitrogen
and Helium working gas at 88 Hz
Re w = 55
Re w = 105
Re w = 155
Re w = 207
10^3
10^4
10^5
Re max

Figure 23

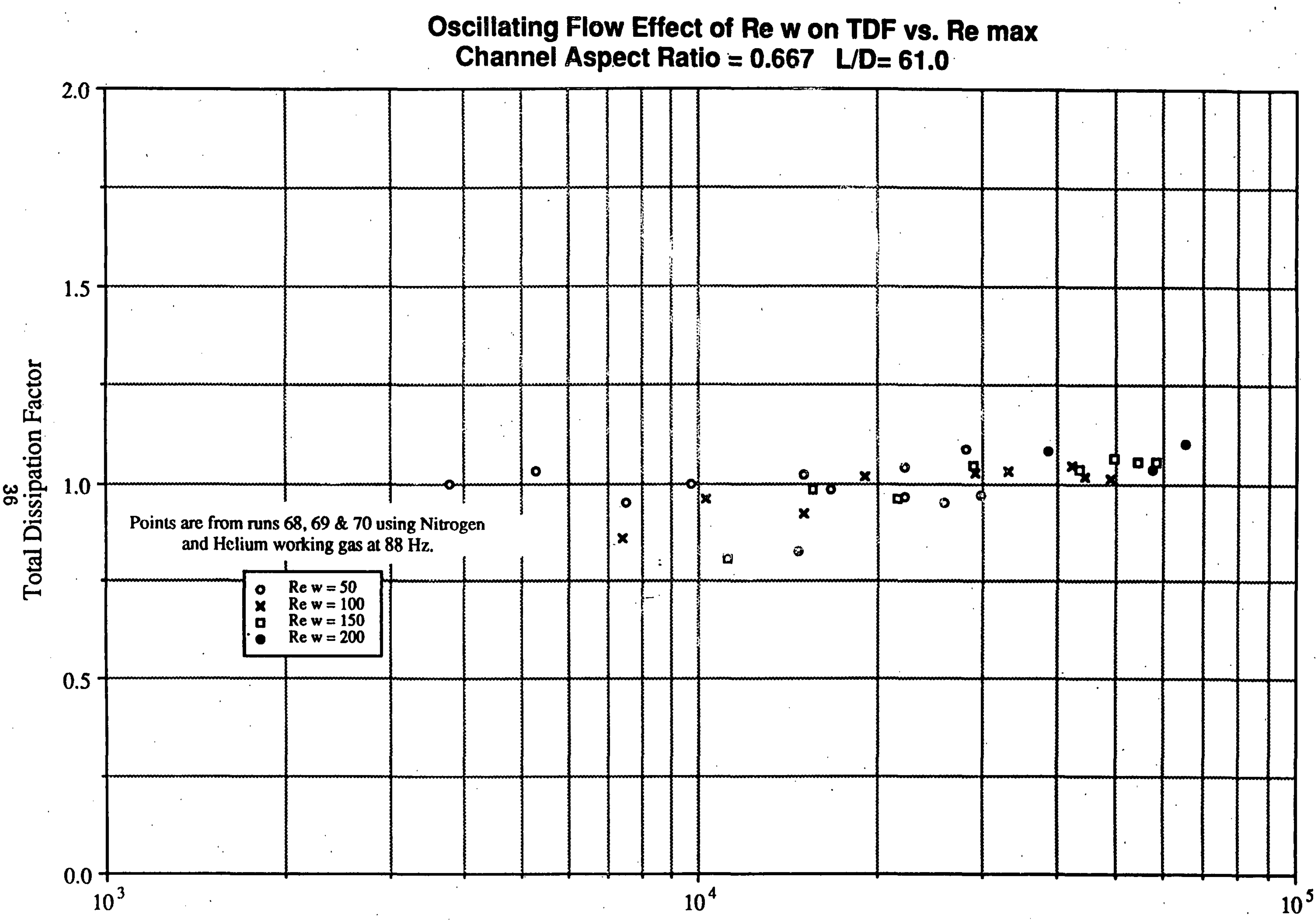
Oscillating Flow Effect of Re w on TDF vs. Re max
Channel Aspect Ratio = 0.667 L/D= 61.0
Total Dissipation Factor
2.0
1.5
1.0
0.5
0.0
Points are from runs 68, 69 & 70 using Nitrogen and Helium working gas at 88 Hz.
Re w = 50
Re w = 100
Re w = 150
Re w = 200
10^3
10^4
10^5
Re max

Figure 24

Oscillating Flow Effect of Re w on TDF vs. Re max
Channel Aspect Ratio = 0.805 L/D= 57.0

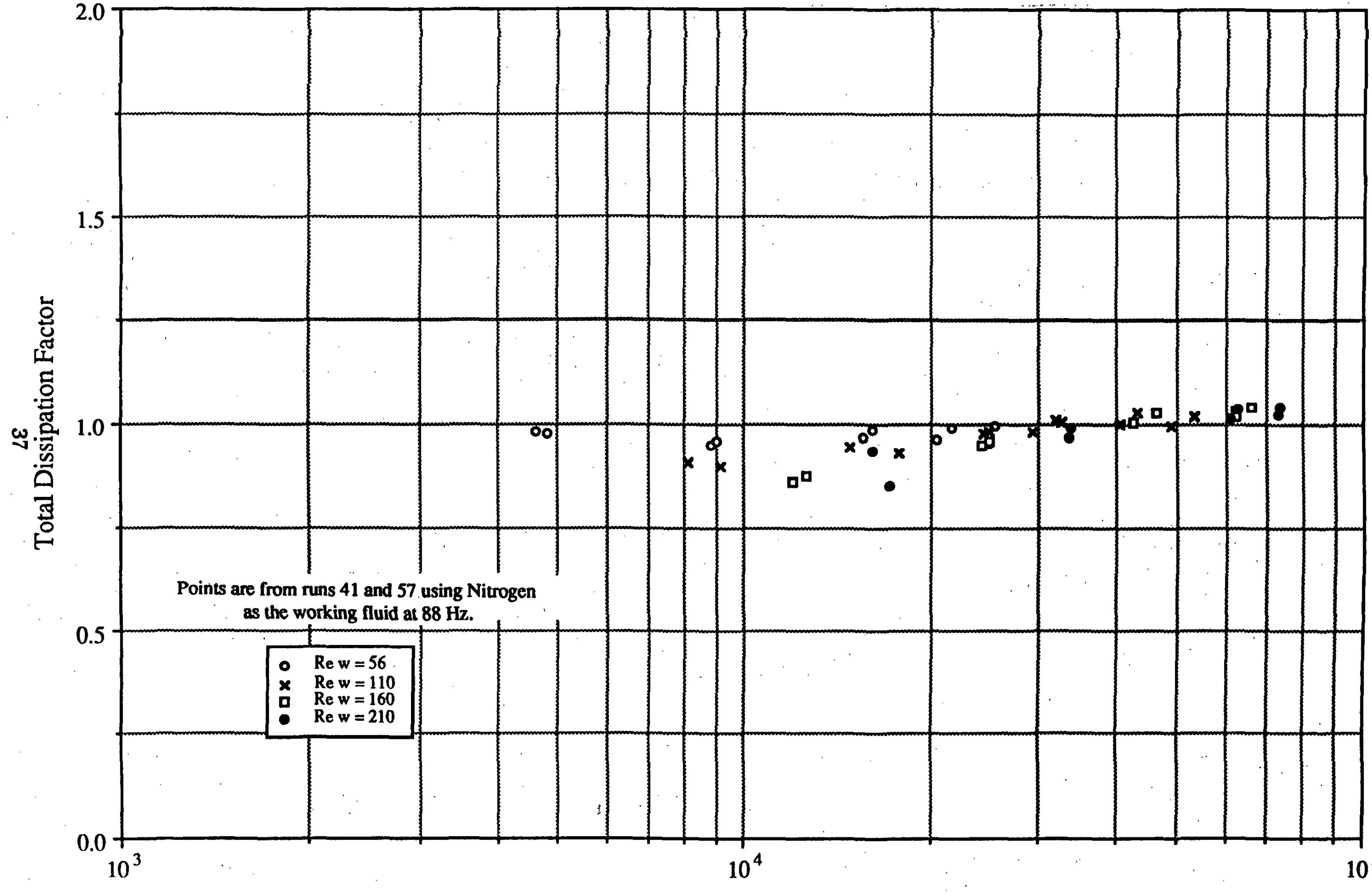

Figure 25

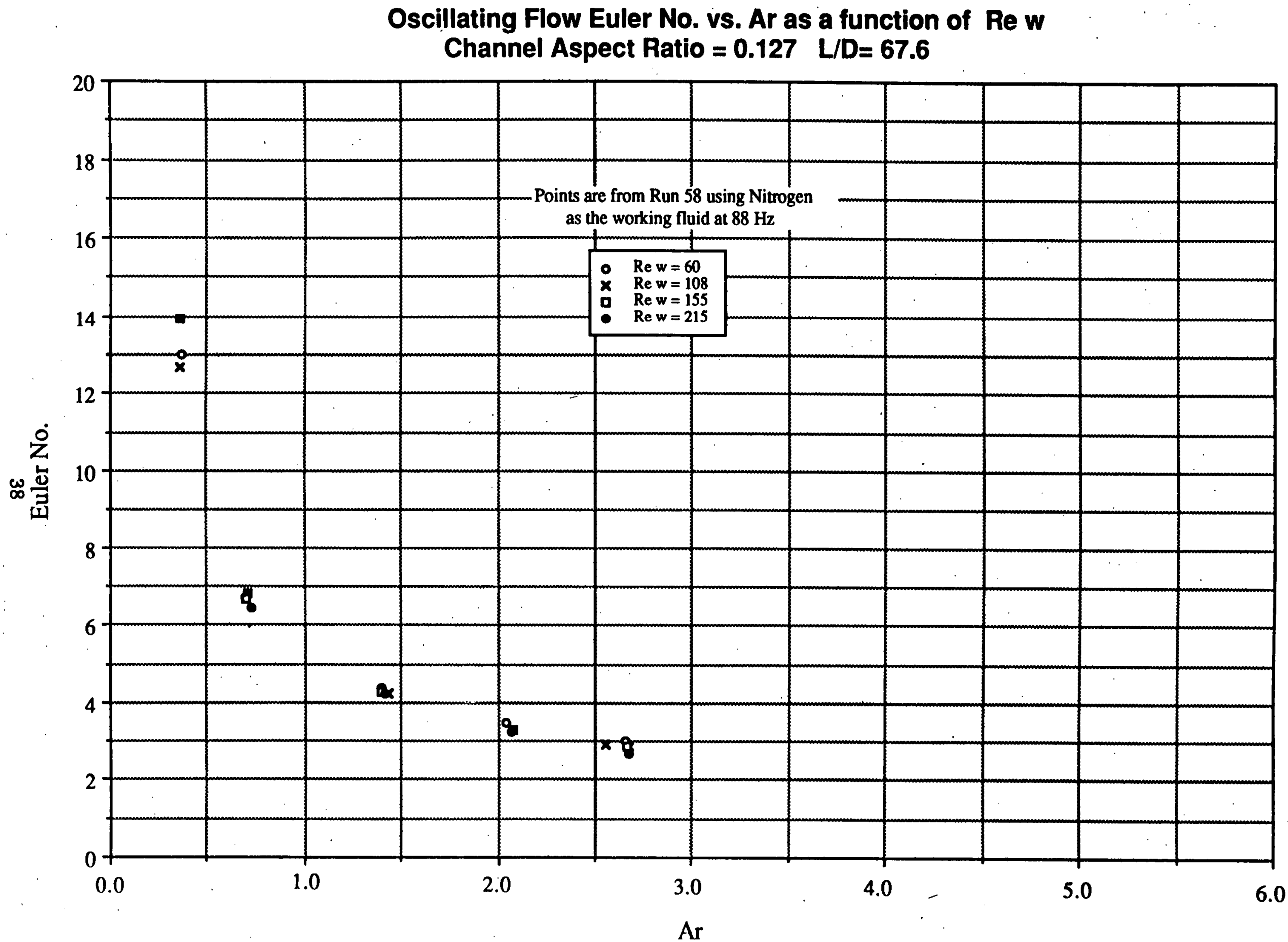
Oscillating Flow Euler No. vs. Ar as a function of Re w
Channel Aspect Ratio = 0.127 L/D= 67.6
Points are from Run 58 using Nitrogen
as the working fluid at 88 Hz
Re w = 60
Re w = 108
Re w = 155
Re w = 215
Euler No.
Ar
0
2
4
6
8
10
12
14
16
18
20
0.0
1.0
2.0
3.0
4.0
5.0
6.0

Figure 26

Oscillating Flow Euler No. vs. Ar as a function of Re w
Channel Aspect Ratio = 0.147 L/D= 81.9

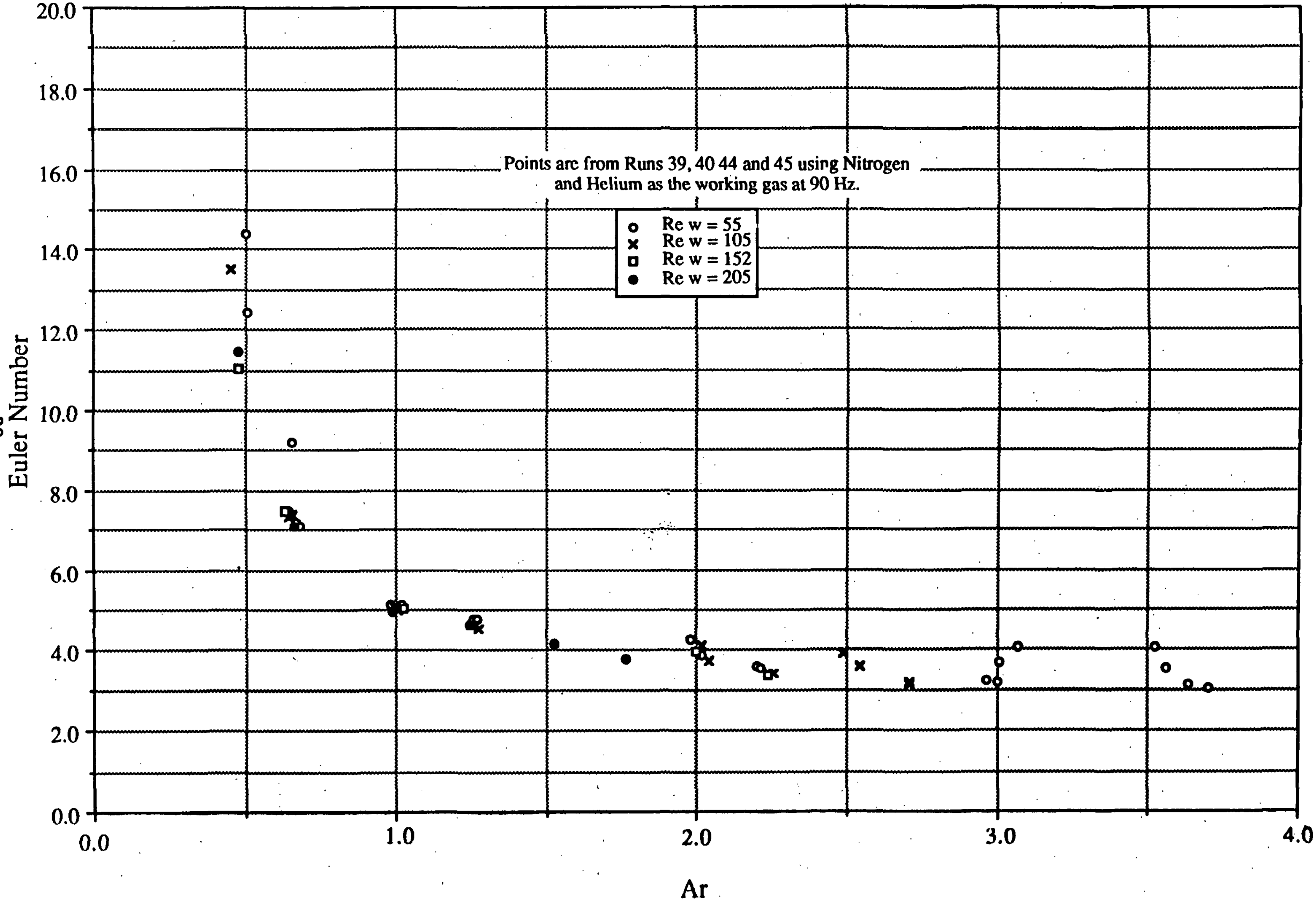

Figure 27

Oscillating Flow Euler No. vs. Ar as a function of Re w
Channel Aspect Ratio = 0.220 L/D= 73.2

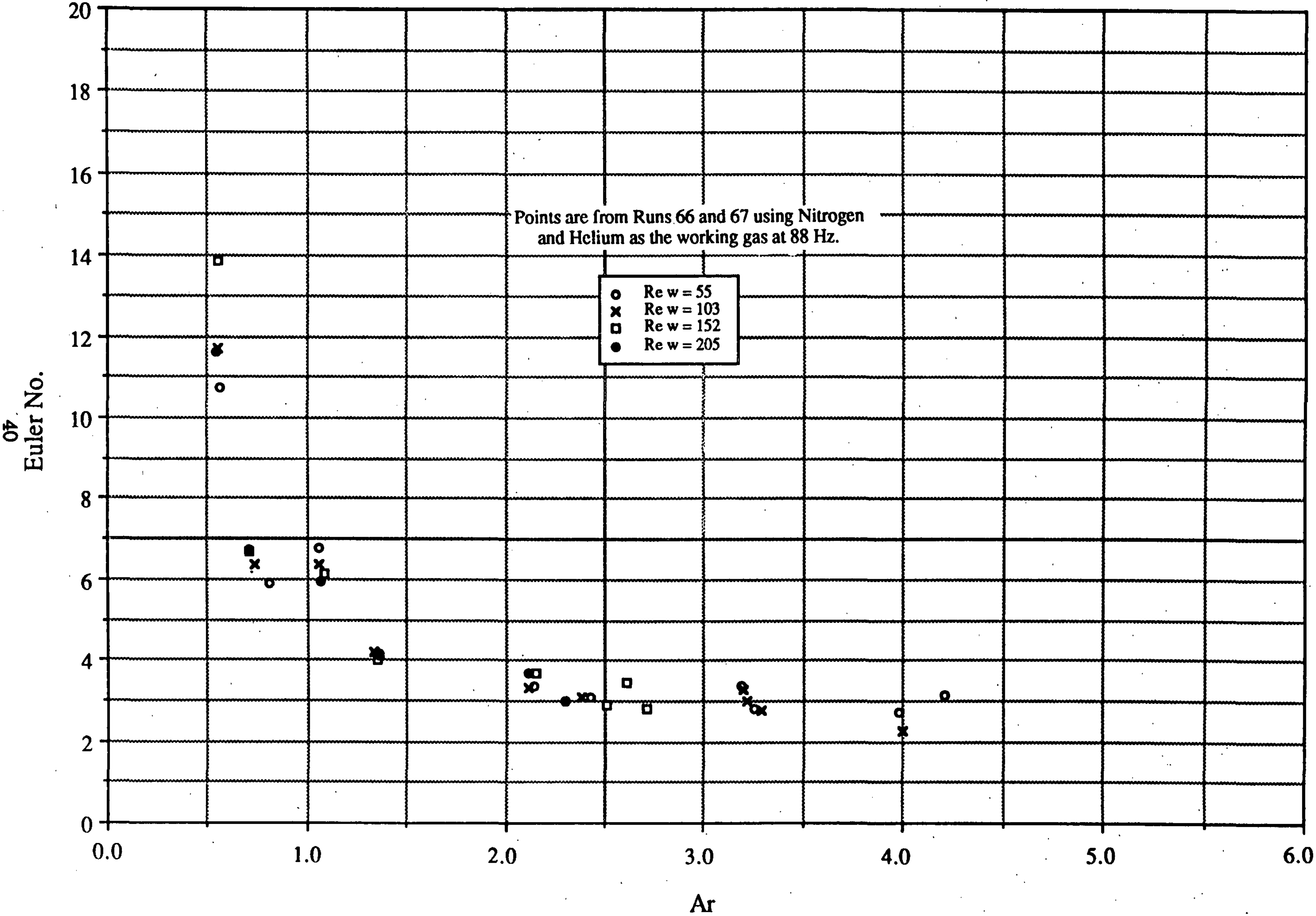

Figure 28

Oscillating Flow Euler No. vs. Ar as a function of Re w
Channel Aspect Ratio = 0.352 L/D= 60.1

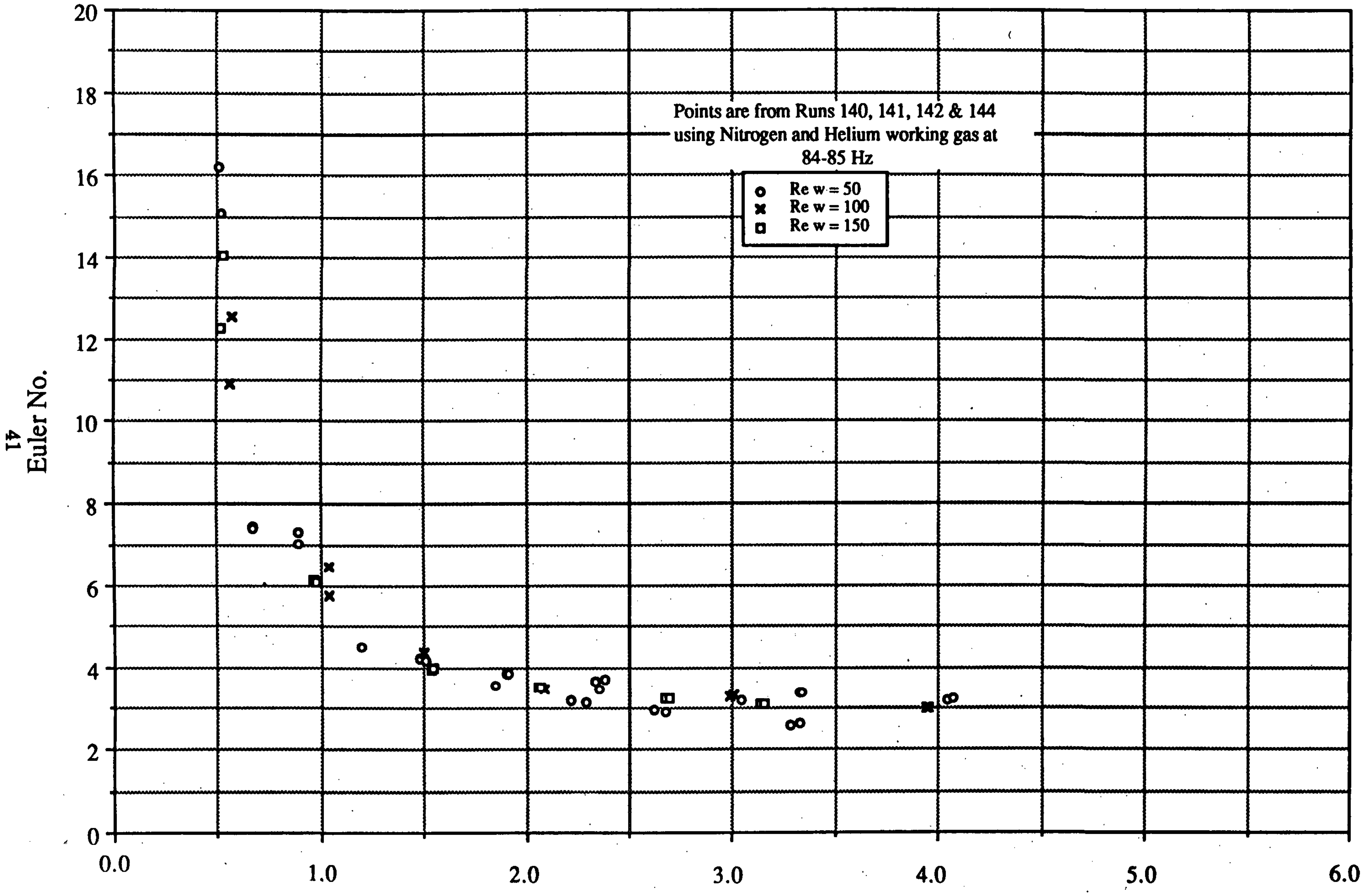

Figure 29

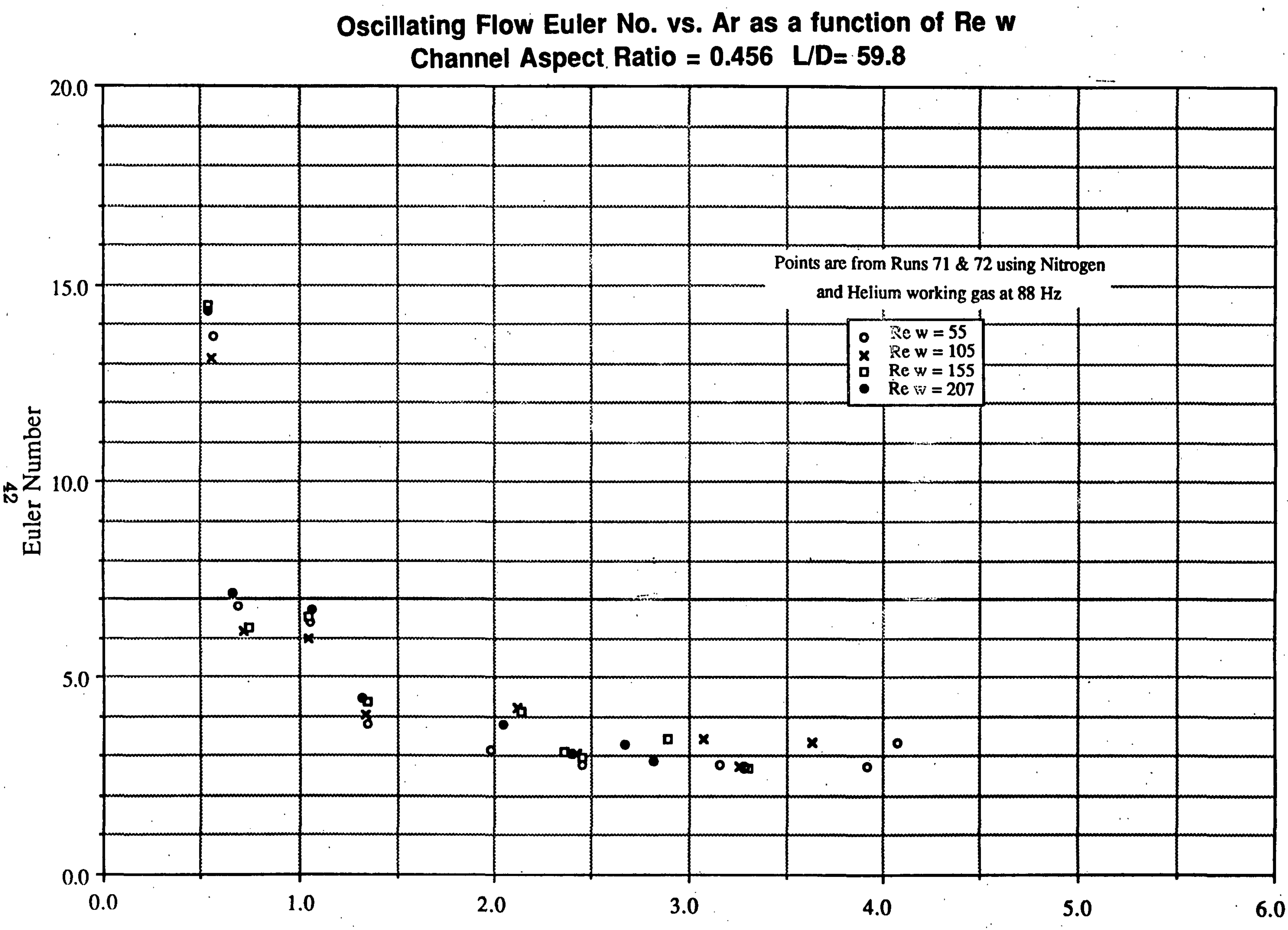
Oscillating Flow Euler No. vs. Ar as a function of Re w
Channel Aspect Ratio = 0.456 L/D= 59.8
Points are from Runs 71 & 72 using Nitrogen
and Helium working gas at 88 Hz
Re w = 55
Re w = 105
Re w = 155
Re w = 207
20.0
15.0
10.0
5.0
0.0
Euler Number
0.0
1.0
2.0
3.0
4.0
5.0
6.0
Ar

Figure 30

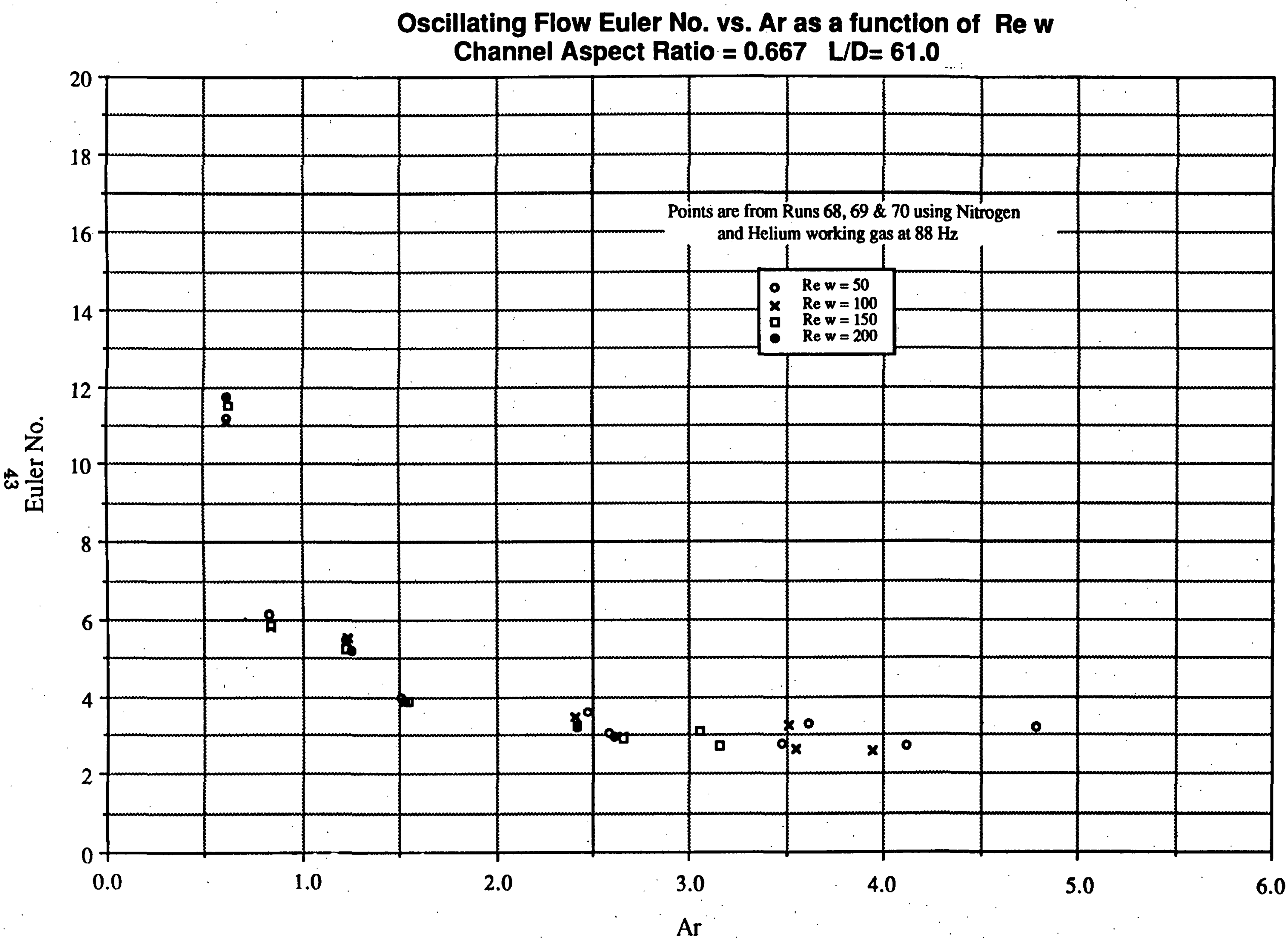
Oscillating Flow Euler No. vs. Ar as a function of Re w
Channel Aspect Ratio = 0.667 L/D= 61.0
Points are from Runs 68, 69 & 70 using Nitrogen
and Helium working gas at 88 Hz
Re w = 50
Re w = 100
Re w = 150
Re w = 200
Euler No.
Ar
0.0
1.0
2.0
3.0
4.0
5.0
6.0
0
2
4
6
8
10
12
14
16
18
20

Figure 31

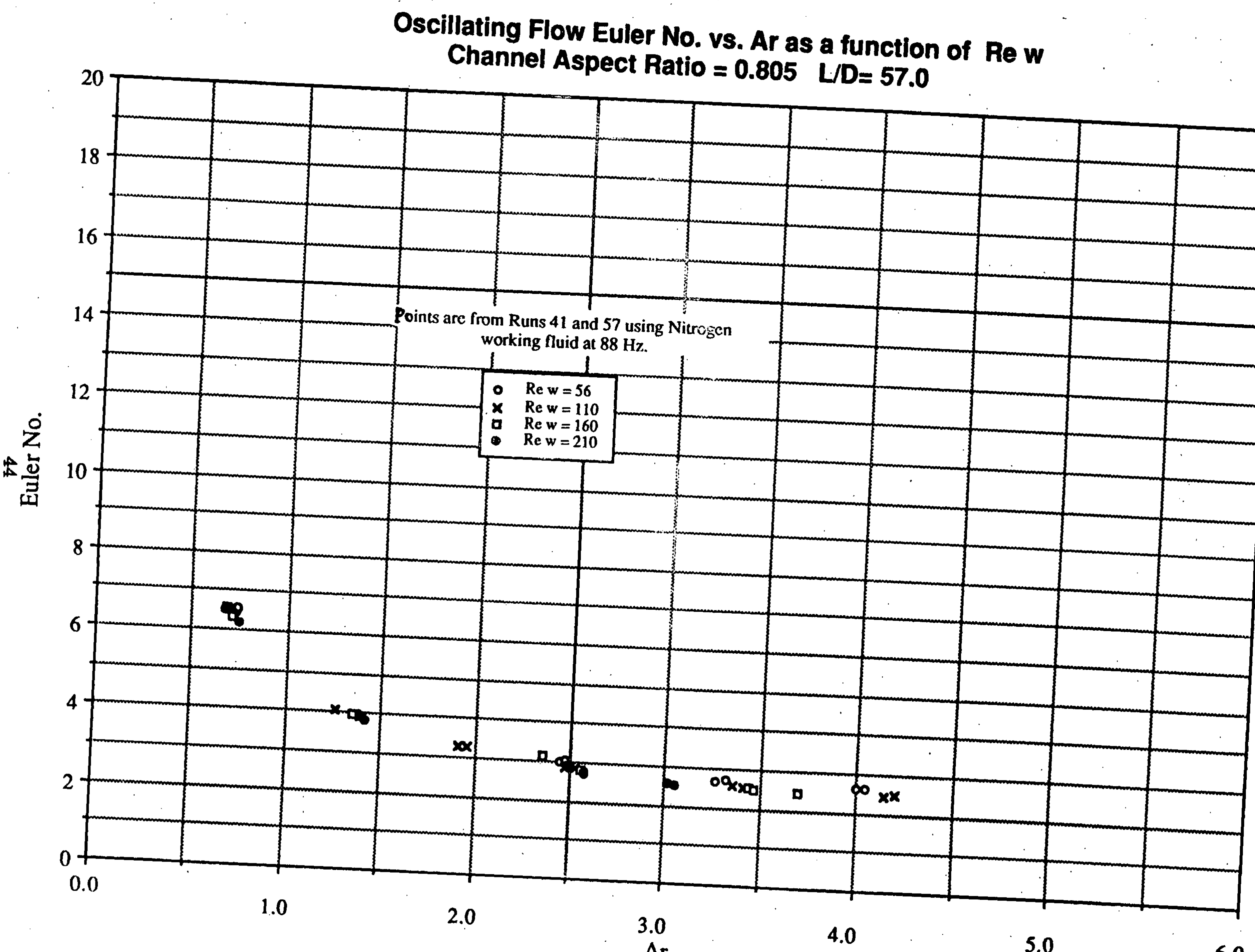
Oscillating Flow Euler No. vs. Ar as a function of Re w
Channel Aspect Ratio = 0.805 L/D= 57.0
Points are from Runs 41 and 57 using Nitrogen working fluid at 88 Hz.
Re w = 56
Re w = 110
Re w = 160
Re w = 210
Euler No.
Ar
0
2
4
6
8
10
12
14
16
18
20
0.0
1.0
2.0
3.0
4.0
5.0
6.0

Oscillating Flow Euler No. vs Re max as a function of Re w
Channel Aspect Ratio = 0.127   L/D = 5.63

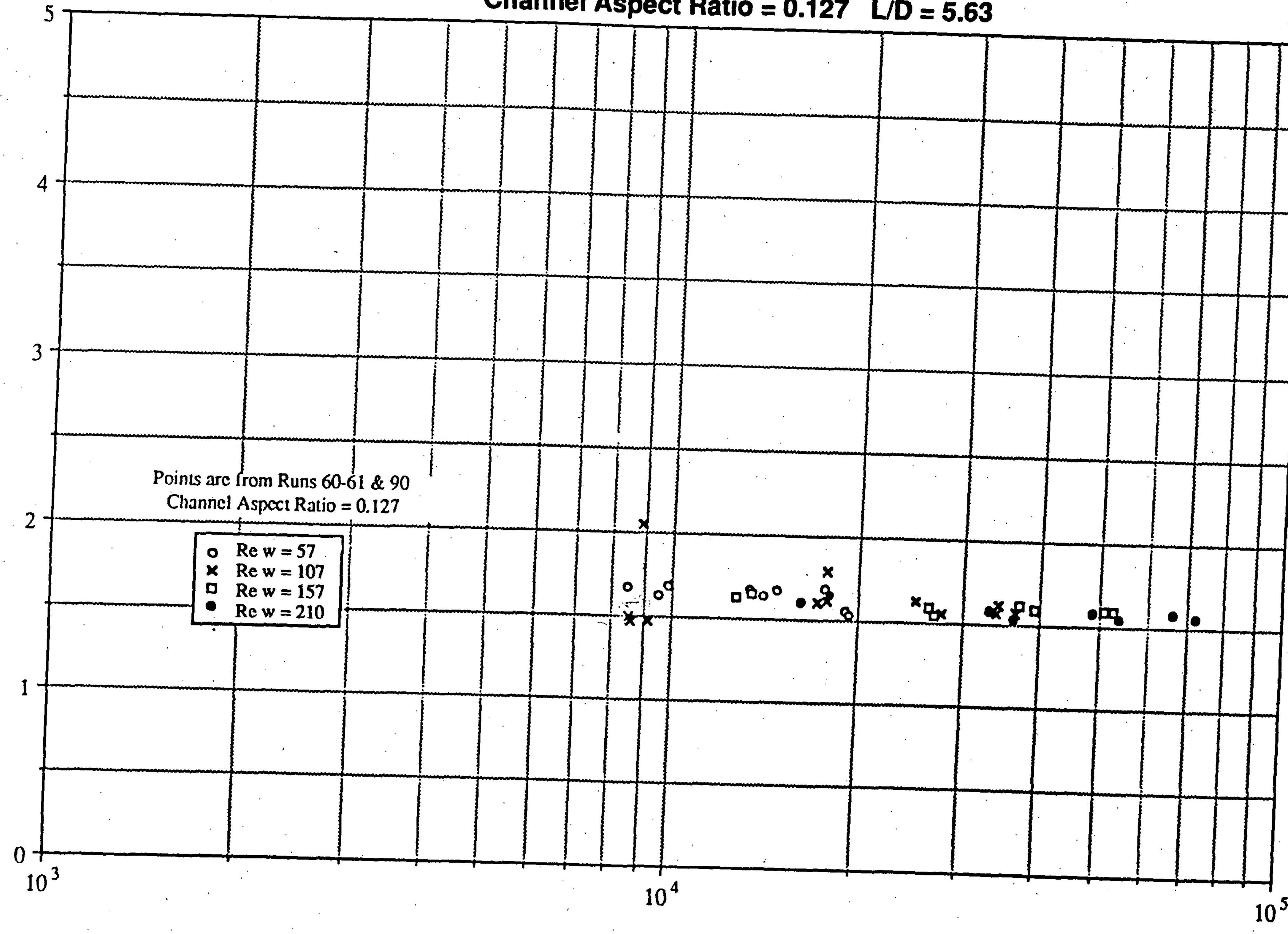

Figure 33

Oscillating Flow Euler No. vs Re max as a function of Re w
Channel Aspect Ratio = 0.442   L/D = 5.15

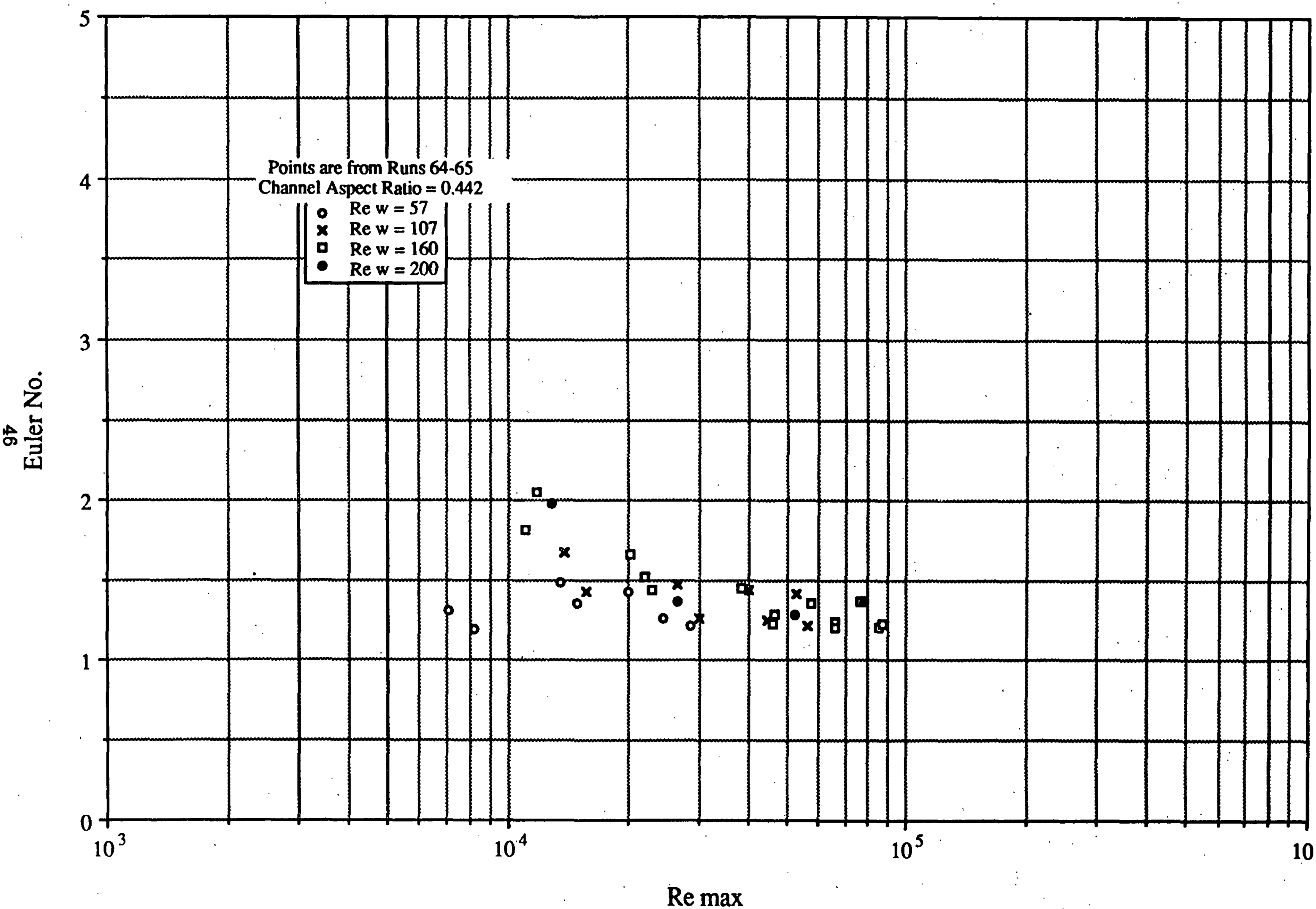

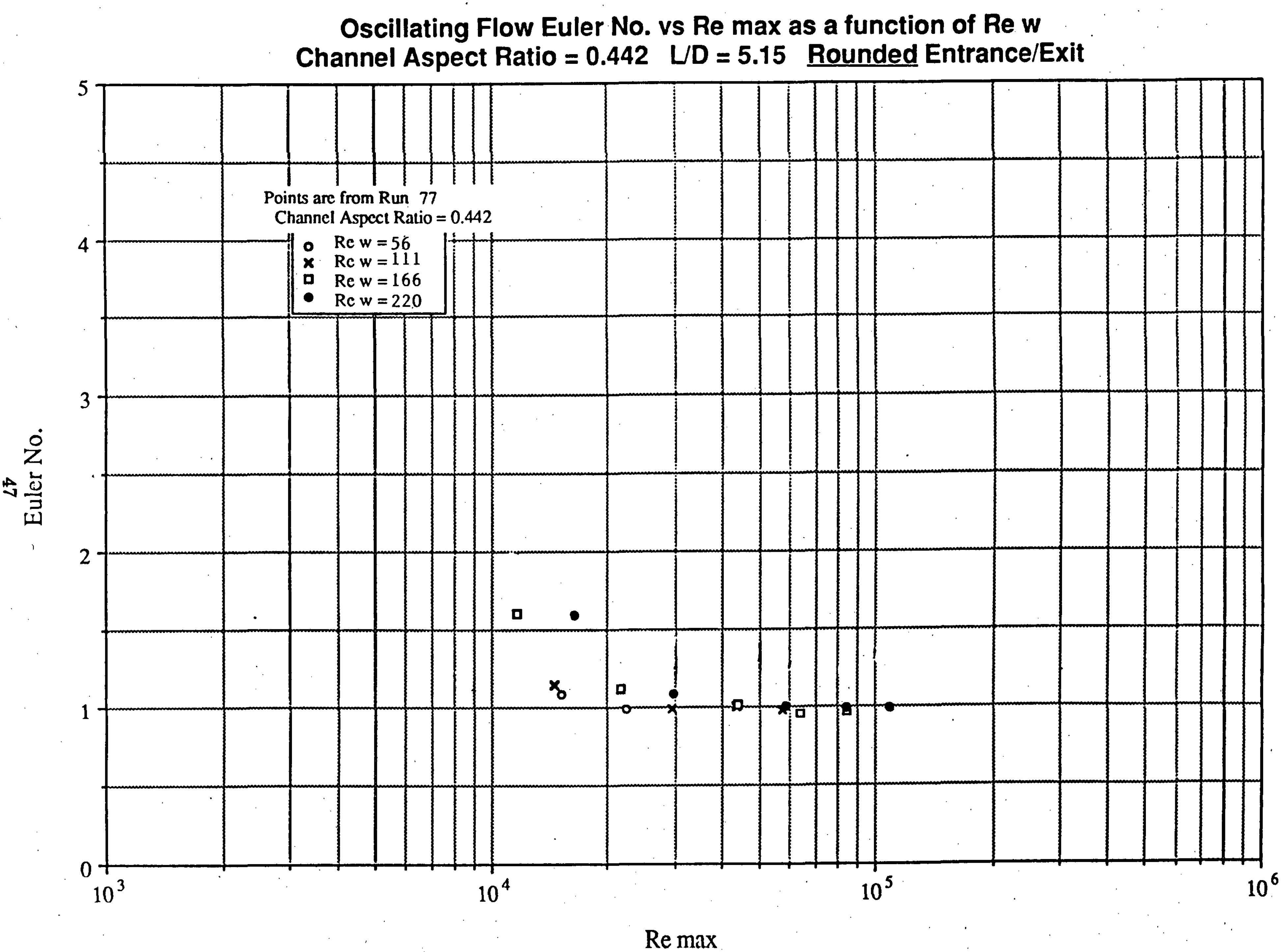

Oscillating Flow Euler No. vs Re max as a function of Re w
Channel Aspect Ratio = 0.442 L/D = 5.15 Rounded Entrance/Exit
Points are from Run 77
Channel Aspect Ratio = 0.442
Re w = 56
Re w = 111
Re w = 166
Re w = 220
Euler No.
0
1
2
3
4
5
10^3
10^4
10^5
10^6
Re max

Figure 35

DISCUSSION OF OSCILLATING-FLOW TEST RESULTS

Before discussing the results of oscillating-flow testing, two concerns which could influence the results should be noted:

First, a possible alignment problem in the hardware existed which could influence the oscillating-flow test results. The insert shown in Figure 5, in which the slots are machined, is the same diameter as the displacement cylinder of the test rig. However, the clearance holes for mounting the sample contained approximately 0.50 mm (0.020 in.) diametral clearance with the mounting bolts.

Thus, the sample could be mounted about 0.25 mm (0.010 in.) off the axis of the displacement cylinder and result in some small blockage of one of the passages. Even if the sample were mounted perfectly aligned with the cylinder, some cylinder wall influence would be expected, especially for the aspect ratios close to 1.0 . It would have been more desirable to have made the insert diameter smaller than the diameter of the displacement cylinder, to avoid these concerns.

Secondly, the mass flow through the sample often contained some higher order harmonics superimposed on the first harmonic. The relative amplitude of any of the higher harmonics was usually less than 10 percent of the first harmonic, but for some test points this ratio approached 20 percent. These higher order harmonics were however handled by the data reduction software so that TDF values presented include the effect of these harmonics.

TDF vs Ar (Figures 12 through 18)

These plots are seen to best compress the effects of Re_ω in the TDF results, although a Re_ω pattern still exists. The most striking pattern of these plots is that TDF appears to level off close to an Ar value of 2.0. Below Ar = 2.0, the TDF generally decreases, with a tendency of the lower Re_ω results to again increase in TDF at very low values of Ar.

As far as compressing the Re_ω effect, an exception is seen in Figure 16 presenting results for the 0.456 aspect ratio sample. The scatter and trends seen in the results for this sample differ from that of all the other samples tested. No explanation could be found for these differences, making these results suspect of error.

One exception to the tendency of the TDF to level off at Ar values greater than 2.0 is seen in Figure 14, as exhibited by the $Re_\omega = 103$ data point at Ar = 4.0. This point indicates a downward turn in TDF with Ar. Since this trend is not exhibited in any of the other results, this point is also suspect of being in error.

There appears to be a pattern to the Re_ω effect in nearly all of these plots. At Ar values around 2.0 and above, there seems to be a small indication of increasing TDF values with increasing Re_ω. However, this trend is generally quite small.

The pattern appears to reverse and become more significant as Ar decreases toward a value of 0.50. A possible explanation for this pattern is an Re_ω influence in the laminar part of the cycle which is more important at low values of Ar.

TDF vs Re_{max} (Figures 19 through 25)

In these plots the effect of Re_ω is fairly pronounced. First, it will be noticed that all of the data plots form a rough, flattened, nearly horizontal, "S" shape. Values of TDF level off somewhere in the middle of the 10^4 cycle of the logarithmic horizontal scale. As Re_{max} decreases to around $Re_{max} = 10^4$, TDF values fall; they then show a tendency to again increase to a value of about 1.0 as Re_{max} decreases toward 3000 to 5000. In general, the magnitude of the drop in the TDF values increases and the curves shift toward the right with increasing Re_ω values.

Again, an exception to the normal pattern is seen for the sample of aspect ratio 0.456. Because of the scatter and the striking differences of these results compared to those of other samples, this data is suspect of being in error.

Euler Number vs Ar (Figures 26 through 32)

For these plots, the Euler Number is based on maximum pressure drop and velocity, see page 23.As seen in the plots, at low Ar values, there is a steep Euler number vs Ar dependency. This is typical of laminar flow conditions where friction factor is inversely proportional to Re. At higher Ar, the Euler number tends to level off, which is typical of turbulent flow where pressure drop is a weak function of Reynolds number.

An interesting feature exhibited by several of these plots is that somewhere around an Ar value of 1.0 there appears to be a transitional region. This is seen in Figures 28, 29 and 30 and can be compared to standard steady flow results. In steady flow, the Euler number is equal to $fL/D+K$ and, in the transition region from laminar to turbulent, the friction factor (f) is known to usually increase.

Euler Number vs Re_{max} (Figures 33 through 35)

These plots show the test results for the short-length samples tested ($L/D \approx 5$) at various values of Re_ω. No discernible effect of Re_ω is indicated in these plots. Comparison of the square-edged to round-edged samples of identical aspect ratio (Figures 34 and 35) shows the expected drop in Euler number caused by round edges.

COMPARISON OF OSCILLATING-FLOW TEST RESULTS TO THEORY

Recently, Joerg Seume of Sunpower has developed a simplified analysis for predicting the effects of oscillating flow. This analysis assumes that flow which starts in the passage remains laminar, while any flow entering the passageway is tripped into and stays turbulent. Steady-flow correlations are used for both the laminar and turbulent flow. An average friction factor is calculated by integrating the laminar and turbulent flows over a cycle using the time varying lengths of flow.

The pumping power is given by:

$$P_p = \text{fave}\ (L/D)\ A/2\ \rho\ u_{max}^3 + 0.424\ K$$

where

A	= flow passage area
fave	= Fturb fst $Re^{-0.25}$ +Flam fsl /Re_{max}
fst	= conventional turbulent flow friction coefficient (0.316 for round tubes)
fsl	= conventional laminar flow friction coefficient (64 for round tubes)
K	= combined steady-flow entrance and exit loss coefficient (1.5 for square edges)
L/D	= sample length divided by hydraulic diameter
ρ	= density of gas
u_{max}	= maximum area-averaged gas velocity

Fturb and Flam values are given in Figure 36.

Seume's technique was used to generate theoretical TDF predictions for comparisons with the test results of this report. These predictions utilized only the first harmonic of the flow through the sample, while the measured TDF values calculated by the data reduction program included higher harmonics in the flow. Also, fst was adjusted for the aspect ratio effect given in Figure 2.6 of Idelchik (5) while the integrated steady-flow correlation on which each TDF is based does not include this effect.

The results of this study for the extremes of Valensi numbers for the 0.127, 0.220, 0.352 and 0.805 aspect ratio test results are presented in Figures 37 through 40. The trends in the test results match fairly well with those predicted by the Seume analysis. The shapes of the curves are similar to that predicted.

Of the four plots presented here, the 0.805 aspect ratio sample deviates the most from the prediction. In this case, no significant dip in measured TDF values for low Valensi number points is seen; however, the limited number of higher Valensi number test points shows signs of the predicted dip. It should be noted that some glue blocked the passages of this sample resulting in very poor entrance and exit conditions; this is described in the section Description of the Test Samples.

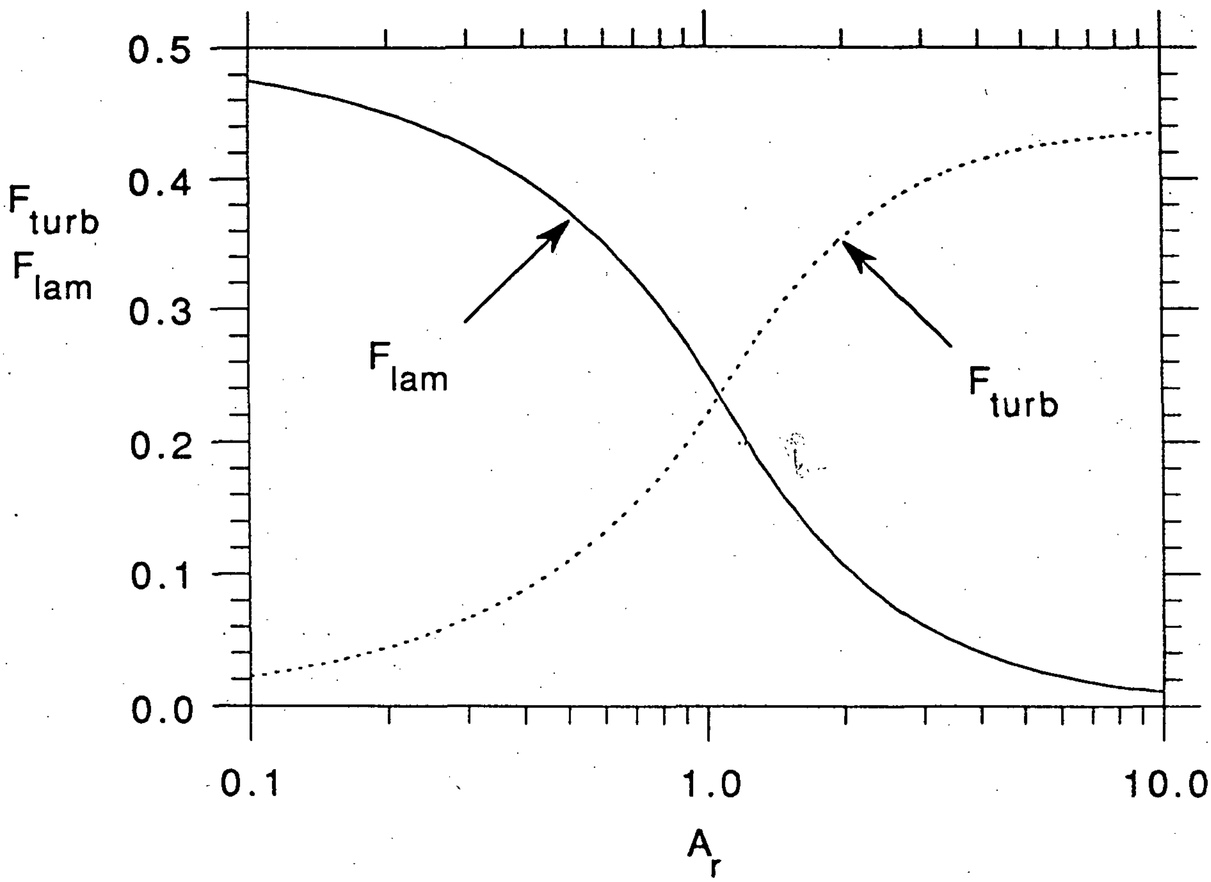

Figure 36 Fturb and Flam Values from Seume's Theory

Oscillating Test Results for Rectangular Passages Compared to Theory
Channel Aspect Ratio = 0.127 L/D = 67.6

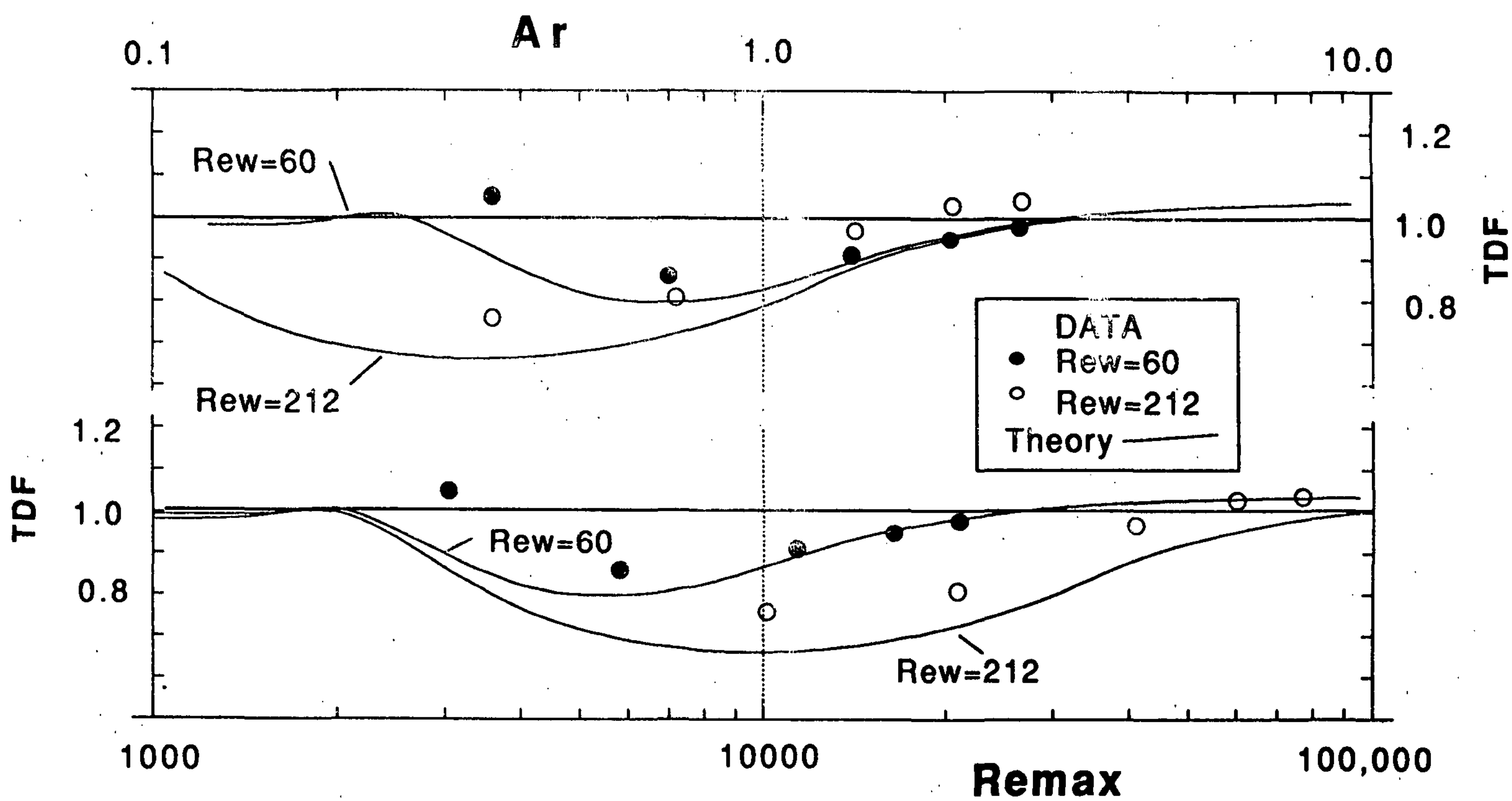

Figure 37

Oscillating Test Results for Rectangular Passages Compared to Theory
Channel Aspect Ratio = 0.220 L/D = 73.2

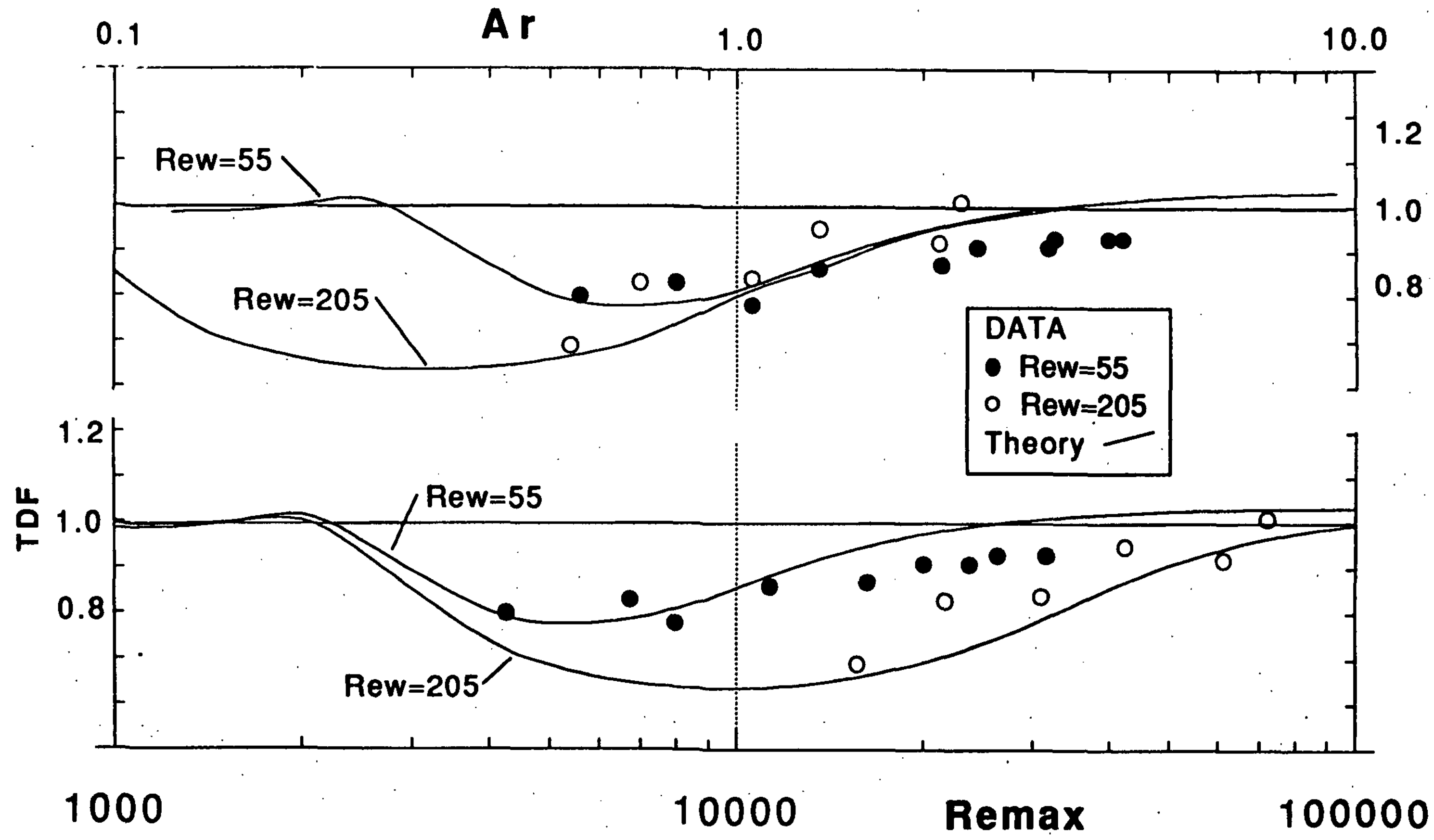

Figure 38

Oscillating Test Results for Rectangular Passages Compared to Theory
Channel Aspect Ratio = 0.352 L/D = 60.1

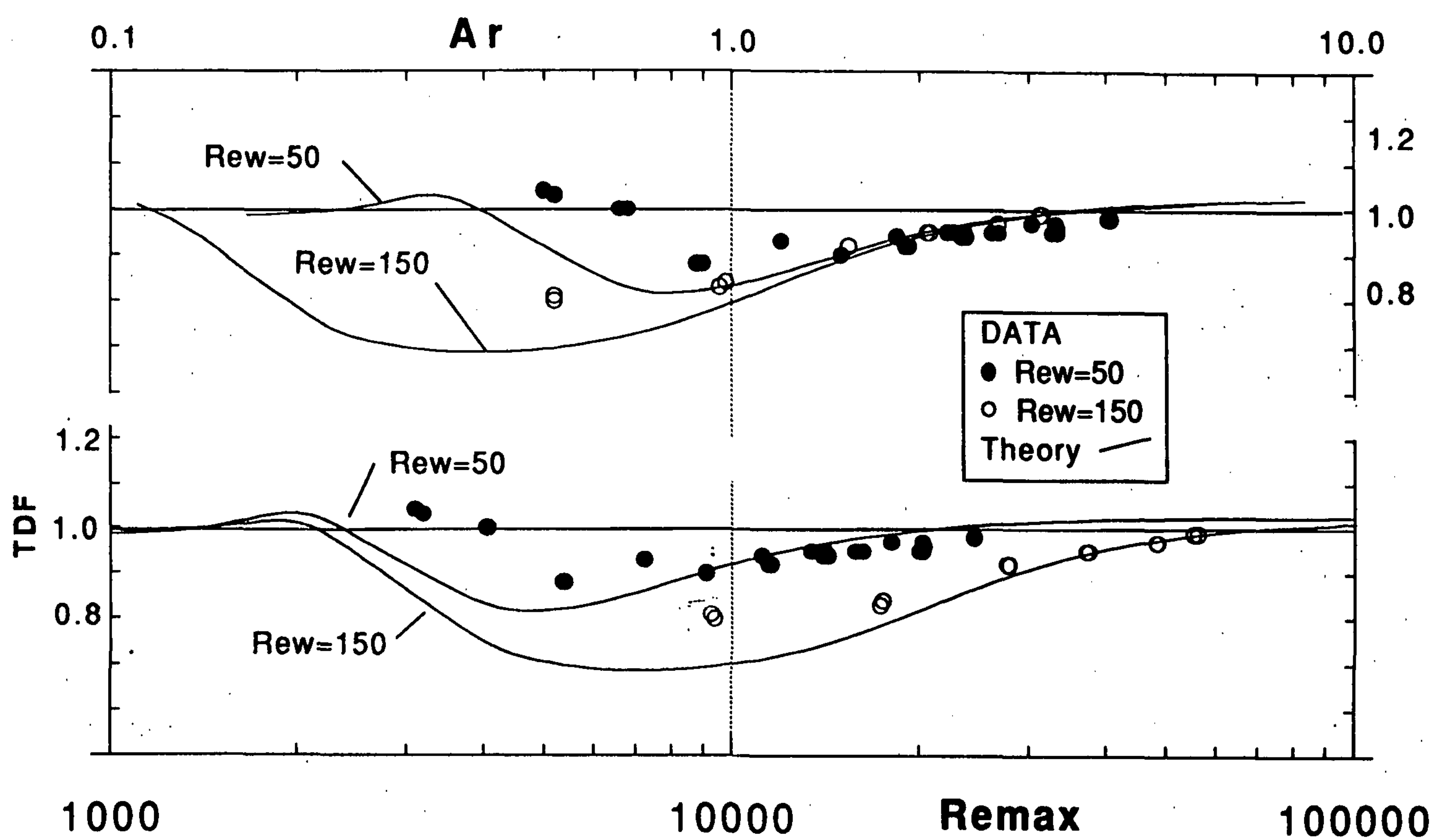

Figure 39

Oscillating Test Results for Rectangular Passages Compared to Theory

Channel Aspect Ratio = 0.805 L/D = 57.0

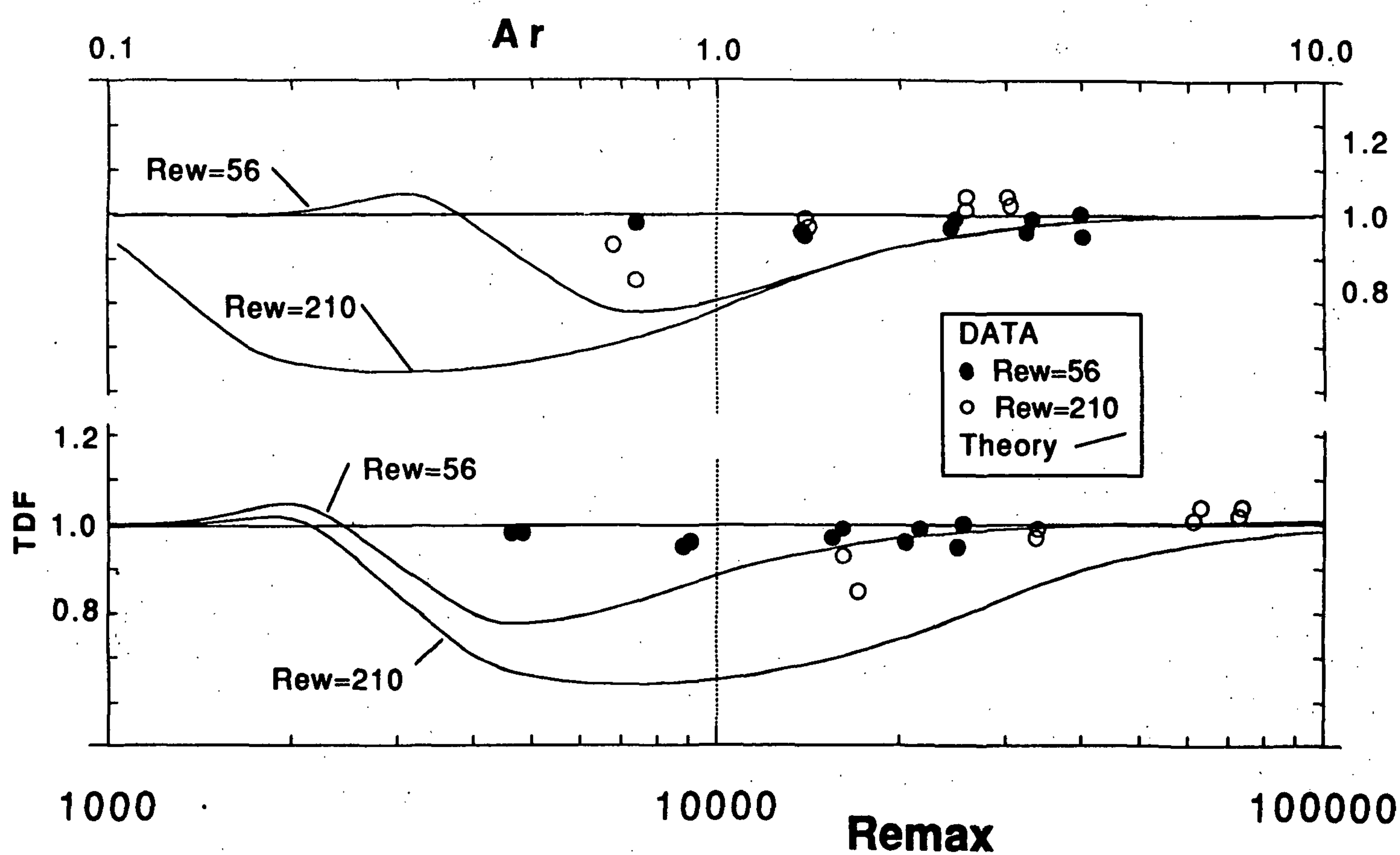

Figure 40

One trend, indicated by the test results but not predicted by the theory, is TDF values increasing slightly with Valensi number above Ar values of around 1 to 2.

Overall, considering possible sample geometry and experimental errors and the neglect of higher harmonics in the analysis, the test results generally support the results of the Seume analysis. Lacking test results on more accurately machined samples, it is recommended that the Seume analysis be utilized to predict oscillating-flow losses.

For more support of this theory, a comparison should be performed against the tube flow results of reference 3. The tube flow results are considered more accurate because of better geometrical accuracy of the samples as well as not having the possible mounting problem on the oscillating-flow rig as described earlier in this report for these samples with rectangular passages.

SUMMARY AND CONCLUSIONS

The intent of this rather limited test program was to obtain a better understanding of pressure drop characteristics in heat exchanger passages of the size and geometry considered for the SSE design. Toward this goal, the test program was structured to also investigate the effects of flow passage aspect ratio.

Due to the sensitivity of the test results to the exact geometry of the passages and end conditions, plus the difficulty of machining accurate small passageways, no discernible effect of aspect ratio was determined. The theoretically expected effect of aspect ratio would have been on the order of 3 percent. This difference was overshadowed by inaccuracy in the test results as well as manufacturing errors in the sample passage geometry and end conditions. It was determined that the precise area and end conditions of passages in this size range are very likely more important than any aspect ratio effect. This realization is important since engine designs which strive for high efficiency tend to utilize very large numbers of extremely small passageways.

Another important outcome of this work is the degree of confidence it imparts to the simplified analysis of oscillating-flow losses performed by Seume. It is thus believed that the ability to predict oscillating-flow losses has been advanced as a result of the work and study reported here.

REFERENCES

[1] L. Barry Penswick, 1050 K Stirling Space Engine Design, NASA Contractor Report 182149, Nov. 1988.

[2] J.G. Wood et al, Description of an Oscillating Flow Pressure Drop Test Rig, 23rd IECEC 1988, also published as NASA Technical Memorandum 100905.

[3] G. Koester et al, Oscillating Flow Loss Test Results in Stirling Engine Heat Exchangers, NASA Contractor Report 182288, May 1990.

[4] R.P. Benedict, Fundamentals of Pipe Flow, John Wiley & Sons, 1980.

[5] I.E. Idelchik, Handbook of Hydraulic Resistance, 2nd Ed., Hemisphere Publishing Corporation, 1986.

Appendix A

The following should be noted with regard to the data contained in the Appendix.

1. Errors listed in these tables are given as a percent of reading.

2. For the oscillating-flow test results:

X_p	=	piston amplitude [mm]
ΔP	=	maximum pressure amplitude [Pa]
P	=	test rig mean charge pressure [bar absolute]
pV	=	rate of work done on the working gas [watts]

Appendix A-1

Steady-Flow Test Results

RUN# 119 L/D = 73.2 Fluid: air Pressure: 7.00 bar
Fins: 120 mm long Aspect Ratio = 0.22 Entrance loss = 1.5
Pressure drop error (Pa) 690 Constant mass flow error (kg/s) 1.64E-4

Point #	Re	Mass Flow (kg/s)	Pressure drop (Pa)	Pratio
3	10338	1.05E-03 ± 15%	2650 ± 26%	0.87 ± 37%
4	16147	1.64E-03 ± 10%	6123 ± 11%	0.89 ± 20%
5	20775	2.11E-03 ± 8%	9867 ± 7%	0.89 ± 15%
6	26092	2.65E-03 ± 6%	15150 ± 5%	0.90 ± 12%
7	31999	3.25E-03 ± 5%	22430 ± 3%	0.91 ± 9%
8	37710	3.83E-03 ± 4%	30350 ± 2%	0.92 ± 8%
9	42830	4.35E-03 ± 4%	38726 ± 2%	0.92 ± 7%
10	48147	4.89E-03 ± 3%	49169 ± 1%	0.95 ± 6%

RUN# 120 L/D = 73.2 Fluid: air Pressure: 7.00 bar
Fins: 120 mm long Aspect Ratio = 0.22 Entrance loss = 1.5
Pressure drop error (Pa) 690 Constant mass flow error (kg/s) 1.6E-4

Point #	Re	Mass Flow (kg/s)	Pressure drop (Pa)	Pratio
3	10240	1.04E-03 ± 15%	2680 ± 26%	0.89 ± 37%
4	10338	1.05E-03 ± 15%	2670 ± 26%	0.87 ± 37%
5	16443	1.67E-03 ± 10%	6379 ± 11%	0.90 ± 20%
6	16344	1.66E-03 ± 10%	6389 ± 11%	0.91 ± 20%
7	22055	2.24E-03 ± 7%	11197 ± 6%	0.91 ± 14%
8	21956	2.23E-03 ± 7%	11186 ± 6%	0.91 ± 14%
9	28258	2.87E-03 ± 6%	18043 ± 4%	0.93 ± 10%
10	28258	2.87E-03 ± 6%	18073 ± 4%	0.92 ± 10%
11	32196	3.27E-03 ± 5%	23067 ± 3%	0.93 ± 9%
12	32295	3.28E-03 ± 5%	23087 ± 3%	0.93 ± 9%
13	38104	3.87E-03 ± 4%	32594 ± 2%	0.96 ± 8%
14	38596	3.92E-03 ± 4%	32965 ± 2%	0.94 ± 7%
15	48639	4.94E-03 ± 3%	50198 ± 1%	0.97 ± 6%
16	48639	4.94E-03 ± 3%	50198 ± 1%	0.96 ± 6%
17	44011	4.47E-03 ± 4%	41143 ± 2%	0.94 ± 6%
18	44011	4.47E-03 ± 4%	41153 ± 2%	0.94 ± 6%

RUN# 121 L/D = 73.2 Fluid: nitrogen Pressure: 18.26 bar
Fins: 120 mm long Aspect Ratio = 0.22 Entrance loss = 1.5
Pressure drop error (Pa) 690 Constant mass flow error (kg/s) 1.2E-4

Point #	Re	Mass Flow (kg/s)	Pressure drop (Pa)	Pratio
1	13530	1.32E-03 ± 9%	1806 ± 38%	0.98 ± 41%
2	13560	1.33E-03 ± 9%	1810 ± 38%	0.97 ± 41%
3	27010	2.64E-03 ± 5%	6320 ± 11%	0.94 ± 14%
4	27010	2.64E-03 ± 5%	6306 ± 11%	0.94 ± 14%
5	43730	4.27E-03 ± 3%	15474 ± 4%	0.94 ± 7%
6	43700	4.27E-03 ± 3%	15485 ± 4%	0.95 ± 7%
7	59280	5.81E-03 ± 2%	27536 ± 3%	0.94 ± 4%
8	59380	5.81E-03 ± 2%	27546 ± 3%	0.94 ± 4%
9	76080	7.45E-03 ± 2%	43453 ± 2%	0.94 ± 3%
10	75910	7.44E-03 ± 2%	43412 ± 2%	0.94 ± 3%
11	89760	8.79E-03 ± 1%	59182 ± 1%	0.93 ± 3%
12	89740	8.80E-03 ± 1%	59268 ± 1%	0.94 ± 3%
13	100500	9.88E-03 ± 1%	73407 ± 1%	0.94 ± 2%
14	100700	9.88E-03 ± 1%	73443 ± 1%	0.94 ± 2%
15	110900	1.09E-02 ± 1%	87357 ± 1%	0.89 ± 2%
16	111600	1.09E-02 ± 1%	87315 ± 1%	0.92 ± 2%

RUN# 122 L/D = 73.2 Fluid: nitrogen Pressure: 18.26 bar
Fins: 120mm long Aspect Ratio = 0.22 Entrance loss = 1.5
Pressure drop error (Pa) 690 Constant mass flow error (kg/s) 1.2E-4

Point #	Re	Mass Flow (kg/s)	Pressure drop (Pa)	Pratio
3	27790	2.72E-03 ± 4%	6566 ± 11%	0.94 ± 13%
4	27780	2.72E-03 ± 4%	6571 ± 11%	0.94 ± 13%
5	43270	4.23E-03 ± 3%	15171 ± 5%	0.94 ± 7%
6	43320	4.24E-03 ± 3%	15181 ± 5%	0.94 ± 7%
7	57080	5.59E-03 ± 2%	25597 ± 3%	0.95 ± 5%
8	57230	5.60E-03 ± 2%	25773 ± 3%	0.95 ± 5%
9	74100	7.26E-03 ± 2%	41557 ± 2%	0.95 ± 3%
10	74030	7.26E-03 ± 2%	41527 ± 2%	0.95 ± 3%
11	90360	8.87E-03 ± 1%	59990 ± 1%	0.93 ± 3%
12	89180	8.86E-03 ± 1%	60253 ± 1%	0.91 ± 3%
13	103700	1.02E-02 ± 1%	78370 ± 1%	0.93 ± 2%
14	104200	1.02E-02 ± 1%	78617 ± 1%	0.94 ± 2%

RUN# 123 L/D = 60.1 Fluid: air Pressure: 7.00 bar
Fins: 120mm long Aspect Ratio = 0.352 Entrance loss = 1.5
Pressure drop error (Pa) 690 Constant mass flow error (kg/s) 1.6E-4

Point #	Re	Mass Flow (kg/s)	Pressure drop (Pa)	Pratio
3	10845	1.03E-03 ± 16%	1981 ± 35%	0.99 ± 44%
19	18004	1.71E-03 ± 9%	5158 ± 13%	1.01 ± 21%
20	24427	2.32E-03 ± 7%	9212 ± 7%	1.01 ± 14%
21	24532	2.33E-03 ± 7%	9264 ± 7%	1.02 ± 14%
22	29797	2.83E-03 ± 6%	13346 ± 5%	1.02 ± 11%
23	29797	2.83E-03 ± 6%	13326 ± 5%	1.02 ± 11%
24	35272	3.35E-03 ± 5%	18312 ± 4%	1.02 ± 9%
25	35377	3.36E-03 ± 5%	18322 ± 4%	1.01 ± 9%
26	41063	3.90E-03 ± 4%	24065 ± 3%	1.01 ± 8%
27	41063	3.90E-03 ± 4%	24036 ± 3%	1.01 ± 8%
28	46538	4.42E-03 ± 4%	30379 ± 2%	1.02 ± 7%
29	46538	4.42E-03 ± 4%	30369 ± 2%	1.02 ± 7%
30	52013	4.94E-03 ± 3%	37426 ± 2%	1.02 ± 6%
31	52013	4.94E-03 ± 3%	37455 ± 2%	1.02 ± 6%

RUN# 124 L/D = 60.1 Fluid: nitrogen Pressure: 18.26 bar
Fins: 120 mm long Aspect Ratio = 0.352 Entrance loss = 1.5
Pressure drop error (Pa) 690 Constant mass flow error (kg/s) 1.2E-4

Point #	Re	Mass Flow (kg/s)	Pressure drop (Pa)	Pratio
3	24990	2.29E-03 ± 5%	3526 ± 20%	1.00 ± 22%
4	25010	2.29E-03 ± 5%	3515 ± 20%	1.00 ± 22%
5	40230	3.68E-03 ± 3%	8685 ± 8%	1.00 ± 10%
6	40310	3.69E-03 ± 3%	8629 ± 8%	1.00 ± 10%
7	54150	4.96E-03 ± 2%	14978 ± 5%	1.00 ± 6%
8	54490	4.99E-03 ± 2%	14978 ± 5%	0.99 ± 6%
9	54520	4.99E-03 ± 2%	14988 ± 5%	0.99 ± 6%
10	54550	5.00E-03 ± 2%	14988 ± 5%	0.99 ± 6%
11	72620	6.65E-03 ± 2%	25480 ± 3%	0.98 ± 4%
12	72610	6.67E-03 ± 2%	25646 ± 3%	0.96 ± 4%
13	89900	8.24E-03 ± 1%	37544 ± 2%	0.96 ± 3%
14	89940	8.24E-03 ± 1%	37792 ± 2%	0.97 ± 3%
15	107500	9.84E-03 ± 1%	51559 ± 1%	0.94 ± 3%
16	106900	9.82E-03 ± 1%	51183 ± 1%	0.94 ± 3%
17	121800	1.12E-02 ± 1%	64462 ± 1%	0.93 ± 2%
18	122200	1.12E-02 ± 1%	64599 ± 1%	0.92 ± 2%
19	133900	1.23E-02 ± 1%	75906 ± 1%	0.93 ± 2%
20	133900	1.23E-02 ± 1%	75906 ± 1%	0.93 ± 2%

RUN# 125 L/D = 57.0 Fluid: air Pressure: 7.00 bar
Fins: 120mm long Aspect Ratio = .805 Entrance loss = 1.5
Pressure drop error (Pa) 690 Constant mass flow error (kg/s) 1.6E-4

Point #	Re	Mass Flow (kg/s)	Pressure drop (Pa)	Pratio
3	12827	1.00E-03 ± 16%	2319 ± 30%	0.97 ± 41%
4	12776	9.96E-04 ± 16%	2328 ± 30%	0.98 ± 41%
5	22833	1.78E-03 ± 9%	6781 ± 10%	0.96 ± 19%
6	22961	1.79E-03 ± 9%	6773 ± 10%	0.96 ± 19%
7	29375	2.29E-03 ± 7%	10915 ± 6%	0.97 ± 14%
8	29247	2.28E-03 ± 7%	10925 ± 6%	0.98 ± 14%
9	36686	2.86E-03 ± 6%	16592 ± 4%	0.98 ± 11%
10	36686	2.86E-03 ± 6%	16623 ± 4%	0.98 ± 11%
11	44126	3.44E-03 ± 5%	23527 ± 3%	0.97 ± 9%
12	44126	3.44E-03 ± 5%	23527 ± 3%	0.98 ± 9%
13	49899	3.89E-03 ± 4%	29610 ± 2%	0.98 ± 8%
14	49899	3.89E-03 ± 4%	29639 ± 2%	0.99 ± 8%
15	55799	4.35E-03 ± 4%	36941 ± 2%	1.00 ± 7%
16	55928	4.36E-03 ± 4%	36931 ± 2%	1.00 ± 7%
17	62983	4.91E-03 ± 3%	46110 ± 1%	1.00 ± 6%
18	62983	4.91E-03 ± 3%	46078 ± 1%	1.00 ± 6%

RUN# 126 L/D = 57.0 Fluid: nitrogen Pressure: 18.26 bar
Fins: 120mm long Aspect Ratio = .805 Entrance loss = 1.5
Pressure drop error (Pa) 690 Constant mass flow error (kg/s) 1.2E-4

Point #	Re	Mass Flow (kg/s)	Pressure drop (Pa)	Pratio
3	38020	2.86E-03 ± 4%	6486 ± 11%	0.96 ± 13%
4	38060	2.86E-03 ± 4%	6473 ± 11%	0.95 ± 13%
5	56030	4.21E-03 ± 3%	13572 ± 5%	0.96 ± 7%
6	55990	4.21E-03 ± 3%	13592 ± 5%	0.96 ± 7%
7	77500	5.83E-03 ± 2%	25139 ± 3%	0.96 ± 5%
8	77540	5.83E-03 ± 2%	25119 ± 3%	0.96 ± 5%
9	93610	7.04E-03 ± 2%	35335 ± 2%	0.95 ± 4%
10	93530	7.04E-03 ± 2%	35335 ± 2%	0.96 ± 4%
11	113200	8.51E-03 ± 1%	50591 ± 1%	0.95 ± 3%
12	113100	8.51E-03 ± 1%	50580 ± 1%	0.95 ± 3%
13	130900	9.89E-03 ± 1%	67322 ± 1%	0.95 ± 2%
14	131200	9.89E-03 ± 1%	67146 ± 1%	0.94 ± 2%
15	145800	1.10E-02 ± 1%	80748 ± 1%	0.95 ± 2%
16	145800	1.10E-02 ± 1%	80772 ± 1%	0.95 ± 2%
17	160500	1.21E-02 ± 1%	92239 ± 1%	0.91 ± 2%
18	161200	1.22E-02 ± 1%	91862 ± 1%	0.89 ± 2%

RUN# 127 L/D = 73.2 Fluid: air Pressure: 7.00 bar
Fins: 120 mm long Aspect Ratio = 0.22 Entrance loss = 1.5
Pressure drop error (Pa) 690 Constant mass flow error (kg/s) 1.64E-4

Point #	Re	Mass Flow (kg/s)	Pressure drop (Pa)	Pratio
3	12504	1.27E-03 ± 13%	3827 ± 18%	0.89 ± 28%
4	12406	1.26E-03 ± 13%	3833 ± 18%	0.89 ± 29%
5	18806	1.91E-03 ± 8%	8067 ± 9%	0.89 ± 17%
6	18806	1.91E-03 ± 8%	8120 ± 8%	0.89 ± 17%
7	24122	2.45E-03 ± 7%	12966 ± 5%	0.89 ± 13%
8	24122	2.45E-03 ± 7%	12966 ± 5%	0.89 ± 13%
9	29144	2.96E-03 ± 5%	18391 ± 4%	0.89 ± 10%
10	29242	2.97E-03 ± 5%	18391 ± 4%	0.88 ± 10%
11	34559	3.51E-03 ± 5%	25490 ± 3%	0.90 ± 8%
12	34658	3.52E-03 ± 5%	25480 ± 3%	0.89 ± 8%
13	39482	4.01E-03 ± 4%	32721 ± 2%	0.91 ± 7%
14	39581	4.02E-03 ± 4%	32751 ± 2%	0.90 ± 7%
15	44110	4.48E-03 ± 4%	40518 ± 2%	0.91 ± 6%
16	44307	4.50E-03 ± 4%	40548 ± 2%	0.91 ± 6%
17	48245	4.90E-03 ± 3%	48140 ± 1%	0.93 ± 6%
18	48343	4.91E-03 ± 3%	48130 ± 1%	0.92 ± 6%

RUN# 128 L/D = 67.6 Fluid: air Pressure:7.00 bar
Fins: 120mm long Aspect Ratio = 0.127 Entrance loss = 1.5
Pressure drop error (Pa) 690 Constant mass flow error (kg/s) 1.6E-4.

Point #	Re	Mass Flow (kg/s)	Pressure drop (Pa)	Pratio
4	9210	1.50E-03 ± 11%	1811 ± 38%	0.91 ± 42%
5	14183	2.31E-03 ± 7%	4138 ± 17%	0.94 ± 21%
6	14244	2.32E-03 ± 7%	4136 ± 17%	0.93 ± 21%
7	18051	2.94E-03 ± 5%	6544 ± 11%	0.94 ± 14%
8	18051	2.94E-03 ± 5%	6536 ± 11%	0.94 ± 14%
9	21797	3.55E-03 ± 5%	9328 ± 7%	0.95 ± 11%
10	21797	3.55E-03 ± 5%	9336 ± 7%	0.95 ± 11%
11	24866	4.05E-03 ± 4%	11976 ± 6%	0.95 ± 9%
12	24989	4.07E-03 ± 4%	11996 ± 6%	0.94 ± 9%
13	27507	4.48E-03 ± 4%	14429 ± 5%	0.95 ± 8%
14	27445	4.47E-03 ± 4%	14419 ± 5%	0.95 ± 8%
15	30270	4.93E-03 ± 3%	17344 ± 4%	0.96 ± 7%
16	30331	4.94E-03 ± 3%	17354 ± 4%	0.95 ± 7%

RUN# 129 L/D = 67.6 Fluid: nitrogen Pressure: 18.26 bar
Fins: 120mm long Aspect Ratio = 0.127 Entrance loss = 1.5
Pressure drop error (Pa) 690 Constant mass flow error (kg/s) 1.2E-4

Point #	Re	Mass Flow (kg/s)	Pressure drop (Pa)	Pratio
3	19240	3.03E-03 ± 4%	2810 ± 25%	0.96 ± 26%
4	19200	3.02E-03 ± 4%	2830 ± 24%	0.97 ± 25%
5	28940	4.55E-03 ± 3%	5949 ± 12%	0.95 ± 12%
6	28970	4.56E-03 ± 3%	5954 ± 12%	0.95 ± 12%
7	38450	6.05E-03 ± 2%	9979 ± 7%	0.94 ± 8%
8	38350	6.03E-03 ± 2%	9981 ± 7%	0.95 ± 8%
9	47000	7.39E-03 ± 2%	14460 ± 5%	0.94 ± 6%
10	47010	7.40E-03 ± 2%	14490 ± 5%	0.94 ± 6%
11	55700	8.77E-03 ± 1%	19701 ± 4%	0.93 ± 4%
12	55530	8.77E-03 ± 1%	19731 ± 3%	0.93 ± 4%
13	64160	1.01E-02 ± 1%	25636 ± 3%	0.91 ± 3%
14	64310	1.01E-02 ± 1%	25666 ± 3%	0.92 ± 3%
15	71290	1.12E-02 ± 1%	31013 ± 2%	0.92 ± 3%
16	71050	1.12E-02 ± 1%	30623 ± 2%	0.89 ± 3%
17	76510	1.20E-02 ± 1%	36063 ± 2%	0.93 ± 3%
18	77420	1.22E-02 ± 1%	36497 ± 2%	0.92 ± 3%

Appendix A-2

Oscillating-Flow Test Results

Run number 39 Sample type: fins L/D = 81.9

120 mm long aspect ratio = 0.147 Entrance loss = 1.5 nitrogen 90 Hz

Point	Xp (mm)	P (bar)	Re max	Re w	Ar/2	Mach#	ΔP (Pa)	pV (W)	Euler#	TDF
1	0.97	1.54	3,227	29.7	0.33	0.06	3.48E3	0.20	7.92	1.03 ±29%
2	2.01	1.54	6,060	29.5	0.63	0.12	7.60E3	1.18	4.87	0.95 ±25%
3	3.95	1.55	10,370	29.3	1.08	0.21	1.75E4	5.65	3.79	0.98 ±28%
4	5.97	1.56	13,980	29.3	1.46	0.28	2.90E4	13.47	3.43	0.98 ±33%
5	7.97	1.57	16,950	29.1	1.78	0.34	4.15E4	24.08	3.30	0.97 ±40%
6	1.00	3.02	6,154	55.2	0.34	0.06	6.23E3	0.33	7.09	0.89 ±17%
7	1.99	3.02	11,410	55.4	0.63	0.12	1.43E4	2.04	4.76	0.95 ±14%
8	3.93	3.03	20,190	55.7	1.11	0.21	3.31E4	10.71	3.55	1.00 ±17%
9	5.93	3.06	27,420	55.7	1.50	0.28	5.50E4	26.18	3.18	1.01 ±22%
10	7.97	3.08	33,480	55.3	1.85	0.35	8.00E4	47.85	3.06	1.00 ±29%
11	0.97	4.60	9,075	84.7	0.33	0.06	8.75E3	0.41	7.06	0.86 ±13%
12	1.89	4.60	16,860	85.2	0.60	0.11	2.01E4	2.66	4.73	0.97 ±11%
13	3.91	4.63	31,260	85.6	1.12	0.21	4.98E4	16.10	3.43	1.03 ±14%
14	5.84	4.65	41,950	85.1	1.51	0.28	8.29E4	38.90	3.13	1.04 ±20%
15	0.96	6.06	11,600	109.7	0.32	0.06	1.15E4	0.51	7.32	0.89 ±12%
16	2.00	6.08	23,330	111.5	0.64	0.12	2.82E4	3.94	4.53	0.98 ±9%
17	3.88	6.09	41,020	112.0	1.12	0.21	6.53E4	20.85	3.41	1.05 ±13%
18	4.98	6.12	49,390	111.2	1.36	0.26	8.81E4	36.44	3.13	1.05 ±16%

Run number 40 Sample type: fins L/D = 81.9

120 mm long aspect ratio = 0.147 Entrance loss = 1.5 helium 90 Hz

Point	Xp (mm)	P (bar)	Re max	Re w	Ar/2	Mach#	ΔP (Pa)	pV (W)	Euler#	TDF
1	0.85	10.87	1,873	26.1	0.22	0.01	2.95E3	0.07	15.39	1.08 ±27%
2	1.94	10.77	4,227	25.9	0.50	0.03	6.13E3	0.59	6.25	0.92 ±12%
3	3.97	10.69	8,571	25.8	1.02	0.07	1.72E4	4.69	4.24	0.97 ±6%
4	5.90	10.72	12,700	25.8	1.50	0.10	3.61E4	14.80	4.06	1.00 ±6%
5	7.86	10.87	16,890	25.9	1.99	0.13	6.17E4	33.68	3.92	1.02 ±6%
6	0.98	21.21	4,178	50.4	0.25	0.02	6.16E3	0.14	12.43	0.85 ±16%
7	1.98	21.65	8,632	51.9	0.51	0.03	1.05E4	1.03	5.12	0.85 ±8%
8	3.94	21.15	16,820	50.9	1.01	0.07	3.05E4	8.02	3.86	0.95 ±4%
9	5.91	21.23	25,120	50.9	1.51	0.10	6.51E4	26.28	3.69	0.99 ±4%
10	7.01	21.28	29,550	50.7	1.78	0.12	8.81E4	42.93	3.57	1.01 ±4%
11	0.99	31.97	6,344	76.2	0.25	0.02	9.02E3	0.19	11.95	0.79 ±13%
12	1.93	32.45	12,600	77.8	0.49	0.03	1.51E4	1.37	5.19	0.86 ±7%
13	4.03	32.53	26,260	77.9	1.03	0.07	4.77E4	12.47	3.78	0.97 ±4%
14	6.03	32.53	38,930	77.4	1.54	0.10	9.87E4	40.73	3.52	1.01 ±4%
16	1.96	42.96	16,830	102.2	0.50	0.03	1.98E4	1.84	5.01	0.87 ±6%
17	3.99	42.74	33,890	101.5	1.02	0.07	6.08E4	15.60	3.75	0.99 ±3%
18	4.99	42.88	42,450	101.8	1.27	0.08	9.08E4	30.06	3.59	1.01 ±3%

Run number 41 Sample type: fins L/D = 57.0

120 mm long aspect ratio = 0.805 Entrance loss = 1.5 nitrogen 88 Hz

Point	Xp (mm)	P (bar)	Re max	Re w	Ar/2	Mach#	ΔP (Pa)	pV (W)	Euler#	TDF
1	0.99	1.47	4,817	57.5	0.37	0.07	3.23E3	0.16	6.56	0.98 ±30%
2	2.00	1.47	9,054	57.5	0.69	0.13	6.95E3	0.99	3.99	0.96 ±25%
3	4.05	1.47	16,120	57.2	1.24	0.23	1.68E4	5.43	3.03	0.99 ±28%
4	6.04	1.48	21,570	57.0	1.66	0.31	2.75E4	12.94	2.74	0.99 ±33%
5	7.88	1.50	25,470	55.9	2.00	0.37	3.83E4	22.44	2.65	1.00 ±38%
6	0.99	2.99	9,142	109.9	0.36	0.07	6.04E3	0.27	6.34	0.90 ±17%
7	2.02	3.00	17,740	111.2	0.70	0.13	1.39E4	1.82	3.94	0.93 ±14%
8	2.97	3.01	24,940	111.8	0.98	0.18	2.26E4	5.02	3.26	0.98 ±14%
9	2.89	3.00	24,480	112.1	0.96	0.18	2.19E4	4.70	3.29	0.97 ±14%
10	4.05	3.02	32,590	113.1	1.26	0.23	3.35E4	10.83	2.87	1.01 ±16%
11	3.97	3.02	31,870	112.5	1.24	0.23	3.26E4	10.29	2.89	1.01 ±16%
12	5.89	3.04	43,070	112.6	1.68	0.31	5.36E4	25.17	2.61	1.03 ±21%
13	8.05	3.04	53,370	111.6	2.10	0.39	7.93E4	48.43	2.48	1.02 ±28%
14	0.97	4.24	12,580	155.6	0.35	0.07	8.07E3	0.33	6.33	0.87 ±14%
15	1.99	4.24	24,900	157.5	0.69	0.13	1.94E4	2.46	3.95	0.96 ±11%
16	4.05	4.27	46,380	159.5	1.28	0.24	4.73E4	15.31	2.82	1.03 ±14%
17	5.98	4.29	62,380	159.3	1.72	0.32	7.68E4	36.85	2.52	1.04 ±19%
18	0.92	5.66	16,140	211.0	0.34	0.06	1.00E4	0.38	6.53	0.93 ±13%
19	2.00	5.66	33,810	212.6	0.70	0.13	2.61E4	3.34	3.91	0.99 ±9%
20	4.07	5.69	62,770	213.8	1.29	0.24	6.33E4	20.58	2.77	1.04 ±13%
21	4.98	5.72	73,440	213.5	1.51	0.28	8.10E4	32.77	2.57	1.04 ±15%

Run number 44 Sample type: fins L/D = 81.9

120 mm long aspect ratio = 0.147 Entrance loss = 1.5 nitrogen 90 Hz

Point	Xp (mm)	P (bar)	Re max	Re w	Ar/2	Mach#	ΔP (Pa)	pV (W)	Euler#	TDF
1	1.00	2.86	5,931	54.0	0.34	0.06	5.73E3	0.30	7.20	0.90 ±18%
2	0.94	2.86	5,825	55.1	0.32	0.06	5.75E3	0.28	7.47	0.90 ±18%
3	2.01	2.86	11,430	55.0	0.63	0.12	1.41E4	2.05	4.75	0.96 ±15%
4	3.94	2.87	19,610	54.4	1.10	0.21	3.19E4	10.32	3.58	1.01 ±18%
5	5.90	2.89	26,240	54.0	1.48	0.28	5.20E4	24.52	3.22	1.02 ±23%
6	7.89	2.90	31,470	52.9	1.82	0.34	7.50E4	44.11	3.13	1.01 ±29%
7	0.96	5.68	11,260	105.3	0.33	0.06	1.13E4	0.50	7.38	0.88 ±12%
8	1.97	5.69	21,880	105.7	0.63	0.12	2.66E4	3.63	4.62	0.97 ±10%
9	3.95	5.71	38,860	105.1	1.13	0.21	6.26E4	20.48	3.42	1.06 ±13%
10	5.03	5.73	46,570	104.9	1.36	0.26	8.39E4	34.97	3.17	1.06 ±16%
11	0.93	8.52	16,230	157.1	0.32	0.06	1.60E4	0.64	7.48	0.89 ±11%
12	1.95	8.53	32,470	158.4	0.63	0.12	3.91E4	5.26	4.63	1.03 ±9%
13	3.87	8.57	57,650	157.4	1.12	0.21	9.11E4	29.23	3.38	1.09 ±12%
14	0.99	11.35	22,830	210.3	0.33	0.06	2.24E4	1.04	7.12	0.98 ±10%
15	1.93	11.36	42,950	210.8	0.62	0.12	5.15E4	6.80	4.63	1.06 ±8%
16	2.88	11.38	60,740	209.8	0.88	0.17	8.45E4	19.23	3.77	1.11 ±9%

Run number 45 Sample type: fins L/D = 81.9

120 mm long aspect ratio = 0.147 Entrance loss = 1.5 helium 90 Hz

Point	Xp (mm)	P (bar)	Re max	Re w	Ar/2	Mach#	ΔP (Pa)	pV (W)	Euler#	TDF
1	1.27	20.33	5,471	50.9	0.33	0.02	7.56E3	0.30	9.18	0.89 ±12%
2	0.97	20.21	4,152	50.7	0.25	0.02	6.85E3	0.15	14.41	0.94 ±16%
3	1.90	20.33	8,191	51.0	0.49	0.03	9.45E3	1.01	5.14	0.94 ±8%
4	3.86	20.26	16,380	50.6	0.99	0.07	3.16E4	8.26	4.25	1.06 ±4%
5	6.02	20.13	25,080	49.8	1.54	0.10	7.22E4	29.84	4.07	1.10 ±4%
6	6.92	20.36	28,770	49.9	1.76	0.12	9.55E4	45.07	4.08	1.12 ±5%
7	0.88	40.45	7,410	100.0	0.23	0.02	1.04E4	0.18	13.51	0.83 ±14%
8	1.94	40.48	16,390	100.5	0.50	0.03	1.91E4	1.88	5.10	0.95 ±6%
9	3.93	40.41	32,980	99.9	1.01	0.07	6.28E4	15.73	4.10	1.07 ±3%
10	4.87	40.34	40,490	99.3	1.24	0.08	9.11E4	29.39	3.92	1.09 ±3%
11	0.94	60.56	11,760	149.3	0.24	0.02	1.44E4	0.29	11.01	0.82 ±12%
12	2.00	60.47	25,040	149.2	0.51	0.03	2.98E4	2.95	5.04	0.98 ±6%
13	3.91	60.54	48,810	148.9	1.00	0.07	8.95E4	22.08	3.97	1.08 ±3%
14	0.94	81.17	15,680	199.2	0.24	0.02	2.00E4	0.37	11.46	0.81 ±12%
15	1.93	81.06	32,350	199.7	0.49	0.03	3.65E4	3.53	4.95	1.00 ±6%
16	2.98	80.89	49,700	198.9	0.76	0.05	7.28E4	12.69	4.16	1.05 ±4%

Run number 57 Sample type: fins L/D = 57.0

120 mm long aspect ratio = 0.805 Entrance loss = 1.5 nitrogen 88 Hz

Point	Xp (mm)	P (bar)	Re max	Re w	Ar/2	Mach#	ΔP (Pa)	pV (W)	Euler#	TDF
1	0.99	1.40	4,618	55.3	0.37	0.07	3.07E3	0.16	6.54	0.98 ±31%
2	2.04	1.41	8,814	55.4	0.70	0.13	6.73E3	0.98	3.93	0.95 ±26%
3	4.02	1.42	15,490	55.5	1.22	0.23	1.58E4	5.04	2.99	0.97 ±29%
4	5.86	1.43	20,460	55.1	1.63	0.30	2.50E4	11.51	2.68	0.96 ±33%
5	8.01	1.45	24,920	54.1	2.02	0.37	3.76E4	21.88	2.63	0.95 ±39%
6	0.96	2.79	8,149	101.8	0.35	0.06	5.33E3	0.23	6.49	0.90 ±18%
7	1.81	2.79	14,760	102.8	0.63	0.12	1.08E4	1.28	4.07	0.94 ±15%
8	3.94	2.81	29,290	103.9	1.24	0.23	2.96E4	9.24	2.87	0.98 ±17%
9	6.02	2.83	40,410	103.9	1.71	0.31	5.01E4	24.07	2.55	1.00 ±22%
10	7.91	2.84	48,890	103.4	2.07	0.38	7.11E4	42.78	2.45	0.99 ±28%
11	0.93	4.27	12,000	155.1	0.34	0.06	7.70E3	0.28	6.58	0.86 ±14%
12	1.94	4.28	24,250	157.1	0.68	0.12	1.87E4	2.28	3.98	0.95 ±11%
13	3.71	4.31	42,650	159.1	1.18	0.22	4.49E4	12.54	3.14	1.01 ±13%
14	6.02	4.34	62,480	158.2	1.73	0.32	7.69E4	37.24	2.48	1.02 ±19%
15	6.73	4.39	66,090	156.9	1.85	0.34	8.68E4	46.05	2.46	1.04 ±21%
16	1.02	5.65	17,110	202.1	0.37	0.07	1.13E4	0.47	6.17	0.85 ±12%
17	2.04	5.70	33,630	208.0	0.71	0.13	2.61E4	3.40	3.83	0.97 ±9%
18	4.05	5.70	61,130	208.2	1.29	0.24	6.15E4	19.82	2.73	1.01 ±12%
19	5.03	5.72	72,590	208.5	1.53	0.28	8.09E4	32.95	2.55	1.02 ±15%

Run number 58 Sample type: fins L/D = 67.6

120 mm long aspect ratio = 0.127 Entrance loss = 1.5 nitrogen 88 Hz

Point	Xp (mm)	P (bar)	Re max	Re w	Δr/2	Mach#	ΔP (Pa)	pV (W)	Euler#	TDF
1	1.00	2.11	3,054	61.1	0.18	0.04	2.38E3	0.07	12.98	1.05 ±31%
2	1.94	2.11	5,821	60.9	0.35	0.07	4.55E3	0.36	6.81	0.86 ±22%
3	3.95	2.13	11,340	60.2	0.70	0.13	1.13E4	2.66	4.39	0.91 ±19%
4	5.94	2.14	16,440	59.6	1.02	0.19	1.91E4	8.25	3.46	0.95 ±20%
5	8.01	2.17	21,060	58.6	1.33	0.25	2.80E4	18.11	2.99	0.98 ±22%
6	0.99	3.95	5,215	106.7	0.18	0.03	3.99E3	0.09	12.66	0.88 ±20%
7	1.97	3.96	10,310	107.2	0.36	0.07	8.34E3	0.59	6.82	0.82 ±13%
8	4.05	3.98	20,950	108.4	0.71	0.13	2.10E4	4.87	4.22	0.92 ±12%
10	7.60	4.05	37,130	107.4	1.28	0.24	4.69E4	28.30	2.93	1.01 ±15%
11	8.01	4.07	38,720	106.9	1.34	0.25	5.04E4	32.42	2.87	1.01 ±16%
12	0.99	5.93	7,599	155.5	0.18	0.03	6.47E3	0.12	13.94	0.81 ±15%
13	1.96	5.93	14,970	157.8	0.35	0.07	1.18E4	0.77	6.68	0.80 ±10%
14	3.96	5.97	30,270	160.0	0.70	0.13	3.04E4	6.58	4.29	0.94 ±9%
15	6.02	6.01	44,940	159.9	1.04	0.19	5.16E4	21.93	3.29	1.01 ±11%
16	7.94	6.04	57,640	159.8	1.33	0.25	7.39E4	46.78	2.85	1.04 ±14%
17	0.98	7.92	10,140	210.1	0.18	0.03	8.50E3	0.14	13.94	0.76 ±14%
18	2.03	7.93	20,920	212.9	0.36	0.07	1.64E4	1.12	6.44	0.81 ±9%
19	4.01	7.97	41,020	214.4	0.71	0.13	4.08E4	8.97	4.20	0.97 ±8%
20	5.97	8.01	60,030	214.7	1.03	0.19	6.73E4	28.38	3.23	1.03 ±10%
21	7.95	8.06	76,930	212.6	1.34	0.25	9.28E4	60.11	2.67	1.04 ±13%

Run number 60 Sample type: fins L/D = 5.63

10 mm long aspect ratio = 0.127 Entrance loss = 0 nitrogen 88 Hz

Point	Xp (mm)	P (bar)	Re max	Re w	Ar/2	Mach#	ΔP (Pa)	pV (W)	Euler#
2	3.96	2.18	9,808	59.8	7.27	0.11	3.32E3	0.87	1.68
3	6.02	2.18	14,680	59.3	10.99	0.17	7.49E3	3.00	1.67
4	8.03	2.20	19,360	59.2	14.51	0.23	1.20E4	6.66	1.53
5	1.97	4.00	8,913	109.0	3.63	0.06	1.84E3	0.19	2.05
6	4.00	3.94	17,810	107.5	7.35	0.11	6.51E3	1.58	1.79
8	7.83	4.03	34,040	106.7	14.16	0.22	2.11E4	11.65	1.56

Run number 61 Sample type: fins L/D = 5.63

10 mm long aspect ratio = 0.127 Entrance loss = 0 nitrogen 82 Hz

Point	Xp (mm)	P (bar)	Re max	Re w	Ar/2	Mach#	ΔP (Pa)	pV (W)	Euler#
4	3.93	2.22	9,498	58.6	7.20	0.11	2.82E3	0.68	1.62
5	5.87	2.21	14,010	58.2	10.69	0.16	6.25E3	2.27	1.64
6	7.90	2.22	19,030	58.9	14.34	0.21	1.07E4	5.49	1.55
8	1.98	4.28	9,165	111.9	3.63	0.05	1.25E3	0.17	1.47
9	3.83	4.30	17,790	112.5	7.02	0.10	5.13E3	1.24	1.61
10	5.93	4.33	27,420	112.5	10.81	0.16	1.18E4	4.51	1.55
11	7.91	4.36	36,460	113.0	14.32	0.21	2.09E4	10.77	1.57
13	1.95	6.36	13,370	165.2	3.59	0.05	2.02E3	0.24	1.65
14	3.95	6.40	26,810	164.6	7.23	0.11	7.70E3	1.95	1.55
15	5.93	6.41	39,210	161.6	10.77	0.16	1.73E4	6.66	1.58
16	7.89	6.46	52,740	163.8	14.29	0.21	3.10E4	15.62	1.59
18	1.96	8.51	17,860	219.7	3.61	0.05	2.71E3	0.32	1.64
19	4.01	8.57	36,130	218.6	7.34	0.11	1.05E4	2.72	1.53
20	5.99	8.63	53,590	218.6	10.88	0.16	2.33E4	9.20	1.55
21	7.92	8.66	71,990	223.1	14.32	0.21	4.11E4	20.85	1.55

Run number 64 Sample type: fins L/D = 5.15

10 mm long aspect ratio = 0.442 Entrance loss = 0 nitrogen 88 Hz

Point	Xp (mm)	P (bar)	Re max	Re w	Ar/2	Mach#	ΔP (Pa)	pV (W)	Euler#
2	2.03	1.72	8,202	59.8	6.66	0.11	1.61E3	0.26	1.20
3	3.94	1.66	14,880	56.9	12.69	0.20	6.37E3	1.71	1.36
5	7.90	1.70	28,540	57.2	24.23	0.38	2.11E4	11.77	1.22
7	2.04	3.33	15,640	113.6	6.69	0.11	3.71E3	0.50	1.43
8	4.00	3.35	30,070	113.3	12.88	0.20	1.22E4	3.49	1.27
9	6.11	3.37	44,480	112.5	19.19	0.30	2.69E4	11.48	1.25
10	7.94	3.40	56,450	112.5	24.36	0.38	4.23E4	23.79	1.22
11	1.00	5.07	11,770	172.4	3.32	0.05	1.99E3	0.10	2.04
12	1.96	5.08	22,790	172.3	6.42	0.10	5.23E3	0.66	1.43
13	4.04	5.12	45,870	171.1	13.01	0.20	1.84E4	5.42	1.23
14	5.98	5.16	65,800	169.7	18.82	0.29	3.77E4	16.42	1.21
15	7.93	5.17	85,110	169.7	24.34	0.38	6.30E4	35.75	1.20
16	1.03	5.11	12,070	172.0	3.41	0.05	2.25E3	0.10	2.19
17	1.88	5.12	21,880	172.1	6.17	0.10	5.15E3	0.59	1.52
18	4.09	5.15	46,410	171.0	13.18	0.21	1.97E4	5.54	1.28
19	5.98	5.17	65,740	169.3	18.86	0.29	3.90E4	16.32	1.24
20	8.19	5.18	86,990	168.4	25.07	0.39	6.81E4	38.82	1.23

Run number 65 Sample type: fins L/D = 5.15

10 mm long aspect ratio = 0.442 Entrance loss = 0 helium 88 Hz

Point	Xp (mm)	P (bar)	Re max	Re w	Ar/2	Mach#	ΔP (Pa)	pV (W)	Euler#
2	2.04	11.95	7,048	52.0	6.58	0.04	1.70E3	0.26	1.31
3	3.94	11.83	13,440	51.4	12.71	0.07	7.14E3	1.85	1.49
4	5.88	11.80	19,870	50.9	18.95	0.10	1.51E4	6.18	1.43
5	7.29	11.80	24,510	50.7	23.47	0.13	2.04E4	12.33	1.26
7	2.02	23.57	13,720	102.0	6.53	0.04	4.20E3	0.48	1.67
8	3.94	23.75	26,680	102.1	12.69	0.07	1.41E4	3.49	1.47
9	5.99	23.69	40,090	101.0	19.28	0.11	3.15E4	12.16	1.44
10	7.93	23.61	52,750	100.3	25.53	0.14	5.39E4	28.33	1.41
11	1.09	35.58	11,070	152.5	3.53	0.02	2.00E3	0.11	1.81
12	2.00	35.35	20,070	151.1	6.45	0.04	6.05E3	0.67	1.65
13	3.87	35.23	38,460	149.6	12.49	0.07	1.97E4	4.82	1.44
14	5.81	35.53	57,760	149.9	18.70	0.10	4.16E4	16.43	1.36
15	7.78	35.35	76,400	148.3	25.01	0.14	7.45E4	39.69	1.37
16	0.95	47.32	12,740	201.0	3.08	0.02	2.20E3	0.10	1.98
17	2.00	47.34	26,550	200.4	6.44	0.04	6.64E3	0.89	1.37
18	3.94	47.64	52,500	200.7	12.70	0.07	2.44E4	6.72	1.28
19	5.96	47.64	78,480	198.7	19.17	0.10	5.88E4	23.03	1.37

Run number 66 Sample type: fins L/D = 73.2

120 mm long aspect ratio = 0.220 Entrance loss = 1.5 nitrogen 88 Hz

Point	Xp (mm)	P (bar)	Re max	Re w	Ar/2	Mach#	ΔP (Pa)	pV (W)	Euler#	TDF
1	1.12	2.34	6,739	57.2	0.40	0.08	5.64E3	0.34	5.89	0.83 ±19%
2	2.02	2.35	11,330	56.7	0.68	0.13	1.14E4	1.58	4.16	0.86 ±17%
3	4.08	2.36	20,020	56.3	1.22	0.23	2.68E4	8.72	3.09	0.91 ±20%
4	6.04	2.39	26,330	55.3	1.63	0.30	4.33E4	20.65	2.80	0.93 ±25%
5	8.02	2.40	31,480	54.1	1.99	0.37	6.20E4	36.96	2.71	0.93 ±31%
6	1.03	4.66	11,510	106.6	0.37	0.07	9.79E3	0.44	6.35	0.79 ±13%
7	1.96	4.66	20,960	107.5	0.67	0.12	2.12E4	2.72	4.20	0.90 ±10%
8	3.90	4.69	37,550	107.8	1.19	0.22	4.98E4	15.66	3.08	0.99 ±14%
9	5.99	4.74	51,460	106.9	1.65	0.30	8.51E4	40.45	2.76	1.00 ±19%
10	7.76	4.72	60,580	103.6	2.00	0.37	1.00E5	63.39	2.24	0.86 ±23%
11	0.99	6.99	16,230	157.3	0.35	0.07	1.40E4	0.54	6.69	0.79 ±11%
12	1.99	7.00	31,570	159.8	0.67	0.13	3.09E4	4.23	3.99	0.92 ±9%
13	4.09	7.06	58,610	159.6	1.26	0.23	7.75E4	25.53	2.89	0.97 ±12%
14	4.52	7.07	63,190	159.1	1.36	0.25	8.78E4	32.19	2.80	0.98 ±13%
15	0.99	9.30	21,700	210.7	0.35	0.07	1.87E4	0.74	6.73	0.83 ±10%
16	1.99	9.31	42,320	212.9	0.68	0.13	4.28E4	5.45	4.11	0.95 ±8%
17	3.66	9.35	72,030	214.0	1.15	0.21	9.04E4	26.22	3.01	1.01 ±11%

Run number 67 Sample type: fins L/D = 73.2

120 mm long aspect ratio = 0.220 Entrance loss = 1.5 helium 88 Hz

Point	Xp (mm)	P (bar)	Re max	Re w	Ar/2	Mach#	ΔP (Pa)	pV (W)	Euler#	TDF
1	1.03	16.66	4,261	52.2	0.28	0.02	5.06E3	0.12	10.73	0.80 ±17%
2	1.96	16.51	7,973	51.5	0.53	0.03	1.13E4	0.73	6.76	0.78 ±9%
3	3.98	16.68	16,260	51.8	1.07	0.07	2.33E4	5.94	3.35	0.87 ±5%
4	5.94	16.65	23,720	50.9	1.59	0.10	5.07E4	19.28	3.34	0.91 ±4%
5	7.87	16.90	31,610	51.3	2.10	0.14	8.40E4	43.99	3.14	0.93 ±5%
6	1.02	33.14	8,239	101.9	0.28	0.02	1.06E4	0.19	11.68	0.68 ±12%
7	1.96	33.04	15,780	101.7	0.53	0.03	2.13E4	1.28	6.37	0.76 ±7%
8	3.92	33.27	31,510	102.0	1.06	0.07	4.40E4	10.61	3.30	0.90 ±4%
9	5.96	33.62	47,600	101.7	1.60	0.10	1.01E5	36.80	3.28	0.93 ±4%
10	5.99	33.63	47,560	101.1	1.61	0.11	9.24E4	36.82	2.99	0.93 ±3%
11	1.02	49.75	12,180	151.4	0.27	0.02	1.87E4	0.25	13.87	0.65 ±11%
12	2.00	49.63	23,960	151.4	0.54	0.04	3.17E4	2.04	6.11	0.80 ±6%
13	3.99	49.94	47,580	151.2	1.08	0.07	7.61E4	16.20	3.70	0.91 ±3%
14	4.85	49.95	57,350	150.2	1.30	0.09	1.04E5	28.70	3.44	0.93 ±3%
15	1.00	65.90	15,670	198.4	0.27	0.02	1.99E4	0.31	11.64	0.69 ±11%
16	1.98	65.77	31,010	198.2	0.53	0.03	3.97E4	2.60	5.93	0.84 ±6%
17	3.93	65.96	61,150	197.6	1.06	0.07	9.66E4	19.89	3.69	0.92 ±3%

Run number 68 Sample type: fins L/D = 61.0

120 mm long aspect ratio = 0.667 Entrance loss = 1.5 nitrogen 88 Hz

Point	Xp (mm)	P (bar)	Re max	Re w	Ar/2	Mach#	ΔP (Pa)	pV (W)	Euler#	TDF
10	0.98	1.56	5,307	52.5	0.41	0.08	4.04E3	0.24	6.13	1.03 ±26%
11	2.00	1.57	9,701	52.7	0.76	0.14	8.74E3	1.33	3.98	1.00 ±24%
12	3.97	1.58	16,580	52.7	1.29	0.24	1.95E4	6.09	3.04	0.98 ±28%
13	6.03	1.59	22,170	52.3	1.74	0.32	3.20E4	14.35	2.75	0.97 ±33%
14	7.78	1.60	25,800	51.4	2.06	0.38	4.38E4	23.54	2.70	0.95 ±39%
15	0.99	3.13	10,230	100.7	0.42	0.08	7.57E3	0.41	5.81	0.96 ±15%
16	1.99	3.15	18,960	101.9	0.76	0.14	1.72E4	2.49	3.91	1.02 ±14%
17	4.01	3.16	33,110	102.2	1.33	0.25	3.93E4	12.51	2.93	1.03 ±17%
18	6.00	3.18	44,210	102.2	1.77	0.33	6.31E4	28.76	2.63	1.02 ±23%
19	7.00	3.20	48,800	101.4	1.97	0.36	7.61E4	39.11	2.57	1.01 ±26%
20	1.00	4.71	15,450	151.2	0.42	0.08	1.16E4	0.61	5.86	0.98 ±12%
21	2.00	4.72	28,830	153.0	0.77	0.14	2.64E4	3.79	3.89	1.04 ±11%

Run number 69 Sample type: fins L/D = 61.0

120 mm long aspect ratio = 0.667 Entrance loss = 1.5 nitrogen 88 Hz

Point	Xp (mm)	P (bar)	Re max	Re w	Ar/2	Mach#	ΔP (Pa)	pV (W)	Euler#	TDF
2	1.97	6.28	38,590	206.9	0.76	0.14	3.47E4	4.90	3.89	1.08 ±9%
3	3.88	6.34	65,370	205.3	1.31	0.24	7.71E4	23.50	2.97	1.10 ±13%
4	3.95	4.76	49,570	153.1	1.33	0.25	5.80E4	18.29	2.88	1.06 ±14%
5	5.00	4.78	58,490	152.0	1.58	0.29	7.65E4	30.07	2.70	1.05 ±17%

Run number 70 Sample type: fins L/D = 61.0

120 mm long aspect ratio = 0.667 Entrance loss = 1.5 helium 88 Hz

Point	Xp (mm)	P (bar)	Re max	Re w	Ar/2	Mach#	ΔP (Pa)	pV (W)	Euler#	TDF
3	1.00	11.15	3,793	50.2	0.31	0.02	4.37E3	0.11	11.21	1.00 ±19%
4	2.00	11.22	7,542	50.5	0.61	0.04	8.39E3	0.73	5.48	0.95 ±10%
5	4.05	11.11	14,920	49.5	1.24	0.08	2.21E4	5.74	3.60	1.02 ±6%
6	5.96	11.41	22,140	50.2	1.81	0.12	4.40E4	17.64	3.29	1.04 ±5%
7	7.93	10.96	28,160	48.3	2.39	0.16	7.20E4	39.93	3.20	1.09 ±7%
8	0.99	22.30	7,438	99.6	0.31	0.02	8.40E3	0.17	11.11	0.85 ±14%
9	2.01	22.33	14,990	99.9	0.61	0.04	1.68E4	1.30	5.51	0.92 ±7%
10	3.94	22.43	29,150	99.4	1.20	0.08	4.07E4	9.97	3.48	1.03 ±4%
11	5.78	22.77	42,270	98.8	1.75	0.11	8.04E4	31.16	3.22	1.05 ±4%
12	1.02	33.33	11,120	146.1	0.31	0.02	1.34E4	0.24	11.53	0.81 ±12%
13	2.00	33.52	21,580	144.7	0.61	0.04	2.34E4	1.87	5.27	0.96 ±6%
14	3.97	33.53	43,450	147.2	1.21	0.08	5.73E4	14.33	3.25	1.03 ±4%
15	5.01	33.63	54,400	146.4	1.52	0.10	8.55E4	28.27	3.07	1.06 ±4%
16	1.00	44.74	14,640	195.4	0.31	0.02	1.77E4	0.30	11.74	0.82 ±11%
17	2.04	44.84	29,730	195.8	0.62	0.04	3.23E4	2.60	5.20	0.97 ±6%
18	3.96	45.12	57,670	196.1	1.21	0.08	7.46E4	18.40	3.19	1.03 ±3%

Run number 71 Sample type: fins L/D = 59.8

120 mm long aspect ratio = 0.456 Entrance loss = 1.5 nitrogen 88 Hz

Point	Xp (mm)	P (bar)	Re max	Re w	Ar/2	Mach#	ΔP (Pa)	pV (W)	Euler#	TDF
1	0.96	1.56	4,712	57.6	0.34	0.07	3.15E3	0.13	6.82	0.85 ±29%
2	2.04	1.57	9,291	57.4	0.68	0.13	6.89E3	0.93	3.81	0.82 ±24%
3	4.05	1.58	16,480	56.3	1.22	0.23	1.65E4	5.20	2.80	0.85 ±25%
4	6.11	1.60	21,970	55.8	1.64	0.31	2.86E4	13.79	2.69	0.95 ±30%
5	8.05	1.63	25,940	55.3	1.96	0.36	4.16E4	24.96	2.74	1.02 ±36%
6	1.03	3.12	9,205	107.1	0.36	0.07	6.05E3	0.25	6.17	0.77 ±17%
7	2.03	3.15	17,420	108.6	0.67	0.12	1.39E4	1.77	4.03	0.91 ±13%
8	4.10	3.17	31,420	108.3	1.21	0.23	3.46E4	11.57	3.06	1.09 ±16%
9	6.00	3.19	42,170	108.2	1.63	0.30	5.57E4	26.91	2.72	1.06 ±21%
11	1.08	4.66	14,010	157.1	0.37	0.07	9.75E3	0.44	6.26	0.88 ±13%
12	3.95	4.72	45,400	160.7	1.18	0.22	4.92E4	15.85	3.09	1.13 ±13%
13	2.06	4.70	25,660	159.2	0.67	0.12	2.25E4	3.22	4.37	1.17 ±11%
14	4.11	4.76	46,880	159.8	1.23	0.23	5.13E4	17.16	2.98	1.10 ±14%
15	6.05	4.80	62,660	158.6	1.65	0.30	8.39E4	40.75	2.69	1.09 ±19%
16	0.96	6.27	16,550	209.8	0.33	0.06	1.17E4	0.48	7.16	1.04 ±12%
17	2.01	6.28	33,570	212.5	0.66	0.12	2.94E4	3.96	4.45	1.18 ±9%
18	4.03	6.34	61,400	214.6	1.20	0.22	6.75E4	22.20	3.08	1.18 ±13%
19	4.95	6.37	71,740	213.0	1.41	0.26	8.77E4	35.32	2.90	1.17 ±15%

Run number 72 Sample type: fins L/D = 59.8

120 mm long aspect ratio = 0.456 Entrance loss = 1.5 helium 88 Hz

Point	Xp (mm)	P (bar)	Re max	Re w	Ar/2	Mach#	ΔP (Pa)	pV (W)	Euler#	TDF
1	1.06	11.02	3,444	51.4	0.28	0.02	4.29E3	0.08	13.67	0.82 ±21%
2	2.00	11.10	6,513	51.6	0.53	0.03	7.17E3	0.42	6.41	0.73 ±12%
3	3.77	11.07	12,090	51.1	0.99	0.07	1.24E4	2.70	3.16	0.79 ±7%
4	6.05	11.22	19,420	51.3	1.58	0.10	2.81E4	10.98	2.79	0.84 ±5%
5	7.84	11.31	24,900	51.1	2.04	0.13	5.61E4	28.03	3.35	1.02 ±6%
6	1.04	22.25	6,630	101.3	0.27	0.02	7.82E3	0.12	13.13	0.74 ±14%
7	1.99	22.13	12,660	101.0	0.52	0.03	1.31E4	0.90	6.00	0.88 ±8%
8	4.04	22.24	25,700	101.5	1.06	0.07	3.78E4	8.20	4.24	1.07 ±4%
9	5.89	22.26	37,630	102.2	1.54	0.10	6.57E4	24.08	3.41	1.04 ±4%
10	6.98	22.46	43,800	100.8	1.82	0.12	8.81E4	39.54	3.35	1.11 ±4%
11	1.01	33.05	9,462	148.4	0.27	0.02	1.20E4	0.15	14.46	0.71 ±13%
12	1.99	33.04	18,720	149.5	0.52	0.03	2.10E4	1.57	6.52	1.09 ±7%
13	4.08	33.21	38,430	150.2	1.07	0.07	5.58E4	12.76	4.13	1.15 ±4%
14	5.53	33.21	51,490	148.9	1.45	0.09	8.46E4	28.98	3.44	1.10 ±4%
15	1.02	44.16	12,760	199.2	0.27	0.02	1.61E4	0.27	14.32	0.97 ±12%
16	2.02	44.19	25,270	199.2	0.53	0.03	2.98E4	2.37	6.74	1.22 ±6%
17	3.92	44.36	48,940	199.4	1.03	0.07	6.32E4	13.98	3.81	1.11 ±4%
18	5.11	44.49	63,570	198.8	1.34	0.09	9.30E4	28.80	3.31	1.06 ±3%

Run number 77 Sample type: fins L/D = 5.15 Rounded

10 mm long aspect ratio = 0.442 Entrance loss = 0 nitrogen 88 Hz

Point	Xp (mm)	P (bar)	Re max	Re w	Ar/2	Mach#	ΔP (Pa)	pV (W)	Euler#
3	4.01	1.67	15,120	56.6	12.98	0.20	5.35E3	1.45	1.09
4	6.03	1.69	22,320	56.4	19.20	0.30	1.07E4	4.63	0.99
7	1.91	3.31	14,520	112.2	6.29	0.10	2.60E3	0.32	1.14
8	3.98	3.32	29,560	111.4	12.89	0.20	9.53E3	2.70	1.00
9	6.06	3.32	43,780	110.2	19.29	0.30	2.13E4	9.04	1.01
10	8.05	3.37	57,560	111.4	25.09	0.39	3.58E4	20.14	0.98
11	1.03	4.95	11,660	166.4	3.40	0.05	1.59E3	0.08	1.60
12	1.91	5.00	21,650	167.9	6.26	0.10	3.81E3	0.47	1.12
13	3.97	5.02	44,040	166.2	12.87	0.20	1.45E4	3.97	1.01
14	5.88	5.05	64,010	165.6	18.76	0.29	2.89E4	12.25	0.95
15	7.86	5.08	83,820	165.4	24.60	0.38	5.06E4	27.82	0.97
16	1.08	6.64	16,260	222.0	3.56	0.06	2.30E3	0.12	1.59
17	1.99	6.65	29,820	221.3	6.54	0.10	5.30E3	0.70	1.08
18	4.01	6.69	58,780	219.6	13.00	0.20	1.94E4	5.31	1.00
19	5.86	6.72	84,210	218.3	18.73	0.29	3.98E4	15.99	0.99
20	7.75	6.77	109,000	217.7	24.30	0.38	6.68E4	35.64	0.99

Run number 90 Sample type: fins L/D = 5.63

10 mm long aspect ratio = 0.127 Entrance loss = 0 helium 90 Hz

Point	Xp (mm)	P (bar)	Re max	Re w	Ar/2	Mach#	ΔP (Pa)	pV (W)	Euler#
3	3.95	14.27	8,446	52.4	7.15	0.04	3.18E3	0.84	1.67
4	6.17	14.46	13,270	52.7	11.17	0.06	7.83E3	3.24	1.67
5	8.27	14.45	17,650	52.4	14.95	0.08	1.40E4	7.79	1.68
7	2.03	28.48	8,579	103.7	3.67	0.02	1.47E3	0.22	1.47
8	2.02	28.48	8,549	103.7	3.66	0.02	1.48E3	0.22	1.50
9	4.05	28.63	17,100	103.6	7.33	0.04	6.38E3	1.73	1.60
10	5.95	28.77	24,950	103.0	10.75	0.06	1.39E4	5.55	1.63
11	8.21	28.82	34,300	102.6	14.83	0.08	2.63E4	14.61	1.62
13	2.04	42.46	12,670	152.7	3.68	0.02	2.40E3	0.32	1.62
14	4.23	42.44	26,190	151.8	7.66	0.04	1.02E4	2.87	1.59
15	6.05	42.64	36,990	150.2	10.93	0.06	2.09E4	8.46	1.61
16	8.28	42.75	50,850	150.8	14.97	0.08	3.89E4	21.83	1.59
18	1.96	56.67	16,140	201.7	3.55	0.02	2.92E3	0.37	1.60
19	4.05	56.78	33,050	200.4	7.32	0.04	1.23E4	3.30	1.58
20	5.99	56.84	48,640	199.5	10.82	0.06	2.68E4	10.73	1.58
21	8.16	57.16	66,110	198.9	14.75	0.08	4.96E4	27.50	1.58

Run number 140 Sample type: fins L/D = 60.1

120 mm long aspect ratio = 0.352 Entrance loss = 1.5 helium 84 Hz

Point	Xp (mm)	P (bar)	Re max	Re w	Ar/2	Mach#	ΔP (Pa)	pV (W)	Euler#	TDF
1	1.09	11.51	3,191	51.3	0.26	0.02	3.93E3	0.07	15.07	1.03 ±23%
2	1.07	11.46	3,103	51.0	0.25	0.02	4.02E3	0.07	16.22	1.04 ±23%
3	1.88	11.33	5,389	50.4	0.44	0.03	5.33E3	0.31	7.03	0.88 ±15%
4	1.88	11.26	5,351	50.0	0.45	0.03	5.50E3	0.31	7.30	0.88 ±14%
5	3.18	11.38	9,101	50.4	0.75	0.05	9.03E3	1.45	4.17	0.90 ±8%
6	3.12	11.30	8,858	50.0	0.74	0.05	8.70E3	1.39	4.21	0.92 ±9%
7	4.04	11.42	11,560	50.3	0.96	0.06	1.35E4	2.94	3.85	0.92 ±7%
8	4.02	11.41	11,470	50.3	0.95	0.06	1.33E4	2.88	3.83	0.92 ±7%
9	5.04	11.44	14,270	49.9	1.19	0.08	1.99E4	5.62	3.68	0.94 ±6%
10	4.98	11.44	14,110	49.9	1.18	0.07	1.82E4	5.49	3.45	0.95 ±6%
11	4.95	11.57	14,020	49.9	1.17	0.07	1.92E4	5.42	3.66	0.94 ±6%
12	6.46	11.53	18,030	49.3	1.52	0.10	2.80E4	11.67	3.18	0.97 ±5%
13	7.09	11.98	20,350	50.8	1.67	0.10	3.72E4	15.54	3.40	0.96 ±5%
14	7.06	11.91	20,220	50.6	1.66	0.10	3.64E4	15.38	3.37	0.97 ±5%
15	8.61	12.01	24,470	50.4	2.02	0.13	5.13E4	27.32	3.20	0.98 ±5%
16	8.67	11.91	24,500	50.1	2.04	0.13	5.20E4	27.82	3.22	0.98 ±5%

Run number 141 Sample type: fins L/D = 60.1

120 mm long aspect ratio = 0.352 Entrance loss = 1.5 helium 84 Hz

Point	Xp (mm)	P (bar)	Re max	Re w	Ar/2	Mach#	ΔP (Pa)	pV (W)	Euler#	TDF
1	1.20	23.53	6,962	101.5	0.29	0.02	7.99E3	0.16	12.55	0.83 ±13%
2	1.19	23.44	6,829	100.9	0.28	0.02	6.73E3	0.15	10.93	0.83 ±14%
3	2.20	23.36	12,630	101.1	0.52	0.03	1.21E4	0.87	5.75	0.84 ±8%
4	2.19	23.35	12,560	100.8	0.52	0.03	1.35E4	0.86	6.47	0.83 ±8%
5	3.17	23.08	17,900	99.3	0.75	0.05	1.89E4	2.59	4.38	0.88 ±5%
6	4.43	23.38	24,890	99.2	1.04	0.07	2.90E4	7.09	3.47	0.94 ±4%
7	4.38	23.33	24,600	99.1	1.03	0.07	2.89E4	6.89	3.53	0.94 ±4%
8	6.34	24.23	36,440	101.6	1.49	0.09	5.80E4	20.91	3.29	0.97 ±3%
9	6.39	24.17	36,360	100.7	1.50	0.09	5.87E4	21.36	3.31	0.97 ±3%
10	8.41	24.27	47,290	99.7	1.97	0.12	9.19E4	47.36	3.01	0.99 ±4%
11	8.39	24.35	47,230	99.8	1.97	0.12	9.13E4	47.14	3.00	0.99 ±4%

Run number 142 Sample type: fins L/D = 60.1

120 mm long aspect ratio = 0.352 Entrance loss = 1.5 helium 85 Hz

Point	Xp (mm)	P (bar)	Re max	Re w	Ar/2	Mach#	ΔP (Pa)	pV (W)	Euler#	TDF
1	1.09	35.49	9,263	149.5	0.26	0.02	9.48E3	0.16	12.28	0.81 ±12%
2	1.11	35.47	9,388	149.2	0.26	0.02	1.12E4	0.17	14.05	0.80 ±12%
3	2.06	35.40	17,480	149.7	0.49	0.03	1.67E4	1.02	6.09	0.84 ±7%
4	2.04	35.44	17,330	149.5	0.48	0.03	1.65E4	1.00	6.12	0.83 ±7%
5	3.27	35.75	27,860	150.1	0.77	0.05	2.76E4	4.23	3.96	0.92 ±4%
6	3.25	35.73	27,730	150.3	0.77	0.05	2.71E4	4.15	3.94	0.92 ±4%
7	4.37	36.17	37,200	150.4	1.03	0.06	4.35E4	10.06	3.49	0.95 ±3%
8	4.39	36.35	37,480	150.8	1.04	0.06	4.43E4	10.22	3.51	0.95 ±3%
9	5.67	36.58	48,250	150.4	1.34	0.08	6.77E4	21.66	3.22	0.97 ±3%
10	5.71	36.55	48,350	149.7	1.34	0.08	6.85E4	22.15	3.22	0.97 ±3%
11	6.71	36.52	56,200	148.3	1.58	0.10	8.94E4	35.40	3.07	0.99 ±3%
12	6.66	36.33	55,340	147.2	1.57	0.10	8.82E4	34.57	3.10	0.99 ±3%

Run number 144 Sample type: fins L/D = 60.1

120 mm long aspect ratio = 0.352 Entrance loss = 1.5 nitrogen 85 Hz

Point	Xp (mm)	P (bar)	Re max	Re w	Ar/2	Mach#	ΔP (Pa)	pV (W)	Euler#	TDF
1	1.09	1.55	4,038	50.4	0.33	0.06	2.90E3	0.14	7.44	1.00 ±31%
2	1.10	1.55	4,062	50.3	0.34	0.06	2.92E3	0.14	7.40	1.00 ±31%
3	2.04	1.57	7,222	50.4	0.60	0.11	5.62E3	0.71	4.50	0.93 ±25%
4	2.05	1.57	7,228	50.2	0.60	0.11	5.64E3	0.71	4.49	0.93 ±25%
5	3.29	1.58	11,190	50.5	0.92	0.16	1.07E4	2.48	3.55	0.94 ±24%
6	3.30	1.58	11,190	50.4	0.92	0.16	1.07E4	2.49	3.55	0.94 ±24%
7	4.22	1.59	13,930	50.7	1.14	0.20	1.45E4	4.66	3.13	0.95 ±25%
8	4.06	1.59	13,420	50.5	1.11	0.20	1.38E4	4.21	3.20	0.95 ±25%
9	5.08	1.61	16,250	50.5	1.34	0.24	1.85E4	7.34	2.90	0.95 ±26%
10	4.94	1.60	15,790	50.2	1.31	0.23	1.78E4	6.86	2.94	0.95 ±26%
11	6.63	1.67	20,230	50.6	1.67	0.29	2.64E4	14.03	2.64	0.95 ±28%
12	6.70	1.68	20,030	50.9	1.64	0.29	2.53E4	13.54	2.59	0.95 ±28%

REPORT DOCUMENTATION PAGE

Form Approved
OMB No. 0704-0188

1. AGENCY USE ONLY *(Leave blank)*

2. REPORT DATE
September 1991

3. REPORT TYPE AND DATES COVERED
Final Contractor Report

4. TITLE AND SUBTITLE
Oscillating-Flow Loss Test Results in Rectangular Heat Exchanger Passages

5. FUNDING NUMBERS
WU-590-13-11
C-NAS3-23885

6. AUTHOR(S)
J. Gary Wood

7. PERFORMING ORGANIZATION NAME(S) AND ADDRESS(ES)
Sunpower, Inc.
6 Byard Street
Athens, Ohio 45701

8. PERFORMING ORGANIZATION REPORT NUMBER
None

9. SPONSORING/MONITORING AGENCY NAMES(S) AND ADDRESS(ES)
National Aeronautics and Space Administration
Lewis Research Center
Cleveland, Ohio 44135-3191

10. SPONSORING/MONITORING AGENCY REPORT NUMBER
NASA CR-185297

11. SUPPLEMENTARY NOTES
Project Manager, Lanny G. Thieme, Power Technology Division, NASA Lewis Research Center, (216) 433-6119.
J. Gary Wood, Consultant, subcontractor to Sunpower, Inc.

12a. DISTRIBUTION/AVAILABILITY STATEMENT
[redacted]
Date for general release September 1993
Subject Category 20

12b. DISTRIBUTION CODE

13. ABSTRACT *(Maximum 200 words)*

Presented in this report are test results of oscillating-flow losses in rectangular heat exchanger passages of various aspect ratios. This work was performed in support of the design of a free-piston Stirling engine (FPSE) for a dynamic space power conversion system. The FPSE design was done by Sunpower, Inc. under contract to NASA-Lewis Research Center as part of the SP-100 program. Oscillating-flow loss testing was performed using an oscillating-flow loss rig which is based on a variable stroke and variable frequency linear drive motor. Test were run over a range of oscillating-flow parameters (Re_{max}, Re_{ω}, and Ar) encompassing the flow regimes of the proposed engine design. Test results are presented in both tabular and graphical form and are compared against analytical predictions.

14. SUBJECT TERMS
Stirling engines; Heat exchangers; Oscillating flow

15. NUMBER OF PAGES
78

16. PRICE CODE
A05

17. SECURITY CLASSIFICATION OF REPORT
Unclassified

18. SECURITY CLASSIFICATION OF THIS PAGE
Unclassified

19. SECURITY CLASSIFICATION OF ABSTRACT
Unclassified

20. LIMITATION OF ABSTRACT

National Aeronautics and
Space Administration

Lewis Research Center
Cleveland, Ohio 44135

Official Business
Penalty for Private Use $300

FOURTH CLASS MAIL

ADDRESS CORRECTION REQUESTED

U.S.MAIL

Postage and Fees Paid
National Aeronautics and
Space Administration
NASA 451

NASA